MONTE CARLO SIMULATION OF ISING CHAINS AND POLYTYPES
and
MODELS FOR LOW SPIN—HIGH SPIN TRANSITIONS IN SOLIDS

A Thesis Submitted
In Partial Fulfilment of the Requirements
for the Degree of
DOCTOR OF PHILOSOPHY

by

S. RAMASESHA

to the

DEPARTMENT OF CHEMISTRY
INDIAN INSTITUTE OF TECHNOLOGY KANPUR
APRIL, 1977

DEPARTMENT OF CHEMISTRY
INDIAN INSTITUTE OF TECHNOLOGY KANPUR, INDIA

CERTIFICATE I

This is to certify that Mr. S. Ramasesha has satisfactorily completed all the courses required for the Ph.D. degree programme. These courses include:

Chm 501	Advanced Organic Chemistry I
Chm 521	Chemical Binding
Chm 523	Chemical Thermodynamics
Chm 524	Modern Physical Methods
Chm 541	Advanced Inorganic Chemistry I
Chm 629	Quantum Chemistry II
Chm 630	Ligand Field Theory
M 601	Mathematical Methods
M 608	Numerical Solutions of Ordinary Differential Equations
Phy 622	Solid State Physics II
MetE 644	Materials Science I

Mr. S. Ramasesha successfully completed his Ph.D. qualifying examination in October 1971.

A. Chakravorty
Professor and Head 11/4/77
Department of Chemistry

D. Devaprabhakara
D. Devaprabhakara
Convener
Departmental Post-Graduate Committee

CERTIFICATE II

Certified that the work contained in this thesis entitled 'MONTE CARLO SIMULATION OF ISING CHAINS AND POLYTYPES and MODELS FOR LOW SPIN-HIGH SPIN TRANSITIONS IN SOLIDS' has been carried out by Mr. S. Ramasesha under my supervision and the same has not been submitted elsewhere for a degree.

C. N. R. Rao
Thesis Supervisor

STATEMENT

I hereby declare that the matter embodied in this thesis entitled "Monte Carlo Simulation of Ising Chains and Polytypes and Models for Low Spin-High Spin Transitions in Solids" is the result of the investigations carried out by me in the Department of Chemistry, Indian Institute of Technology, Kanpur, India, under the supervision of Professor C. N. R. Rao.

In keeping with the general practice of reporting scientific observations, due acknowledgement has been made whenever the work described is based on the findings of other investigators. Any omissions which might have occurred by oversight or error in judgement is regretted.

S. Ramasesha

ACKNOWLEDGEMENTS

It is my pleasant duty to thank Professor C. N. R. Rao for suggesting the problems, inspiring guidance, constant encouragement and forbearance without which this thesis would not have taken shape. I am also highly indebted to him for taking keen interest in my personal welfare despite my many failings.

I thank Professor T. V. Ramakrishnan for willingly sparing much of his valuable time, for many helpful discussions and useful suggestions, during the course of this work.

My thanks are also due to

Professor C. K. Mazumdar for a helpful discussion.

my lab colleagues, in particular, Dr. P. Ganguly, Mr. M. K. Uppal and Mr. U. P. Agrawal for the help received at various stages of this work.

my friends for making my stay here pleasant and enjoyable.

the members of my family for their immense patience and constant encouragement.

Mr. Nihal Ahmad for excellent and expeditious typing of the manuscript.

S. Ramasesha

CONTENTS

PREFACE

Ising chains with finite-range interactions do not show phase transitions. However, Ising chains with infinite-range interactions do show a phase transition, when the interaction potential is of a particular form. Particularly interesting are Ising chains with short-range antiferromagnetic interaction and an infinite-range ferromagnetic interaction. Such systems have been studied by Nagle and Theumann and Høye. Nagle studied spin-half Ising chains with nearest neighbour antiferromagnetic interaction and equivalent neighbour ferromagnetic interaction and found first order phase transition with temperature, both in a field and in the absence of a field, for certain range of relative interaction strengths ($J_{short-range}/J_{long-range}$). Theumann and Høye extended the range of antiferromagnetic interactions to the second neighbour and introduced Kac potential for long-range interactions. These workers have reported a zero temperature phase diagram for the system with strength of interactions as parameters. In certain regions of their phase diagram, the Ising chain shows as many as four first order phase transitions, while in other regions the chain exhibits one, two or three phase transitions.

In Chapter I, we have presented results of a Monte Carlo simulation of spin-half Ising chains with (i) nearest-neighbour antiferromagnetic interaction and equivalent neighbour ferromagnetic interaction and (ii) nearest and next nearest neighbour antiferromagnetic interaction and equivalent neighbour ferromagnetic interaction. We have estimated thermodynamic properties such as internal energy, specific heat, staggered susceptibilities, sublattice magnetizations and correlation functions. The main aim of this work was to find out if different spin orderings were present in the different regions of the phase diagrams of Nagle and Theumann and Høye and to study changes in spin ordering as a function of temperature, for a given set of interaction strengths, in a given region. In (i), we find a first order phase transition in the presence of a field while in the absence of a field, the system is in a metastable state and thus, does not show any phase transition. In (ii), we observe first order phase transition in the presence and absence of a field, in one of the regions. In the rest of the regions, we find blips in specific heat vs. temperature curves, probably indicating that the transitions are of a higher order. We find different spin arrangements, in different regions of the phase diagram at low temperatures. We do not see any significant changes in short-range spin-ordering, within a region as the temperature is varied, except in the case where a first order phase transition is observed. However, from the asymptotic

correlation functions computed in one of the regions, we observe that the long-range ordering of spins changes from a four-sublattice structure to a three-sublattice structure at the transition temperature.

The above studies on magnetic Ising chains were partly prompted by our interest in the origin of polytypism. It is well known that substances like SiC, ZnS, CdI_2 and TaS_2 exhibit polytypism wherein different polytypic forms differ only in the c parameter of the unit cell (the other two remaining essentially constant). This is due to different stacking arrangements of the layers in different specimens. The nature of interactions responsible for polytype formation is not clearly known and the existing theories are inadequate.

In Chapter II of this thesis, we have presented results of the Monte Carlo simulation of polytypes based on the Ising chains of Chapter I. We have first started with the fact that each layer in a polytype can be classified either as a cubic layer or as a hexagonal layer. Therefore generation of a polytype is equivalent to the generation of a spin-half Ising chain. Since the properties of polytypes closely resemble those of the magnetic Ising chains studied in Chapter I, we assumed that the interaction between layers are similar to the interaction between spins in the Ising chains. However, to simulate polytypes we had to consider different growth mechanisms since the spin-flip mechanism used to generate magnetic Ising chain

states is not physically meaningful in the case of polytypes. Three different mechanisms to rearrange the layer sequence were construed viz. (i) rearrangement of a single layer (e.g., ----ABBCAB---- ----ABACAB----), (ii) transposition of two layers (e.g., ----ABCACB---- ----ACBACB----), and (iii) general rearrangement of two layers (e.g., ----ABCACB---- ---ABCBAB----). It was found that the first two mechanisms presented ergodic problems, i.e. the number of trys required to move the chain from one configuration to another was unmanageably large. The third mechanism did not present any such problem and hence appeared to be a more reasonable mechanism. Using this mechanism and with competing interaction of different ranges between layers, we have been successful in generating polytypes up to a repeat length of 12 layers.

Though the interaction terms need justification, infinite range equivalent neighbour interaction at least is known in solid state systems, consisting of ions of different volumes. The method of simulation presented here can also be used for testing interaction models that may be put forth in the future for explaining polytypism.

Some inorganic solids (e.g., MnAs, $LaCoO_3$ and $HoCoO_3$) and inorganic complexes in the solid state (e.g., $[Fe(Phen)_2(NCS)_2]$), which contain a transition metal ion capable of showing a crossover in the ground state with change in crystal field strength, exhibit gradual or abrupt

spin-state transitions. These spin-state transitions are often accompanied by a change in crystal structure. Bari and Sivardiere put forth some models to explain such spin-state transitions, based on coupling of the spin states to the lattice, with some success. Because of considerable experimental interest in spin-state transitions, in this laboratory, we have undertaken a re-examination of the models of Bari and Sivardiere and also have investigated some new models for spin-state transitions in solids.

The one and two-sublattice models of Bari and Sivardiere do not exhibit a phase transition when a kinetic energy term is added to their Hamiltonian. This is an exact result. Similarly a dynamic model in which the spin-states are coupled to an optical mode, with the coupling capable of mixing spin states, also does not exhibit a phase transition, though it explains non-zero high-spin state population observed at absolute zero. It appears from these results that kinetic energy plays an important role in determining the existence of a phase transition. To include the kinetic energy term and at the same time obtain a free energy expansion in terms of an order parameter we employed the path integral method for computing the partition function. The results from this method for the two-sublattice model predicted a phase transition, in apparent contradiction to the exact results. To resolve the discrepancy we have examined the order parameter method closely and have concluded that the phase transition

results from a tacit inclusion of the coupling of displacements on different sites, and is inherent in the order parameter expansion. To explain the observed first order phase transitions we have considered coupling of the spin states to the cube of the lattice displacement and proceeding by the path integral method and order parameter expansion, we indeed observe first order phase transition in the model. We have also investigated a two phonon model to satisfactorily explain the observed behaviour in the spin-state transition systems. In this model, the spin-states are coupled to a breathing mode and an optical mode. The coupling to the optical mode mixes the two spin-states, while coupling to the breathing mode is linear in displacement and without mixing. Preliminary results show that this model can exhibit a phase transition and explain the observed jumps in spin-state populations, in addition to explaining non-zero population of the high-spin state at absolute zero. These results form the contents of Chapter III.

CHAPTER I

MONTE CARLO SIMULATION OF ISING CHAINS WITH PHASE TRANSITIONS

I.1 Introduction

One-dimensional systems are of considerable interest in the study of phase transitions as they are often amenable to rigorous mathematical treatment. Gürsey[1] first showed that a one-dimensional gas of molecules interacting via a short-range potential with negligible interaction across molecules (i.e. only nearest-neighbour interactions are of importance) does not undergo a phase transition. The system, however, behaves like a perfect gas at high-temperatures and like a linear crystal near absolute zero*, for an attractive potential, though the partition function is analytic through out. A similar conclusion has been arrived at for a one-dimensional system of spins represented by a

*This is because the model is classical. In a quantum-mechanical system, zero-point motions preclude the possibility of ordering at 0 K.

Heisenberg Hamiltonian, in the nearest-neighbour approximation. It is most straightforward to demonstrate the absence of a phase transition in a one-dimensional spin-1/2 Ising model with nearest-neighbour interaction.[2] For the sake of simplicity, let us consider the interaction to be ferromagnetic. At absolute zero, the chain is completely ordered with all spins pointing in the same direction. The existing long-range order[3] can be destroyed completely by introducing a single break. The free energy change in introducing a single break is,

$$\Delta F = 2J - k_B T \ln N \qquad (I.1.1)$$

The first term is due to the increase in internal energy as a pair of spins gets alligned anti-parallel. The second term is due to the increase in entropy since the break can be introduced at any of the N sites. In the thermodynamic limit since $N \to \infty$, we notice that a break can always be introduced at any temperature above absolute zero. Thus, there can be no long-range order in the system at any non-zero temperature thereby ruling out a phase transition.

Montroll[4] has shown that for an Ising chain to undergo a phase transition, it is essential that the highest eigen-value of the corresponding transfer matrix be degenerate. Since the transfer matrix will always have

all positive elements we can apply Frobenius[5] theorem (to see whether the highest eigen value is degenerate). The theorem states that the highest eigen value of any matrix of finite order with all positive elements is always nondegenerate. The order of the transfer matrix is finite for interactions of finite-range (in fact the order is $2^n \times 2^n$ in the presence of a field where n implies that the interaction up to nth-neighbour is non zero). Hence one-dimensional systems cannot undergo phase transitions if the range of interaction is finite. Dobson[6] calculated partition functions for one-dimensional chains interacting up to the 7th-neighbour using interaction potentials of different forms some of which in the infinite-range lead to a phase transition while others do not. Dobson's calculations, however, failed to show either a phase transition or any significant difference between the two classes of potentials, thus rendering support to Montroll's ideas.

The partition function of a one-dimensional Ising model with infinite-range interactions was first computed by Kac[7] for the potential of the following form:
$V(x) = +\infty$ for $0 \leq x < \delta$, $V(x) = -\alpha \exp(-\gamma x)$ for $x \geq \delta$
This form of the potential is now known as Kac potential. Kac's result showed no phase transition for finite non-zero γ. Baker[8] computed the partition function in the limit $\gamma \to 0$

or $e^{-\gamma} \to 1$. There were two different situations: (i) $\lim e^{-\gamma} \to 1$ and $\lim e^{-N\gamma} \to 0$ as $N \to \infty$; (ii) $\lim e^{-\gamma} \to 1$ and $\lim e^{-N\gamma} \to 1$ as $N \to \infty$. In case (i), Baker observed a second order phase transition while results of case (ii) were equivalent to the Bragg-Williams approximation.[9] Kac, Uhlenbeck and Hemmer[10] determined the partition function exactly in the thermodynamic limit for the Kac potential and showed that when the range of attractive force goes to infinity (with strength becoming porportionately weaker), a phase transition occurs.

For an Ising chain with infinite-range interaction the Hamiltonian is given by,

$$H = -\sum_{i>j}^{*} J(i-j)\, S_i S_j, \quad j \varepsilon (-\infty, \infty), \; J(n) \geq 0 \qquad (I.1.2)$$

We can see that there can be no phase transition if M_o defined by,

$$M_o = \sum_{n=1}^{\infty} J(n) \qquad (I.1.3)$$

is infinite, simply because there is an infinite energy gap between an ordered ground state and all other states.

On the other hand, we have already discussed the case in which only finite number of $J(n)$ are non-zero and arrived at the conclusion that there can be no phase transition and that the system is disordered at all non-zero temperatures. It has been proved that the above system

is disordered at all finite temperatures and therefore there is no phase transition, provided that M_1 defined by

$$M_1 = \sum_{n=1}^{\infty} n\, J(n) \quad , \qquad (I.1.4)$$

is finite. This is intuitively clear as $2M_1$ is the energy required to have a single break in the completely ordered phase. Finite M_1 implies that breaks in ordering must appear with non-zero density along the chain at temperatures above zero and consequently no long-range order can be expected. Kac and Thompson,[11] after studying some particular examples, conjectured that the above system with finite M_o and infinite M_1 has a phase transition above absolute zero. This is satisfied if and only if $J(n)$ has the form $n^{-\alpha}$ with $1 < \alpha \leq 2$. The existence of a phase transition for the above potential for $1 < \alpha < 2$ has been proved by Dyson;[11a] for $\alpha = 2$ it is believed that there is no phase transition.

So far, we have stated that in one-dimension, a phase transition can occur only if the interaction potential has an infinite-range. This is true as long as we restrict ourselves to a pairwise interaction potential or a many body interaction potential to a finite order. Fisher[12] has exactly solved a one-dimensional model in which there is many body interaction to an infinite order though the range of the interaction potential is finite.

He has shown that if the many body interaction potential ϕ_s (s refers to the number of particles interacting) decays slower than s^{-2}, the system exhibits a phase transition. However, here one can argue that the role of infinite-range interaction is taken over by the infinite-order many body interaction.

Ising systems of interest to us are one-dimensional systems in which both short-range and long-range interactions are operating. A system with short-range and long-range interaction was first studied by Baker[13] in higher dimensionality. In one-dimension, Suzuki[14] was the first to study systems in which both short- and long-range interactions were present. Suzuki's Hamiltonian is given by,

$$H = -\sum J\,(S_i^x S_{i+1}^x + S_i^y S_{i+1}^y) - J_1 \sum_{i,j} S_i^z S_j^z - mH \sum_i S_i^z \qquad (I.1.5)$$

As we can see, in the above Hamiltonian, the short-range interaction is between the transverse components of the spin and the long-range interaction is represented by an infinite-range equivalent neighbour interaction term first studied by Temperley.[15] Another point to note is that the short-range and long-range interaction constants are of the same sign. Suzuki solved this model exactly and showed the existence of a phase transition. Anderson, Yuval and

Hamann[16] have studied a one-dimensional Ising system with competing short-range and long-range interactions. Their long-range interaction term was ferromagnetic and decayed as r^{-2}. They showed that two phase transitions exist in the system for strong nearest-neighbour antiferromagnetic interaction coupled with infinite-range interaction. However, approximations in their theory break down for the short-range interaction values considered by them. Nagle[17] has considered the same system with equivalent neighbour interaction in place of the r^{-2} interaction of Anderson et al. This system showed interesting phase behaviour although there was only a single transition in zero field. Theumann and Høye[18] extended the short-range interaction to second-neighbour and used the Kac potential in the limit $\gamma \to 0$ for the infinite-range ferromagnetic term. They observed that for a certain range of values of the interaction strengths the system showed as many as four first-order phase transitions at zero temperature.

In the present study, we have carried out a Monte Carlo simulation of the models of Nagle and Theumann and Høye, as a function of temperature, in the different regions of their phase diagrams, in order to understand the changes in spin ordering accompanying phase transitions. We shall discuss these two models in some detail in the next section. This study was also prompted to some extent

by our interest in long period polytypes (discussed in Chapter II of the thesis) which can be treated as a spin-1/2 Ising chain with different spin orderings.

1.2 Ising Models of Nagle and Theumann and Høye

Nagle[17] studied the competing interaction model, to see whether such an Ising chain exhibited metamagnetism, i.e., to see whether there exist two critical temperatures - a lower critical temperature at which the chain becomes ferromagnetic from a lower temperature antiferromagnetic phase and a higher critical temperature at which the ferromagnetism vanishes. His reasoning was based on the fact that Ising chains with an infinite-range interaction of the form $r^{-1-\sigma}$ show a decreasing T_c as σ increases, provided the total interaction strength is kept constant. This implies that longer range interactions are more effective at higher temperatures. Thus, an Ising chain with long-range ferromagnetic interaction and short-range antiferromagnetic interaction, at low temperatures, is expected to be in an antiferromagnetic state. As the temperature is increased, the longer range ferromagnetic interaction takes over and the chain becomes ferromagnetic from an antiferromagnetic state at a lower critical temperature. This ferromagnetism vanishes at an upper critical temperature.

Nagle's Hamiltonian is given by,

$$H = -J_{Sr} \sum_{i=1}^{N} \mu_i \mu_{i+1} - \frac{J_{lr}}{N} \sum_{j,i=1}^{N} \mu_i \mu_j - H \sum_{i=1}^{N} \mu_i ,$$

$$J_{Sr} < 0, \; J_{lr} > 0. \qquad \text{(I.2.1)}$$

The free energy expression corresponding to this Hamiltonian was exactly derived by Nagle. The above Hamiltonian without the long-range part was considered and the free energy expression corresponding to this (Nagle's Hamiltonian without the long-range part) is obtained as a function of temperature and the magnetic field, H_o. A Legendre transformation[19] was effected to transform the variables in the free energy expression from H_o and T to M and T. The contribution to free energy from the long-range part was calculated to be $-J_{lr}M^2$. The free energy expression corresponding to Nagle's Hamiltonian as a function of M and T is thus obtained. To locate the critical points, free energy was expanded in a power series in M:

$$A\,(M,T) = a_o(T) + a_2(T)\, M^2 + a_4(T)\, M^4 + \ldots \text{(I.2.2)}$$

Expression for a_o, a_2 etc. are known exactly as we know the free energy expression. The critical points are given by the conditions,[20]

$$a_2\,(T_c) = 0, \quad a_4\,(T_c) > 0. \qquad \text{(I.2.3)}$$

Both the conditions are satisfied for $-J_{lr}/J_{sr} > R \approx 3.1532$ and one finds a classical transition. When $-J_{lr}/J_{sr} < R$, we can define a temperature T^* at which $a_2(T^*)=0$ but $a_4(T^*) < 0$ so at a higher temperature T_1, the M=0 state becomes unstable and a first-order transition results in zero field. At $-J_{lr}/J_{sr}=R$ there is a confluence point and the critical exponents are determined for this point. The model also exhibits a first order transition in a magnetic field.

Stell and Hemmer[21] studied the analogous linear gas - with a hard core, a short-range repulsive interaction and an infinite-range attractive interaction - and arrived at similar results. Nagle and Bonner[22] studied Nagle's model with an additional staggered field and obtained phase diagrams in the space of staggered and direct fields and interaction strengths. We shall not discuss this model any further since it is not relevant to the present study.

Theumann and Høye[18] extended the range of short-range interactions up to second neighbour and studied the following Hamiltonian:

$$H = -J \sum_{i=1}^{N} \mu_i \mu_{i+1} - K \sum_{i=1}^{N} \mu_i \mu_{i+2} - \sum_{i>j=1}^{N} \phi(i-j) \mu_i \mu_j - H \sum_{i=1}^{N} \mu_i \qquad (I.2.4)$$

$$\mu_i = \pm 1, \; J < 0, \; K < 0$$

and $$\phi(j) = a\gamma \, e^{-\gamma|j|}, \; a > 0. \qquad (I.2.5)$$

The long-range part in the limit $\gamma \to 0$ is equivalent to the long-range part of Nagle. The free energy of this model was exactly obtained by using the magnetic analogue of Lebowitz-Penrose solution[23] for systems with long-range and short-range interactions. Lebowitz-Penrose solution when applied to a magnetic system, for non-negative $\phi(j)$ in the limit $\gamma \to 0$, gives the exact free energy, $A(M,T)$, from the expression.

$$A(M,T) = CE\ [A_s(M,T) - a\ M^2], \qquad (I.2.6)$$

$$a = \frac{1}{2} \sum_{i=-\infty}^{\infty} \phi(i) \qquad (I.2.7)$$

where CE stands for convex envelope and $A_s(M,T)$ is the free energy of the system with the long-range part being zero identically. $A_s(M,T)$ is obtained by calculating the partition function of the corresponding Hamiltonian, along the lines of Dobson[6] and later performing a Legendre transformation to the variables (M,T). The critical points are determined by solving for the isotherms. The isotherms are given by the equation

$$H = MC\ [H_o - 2aM], \qquad (I.2.8)$$

where MC stands for Maxwell construct[9,24] and H_o is the isotherm of the system in the absence of long-range interactions.

The zero temperature phase diagram of Theumann and Høye as a function of interaction strengths is shown in Fig. I.1. We see that in some regions the system shows as many as four first order transitions. This was also observed by Stell and Hemmer[25] in the case of an analogous linear gas and four different types of ordering were observed at zero temperature. Theumann and Høye extended the phase diagram to non-zero temperatures without significant changes in the regions. They further determined the critical temperatures of the system for some given sets of interactions and observed many phase transitions in both zero and non-zero fields. Another interesting feature of this model (of relevance to polytypes) is the coexistence of as many as five phases for a given set of interactions. This seemingly violates Gibb's phase rule as the system in question is a single component system. However, since the variables in the phase diagram are not strictly thermodynamic, there is really no violation of the phase rule.

Because of our interest in polytypism and its relation to Ising chains (for details, see Chapter II), we have carried out a Monte Carlo simulation on these Ising chains. We have attempted to find out the changes in the ordering of spins, as a function of temperature in each region of the phase diagram of Theumann and Høye. Monte Carlo simulation was decided upon since this method in addition to giving

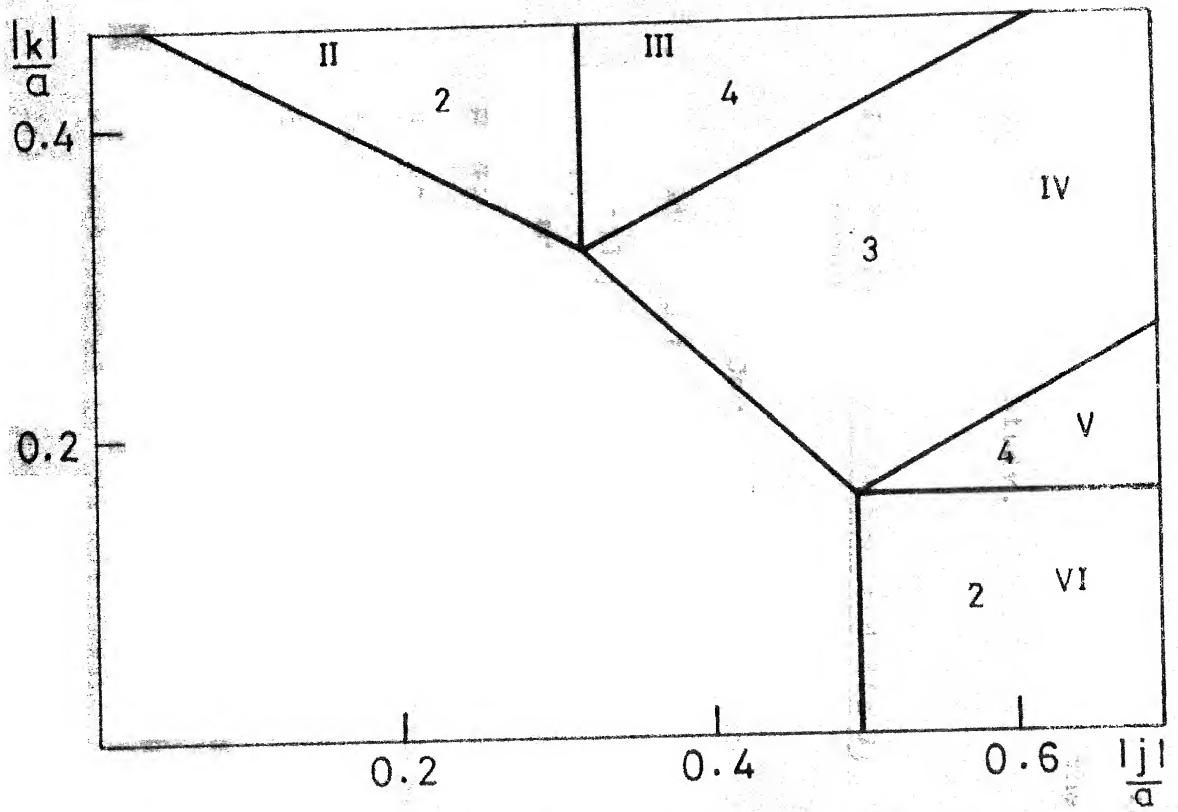

Phase diagram of Theumann and Høye. j, k and a refer to the nearest-neighbour, next-nearest-neighbour and infinite-range interaction strengths respectively. Roman numerals define the division of the diagram into regions. Arabic numbers give the number of phase transitions in the respective region, at 0 K.

thermodynamic properties of the system, allows us to take a direct look at any of the systems of the canonical ensemble. A brief introduction to the Monte Carlo method and its application to estimation of thermodynamic properties is given in the next section. This is followed by a description of the programs and their testing, employed in the present study.

I.3 Monte Carlo Method and its Applications to Thermodynamics

Monte Carlo method[26-28] involves the use of random sampling to approximate the solution of mathematical or physical problems. Mathematical problems solved by Monte Carlo method are mostly confined to the evaluation of multi-dimensional integrals. Other mathematical problems solved by Monte Carlo method (although the method is much inferior compared to the standard numerical methods) are, determination of eigen values and eigen functions of matrices, solutions of differential and integral equations, inversion of matrices and such others. Monte Carlo method is most useful in the evaluation of multi-dimensional integrals, where the conventional numerical methods become unmanageable as the dimensionality of the integral becomes large. The error in the Monte Carlo method applied to mathematical problems is proportional to $\sigma^2/\sqrt{N}$, where σ^2

is the sampling variance of the estimator and N is the sample size. Thus, error in Monte Carlo estimates can be reduced by either increasing the sample size or by decreasing the variance. The former method of increasing accuracy is often not practical as a reduction in error by ten-fold demands a hundred-fold increase in sample size or correspondingly a hundred-fold increase in computer time. Efficient Monte Carlo methods should therefore depend more on reducing the variance of the estimator. In recent times, a combination of fast computers and good variance reduction techniques have made accurate estimation of multi-dimensional integrals by Monte Carlo method plausible.

Several other mathematical problems mentioned earlier have been solved by devising ingenious stochastic processes such that the distribution of the so devised stochastic process or some set of its parameters satisfy the mathematical equation in question. One of the earliest problems solved was the Buffon needle problem for estimating π - the value of π was obtained by determining the fraction of times a needle of given length, when dropped randomly between a pair of parallel lines separated by a known distance, intersected one of the lines.

Direct Monte Carlo simulation has been used to study: (i) physical problem of a complex nature where no analytical formulation is practicable, and (ii) to gain insight into

the physical processes taking place in a system. Direct simulation involves playing a game of chance in the system, simulated say on a computer, with the rules of the game being such that the actual deterministic and random features of the physical process are step by step exactly imitated by the game. Relevant parameters of the physical system can be obtained fairly accurately when the game is played for a sufficient length of time. Large number of problems from diverse fields are being solved by direct Monte Carlo simulation examples being neutron transport problems and nuclear reactor criticality,[29] quality and reliability of complsx systems, mass servicing systems, percolation problems,[26] chain conformation, molecular weight distributions and polymerization rates of polymers[30] and so on.

Any Monte Carlo calculation involves the generation of random numbers belonging to a specified distribution. The random numbers so generated should satisfy appropriate statistical tests such as frequency tests, moments tests, chi-squared test etc. This is important since errors in the estimates can be reduced by using a well distributed set of random numbers. Furthermore, the time taken for each random number generation must be as small as possible and the random number sequence so generated must have long periodicity. There are several algorithms for fast generation of well distributed random numbers.[31,32] The

random number generation algorithm used in the present study as well as the results of statistical tests carried out on the first thirty thousand random numbers generated by using this algorithm are given in the Appendix at the end of this chapter.

Before considering the applications of Monte Carlo method to estimate thermodynamic properties, a brief review of Markov chains is in order.[33,34] An nth order Markov chain is one in which the probability of outcome of a particular trial depends on the previous n outcomes and none else (for n=0, we have independent outcomes for each trial and the process is known as Bernoulli trials). We shall be concerned only with first order Markov chains or simple Markov chains where probability of outcome of a particular trial is dependent on the outcome of the previous trial only. All possible outcomes of a Markov chain are said to form a state space. A Markov chain with a finite state space is known as a finite Markov chain. A Markov chain is completely described if the initial probability function $p_i^{(0)}$ ($p_i^{(0)}$ is the probability that the chain is in state i at time zero), the one-step transition probabilities $p_{ij}^{(1)}$ and the state space of the chain are given. A finite Markov chain is ergodic if there exist probabilities π_j such that $\lim_{n\to\infty} p_{ij}^{(n)} = \pi_j$ for all i and j. $p_{ij}^{(n)}$ is the probability of going from

state i to state j in exactly n steps. All states of the Markov chain belong to the same ergodic class, if there exists an n such that $p_{jk}^{(n)} > 0$ for all j and k. We have a a theorem governing the limiting behaviour of an ergodic Markov chain with all its states belonging to the same class by which we have

$$\text{(i)} \quad \pi_k > 0 \quad \text{and} \quad \sum_{k=1}^{S} \pi_k = 1 \qquad \text{(I.3.1)}$$

$$\text{(ii)} \quad \pi_k = \sum_{j=1}^{S} \pi_j \, p_{jk}, \; k = 1,2,\ldots S \qquad \text{(I.3.2)}$$

We shall use these results in arriving at a Monte Carlo scheme for the estimation of thermodynamic properties of a classical system.

Equilibrium statistical mechanics is concerned with averages of the type

$$\langle F \rangle = \sum_{i}^{\text{over all states}} e^{-\beta E_i} F_i \Big/ \sum_{i}^{\text{over all states}} e^{-\beta E_i}, \qquad \text{(I.3.3)}$$

where E_i is the energy of state i, F_i is the value of the variable F in state i and $\beta = \frac{1}{k_B T}$. This sum is reduced to an integration over configuration space for classical systems. We would however be concerned mostly with properties of the system which depend only on space coordinates. Hence the above sum would be reduced to an integration of the form,

$$\langle F \rangle = \int F(r)\, e^{-\beta U(r)}\, dr \,/ \int e^{-\beta U(r)}\, dr \qquad (I.3.4)$$

where $U(r)$ is the potential energy of interaction among the particles and r designates all the space variables of the system. Thus evaluation of average properties of the system reduces to an evaluation of multi-dimensional integrals. The exponential factor in the integrand implies that a significant part of the integral is concentrated in a very small region. Hence estimation of $\langle F \rangle$ appears at the outset to be just a straight-forward estimation of the multi-dimensional integral by an 'importance sampling' method in which the random variables are drawn from a distribution given by $e^{-\beta U_i} / \int e^{-\beta U(r)}\, dr$. This means that we should know the denominator to get the distribution function. Knowing the denominator is equivalent to solving the problem itself since it is proportional to the partition function of the system. We set out to estimate the thermodynamic properties by Monte Carlo method since determination of the partition function by other means is not possible. Now it appears that we have ended up in a vicious circle. A way out of this was devised by Metropolis, Rosenbluth, Rosenbluth, Teller and Teller.[35] They devised a Markov chain such that the ratio of the limiting probabilities of any two states of the chain is equal to the ratio of the equilibrium probabilities of the corresponding two states of the system:

$$\pi_i/\pi_j = e^{-(E_i-E_j)\beta} \qquad (I.3.5)$$

Here, π_i and π_j are the limiting probabilities of the states i and j of the Markov chain. Hence if the Markov chain is propagated for a sufficient length of time, the states of the Markov chain would be distributed with probabilities given by the equilibrium probabilities of the given system. Thermodynamic averages of the system can now be estimated as the average over all states of the Markov chain, taken over a large number of states, after the Markov chain has attained limiting behaviour. In this method, since only the ratios of the limiting probabilities of any two states need be known, the problem of evaluating the denominator in eq. (I.3.4) is overcome.

The Markov chain of Metropolis et al.[35] for a system under study is defined by initial probabilities taken to be the thermodynamic probabilities for the states of the system in equilibrium at T=0 or T= ∞ (completely ordered or completely disordered system). The one step probabilities for the chain to go from a state 'r' to state 's' is unity if the energies of the corresponding states of the system are such that $E_r \geq E_s$ otherwise it is given by $\exp[(E_r-E_s)\beta]$. The state space of the Markov chain is completely defined and the process of going from one state to other is such that all the states of the state space

are accessible from any state. These conditions ensure that corresponding to any two states 'r' and 's' of the canonical ensemble, we generate ν_r and ν_s systems, respectively, such that

$$\nu_r/\nu_s = e^{-(E_r-E_s)\beta} \qquad \text{(I.3.6)}$$

This is because the probability with which we pick a state 'r' to move to state 's' is equal to the probability with which we pick the state 's' to move to state 'r', i.e., $P_{rs} = P_{sr}$. Now, if $E_r \geq E_s$, the number of systems moving from state 'r' to state 's' is $\nu_r P_{rs}$ and the number of systems moving from state 's' to state 'r' is $\nu_s P_{rs} \exp[-(E_r-E_s)\beta]$. The net number of systems moving from state 's' to state 'r' is,

$$N_{s\to r} = \nu_s P_{rs} \cdot \exp[-(E_r-E_s)\beta] - \nu_r P_{rs} \qquad \text{(I.3.7)}$$

If $\nu_r/\nu_s < \exp(-E_r\beta)/\exp(-E_s\beta)$ on an average more systems move from 's' to 'r'. This coupled with the condition that all states should be attainable by the process enables the relation (I.3.5) to be satisfied.

The one step probabilities assumed by Metropolis et al.[35] to define the Markov chain is not unique. Wood and Parker[36] recognized that the Markov chain we are dealing with is an ergodic Markov chain with all its states belonging to the same class and used the relations (I.3.1)

and (I.3.2) to arrive at the conditions the one step probabilities of such a Markov chain should satisfy. By inspection, we see the conditions are normalization and microscopic reversibility, i.e.

$$\sum_{k=1}^{S} p_{kj}^{(1)} = 1 \text{ for all } j = 1,2,\ldots S \text{ and} \qquad \text{(I.3.8)}$$

$$\pi_j p_{jk} = \pi_k p_{kj}. \qquad \text{(I.3.9)}$$

In our case the limiting probability of the Markov chain should be proportional to the thermodynamic probability at equilibrium, $\pi_j = c \exp(-E_j\beta)$. Wood and Parker used the following one step probabilities to obtain Monte Carlo equation of state of interacting molecules

$$p_{jk} = A_{jk} \quad \text{for} \quad E_j \leq E_k$$

$$p_{jk} = A_{jk} \exp[-(E_j - E_k)\beta] \quad \text{for } E_j > E_k \qquad \text{(I.3.10)}$$

and $p_{jj} = 1 - \sum_{k \neq j} p_{jk}$.

Computation methods for Monte Carlo estimation of thermodynamic properties is straight forward. The system is created on the computer* with the given initial probabilities. The location (inside the system) at which a change is to take place is selected by a random process. The nature of the change at the location may be probabilistic

*The present study was carried out on an IBM 7044/1401 computer system of this Institute.

or deterministic, depending on the problem. In the former case the nature of the change is decided with the help of a random number drawn from an appropriate distribution. Probability for the change is computed from the one step probability functions. If the probability is unity, the change is carried out. If the probability is less than unity, a random number between 0 and 1 is generated and the change is effected if the random number is less than the probability, if not, the original state is retained. After repeating this process sufficient number of times, the effect of initial configuration vanishes. From this point onwards, in the calculation, exact thermodynamic variable corresponding to the state of the system is calculated at each step. The ensemble average is taken to be the average of the thermodynamic properties over all the Monte Carlo cycles performed after we started computing the thermodynamic variable. Unsuccessful tries should also be included in the averaging process as not to include them is equivalent to removing from the ensemble those systems which tried to move but were forbidden.

In all Monte Carlo calculations, it is important to know, (i) the statistical error[37,38] involved in the method, and (ii) the number of Monte Carlo steps required for the effect of initial configuration to vanish,[37] thereby bringing

the system to thermodynamic equilibrium at the specified values of the external variables (temperature, magnetic field etc.). To estimate these, let us start with the relations defining the relaxation functions $\phi_{\delta A \delta B}(t)$ and $\phi_{\delta A}^{\Delta e}(t)$:

$$\phi_{\delta A \delta B}(t) = \{\langle A(0)\, B(t)\rangle - \langle A\rangle\langle B\rangle\} / \{\langle AB\rangle - \langle A\rangle\langle B\rangle\} \quad \text{(I.3.11)}$$

and $$\phi_{\delta A}^{\Delta e}(t) = \{\langle A(t)\rangle_{e'} - \langle A(\infty)\rangle_{e'}\} / \{\langle A(0)\rangle_{e'} - \langle A(\infty)\rangle_{e'}\}, \quad \text{(I.3.12)}$$

A and B are the variables of interest. $\phi_{\delta A \delta B}$ is the equilibrium relaxation function and gives the dynamics of fluctuations around equilibrium. $\phi_{\delta A}^{\Delta e}(t)$ is the non-equilibrium relaxation function and gives the dynamics of change in A as the external variable e is changed from e' for $t < 0$ to $e' + \Delta e$ at $t=0$. The averages in the expression are calculated over the states for which the external variable is e'. Using these functions two relaxation times, $\tau_{\delta A \delta B}$ and $\tau_{\delta A}^{\Delta e}$, are defined by the relations

$$\tau_{\delta A \delta B} = \int \phi_{\delta A \delta B}(t)\, dt \quad \text{(I.3.13)}$$

and $$\tau_{\delta A}^{\Delta e} = \int \phi_{\delta A}^{\Delta e}(t)\, dt. \quad \text{(I.3.14)}$$

The number of Monte Carlo steps, n, that should be excluded to get rid of the effect of initial configuration, after

the change Δe is effected, must satisfy $\frac{n}{N} >> \tau_{\delta A}^{\Delta e}$ where N is the size of the system. The expected statistical error $\delta \bar{A}$ of an estimate $\bar{A}$, after m Monte Carlo steps is

$$(\delta \bar{A})^2 \sim \frac{1}{m} [\langle A^2 \rangle - \langle A \rangle^2] \ (1 + 2\tau_{\delta A \delta A}), \ \frac{m}{N} >> \tau_{\delta A \delta A}.$$

The quantities $\tau_{\delta A}^{\Delta e}$ and $\tau_{\delta A \delta A}$ can be estimated a priori from the theory of stochastic model systems.

In the present study, instead of making these estimates, we have relied on comparison with exact results for testing the accuracy of the method. Such comparisons have been made by earlier workers[38,39] in other statistical mechanical problems and Monte Carlo method has been shown to be quite accurate. The main sources of error in the Monte Carlo method are due to finite sample size, finite size of the system and systematic errors. Finite sample size leads to (a) a statistical error, proportional to thermodynamic fluctuations, which is always present even if the sample is drawn from a true ensemble with perfect randomness, and (b) an error present due to correlation among states closely succeeding one another. The error from (b) has the effect of marginally reducing the efficiency of the Monte Carlo method. Errors due to finite size of the system can be eliminated using theories which provide information about the finite size effects. In a study of phase transitions finite size has the effect of smoothening out the variations of appropriate thermodynamic quantities,

which otherwise should show sharp breaks at the transition points. Systematic errors can be eliminated by using good random variables in the calculation and by proper debugging of the programs.

Monte Carlo method has been applied in statistical mechanics to study a variety of problems such as order-disorder transformation in b.c.c. systems,[40] phase transition of three and two-dimensional Ising system with a variety of interactions,[41-43] equations of states of molecules interacting with different potentials[35,36,44] and so on.

The method of Metropolis et al.[35] is applicable only to obtain canonical ensemble averages of classical systems. A study of phase transitions by canonical ensemble method requires a fairly large system. This is not a problem in one-dimension. However in 2 and 3-dimensions the system size required in some cases may become unmanageably large. We can overcome this difficulty if we can obtain thermodynamic averages of a grand canonical ensemble by Monte Carlo method. The system size required to study a phase transition by dealing with a grand canonical ensemble is quite small. Filinov and Norman[45] have given a method by which we can generate a Markov chain with state space consisting of the states of a grand canonical ensemble.

To deal with quantum statistical mechanics by the Monte Carlo method, we have to make modifications of the

method of Metropolis et al.[35] The problem arises since in quantum statistical mechanics the partition function cannot be represented by a configurational integral and we need to know the eigen values of the system, which is often difficult to obtain. Handscomb[46] and Fosdick[47] have given methods for estimating thermodynamic properties of the system by a Monte Carlo calculation. Handscomb's method involves a partitioning of the Hamiltonian and expressing the thermodynamic averages as a sum of traces taken over different parts of the Hamiltonian and estimating this sum by a method similar to Metropolic method, provided the traces appearing in the sum are easily calculated. Fosdick[47] writes the partition function as a Wiener integral and represents this Wiener integral by an n-fold Riemann integral, the evaluation of the latter is done by standard Monte Carlo methods.

Monte Carlo method has been applied for the extraction of critical exponents of a system.[48] In this method, the transformation of interaction parameters, defining the model, under a change of length scale is obtained by Monte Carlo method. The average lifetimes of a single spin in up and down state and the average lifetimes of a block of spins in up and down states of the block, are estimated by Monte Carlo method. These give the transformation of parameters under a change of length scale, which in turn is related to the critical exponents of the system.

I.4 Programs and Testing

In the present study, we have simulated an Ising chain with one thousand spins. The up and down states of a spin are designated by the numbers one and two. To begin with, the interaction parameters, the temperature and a variable which decides the initial state of the chain are read in. If the initial state to be generated corresponds to a completely ordered chain, number 1 is assigned to all the sites. If the initial state to be generated happens to be a disordered state, we pick the first site, call a random number between 0 and 1 and assign 1 to the site if the random number is less than 0.5 and assign 2 otherwise. On repeating this with all the sites we get the chain in a disordered state. The initial energy of the chain is computed in two parts viz., (i) the contribution from short-range interactions and (ii) the contribution from the long-range part. The contribution from (i) is calculated by starting from the first site and evaluating its interaction energy by finding out the state of the spins at the first and second-neighbour positions. This is repeated for all the thousand sites and the total short-range interaction energy is obtained by summing up all these contributions. A cyclic boundary condition is used in all the calculations. The long-range contribution to initial energy is given by $J_{lr} M^2$ where J_{lr} is the long-range

interaction strength and M is the magnetization of the chain in the initial state. Magnetization is given by the number of '1 sites' minus the number of '2 sites'. In all our calculations we have used equivalent-neighbour interaction for the long-range part. The initial energy is the sum of contributions from (i) and (ii).

The chain which is now at T=0 or T=∞, depending on whether its state is ordered or disordered, has to be brought into equilibrium at the temperature at which we intend to calculate the thermodynamic properties. This is achieved by flipping the spins in the following way. We select a site at random with the help of a random integer between 0 and 1000. We calculate the change in energy of the chain, ΔE, when the spin at this site is flipped. ΔE is calculated as the sum of ΔE_{sr}, the change in short-range interaction energy of a segment of the chain before and after flipping the spin (the segment of the chain includes all the spins whose short-range interaction energies are affected by the spin flip) and ΔE_{lr}, the change in long-range interaction energy caused by the change in magnetization accompanying the spin flip. The spin is flipped if ΔE is negative or zero. If ΔE is positive, a random number between 0 and 1 is generated and compared with P given by $\exp(-\Delta E/T)$. If the random number is smaller than P the spin is flipped otherwise the original

state is retained. The total energy of the chain is changed by ΔE if the spin has been flipped otherwise the original value is left unchanged. The whole process is repeated starting from the selection of a random site. Depending upon the temperature, 3000 to 60000 tries are required to bring the chain to equilibrium. In equilibrium, the internal energy starts fluctuating around a mean and the test of having reached equilibrium lies in looking for fluctuations in the internal energy which is printed out at the end of every hundred or hundred and fifty spin flips.

Once having ensured that the system has reached equilibrium, we can start computing the thermodynamic properties. The thermodynamic properties computed are the internal energy, square of the internal energy, sublattice magnetizations and correlation function describing correlation of spins on different sites. To get these, the respective sums (formed by adding up the actual value of the quantities at the end of each Monte Carlo step including unsuccessful tries) are calculated. The averages are given by dividing these sums by the number of tries made after first computation of these quantities. The sublattice magnetizations are estimated assuming the existence of two sublattices viz. all the odd numbered sites forming one sublattice and all the even numbered

sites forming the other. The correlation function of the chain is initially calculated as,

$$g^{(i)}(k) = \sum_j \mu(i)_j \; \mu(i)_{j+k}, \quad k = 1, 2, \ldots 20 \qquad (I.4.1)$$

where (i) refers to the initial calculation. Subsequent calculations of g(k) involved making appropriate changes whenever a spin was flipped. Specific heat is given by fluctuations in internal energy by the relation

$$C_m \; \alpha \; \frac{1}{T^2} \; \{\langle E^2 \rangle - \langle E \rangle^2\} \qquad (I.4.2)$$

Since we have computed $\langle E^2 \rangle$ as well as $\langle E \rangle^2$, specific heat estimate can be made from our calculations. Uniform susceptibility is given by

$$\chi \; \alpha \; \frac{1}{T} \iint g(r,r')\, dr\, dr' \qquad (I.4.3)$$

where g(r,r') is the correlation function for magnetization, which we have estimated for our discrete chain and hence we can calculate susceptibility by our simulation. In fact, we have estimated staggered susceptibilities, assuming different orderings of the spin, by forming appropriate partial sums of the correlation function.

In all our calculations the number of tries required to reach equilibrium at any given temperature is read in at the beginning of the program. This is estimated, over all temperatures of interest, from trial runs on a purely anti-ferromagnetic chain with a disordered initial configuration.

An examination of the internal energy that is printed out at intervals of every hundred spin flips shows that the number of tries excluded from the averaging process is generally sufficient to remove the effect of initial configuration. Averages of thermodynamic properties are taken over sixty to seventy thousand tries. The time taken per Monte Carlo cycle was between 3 to 6 milliseconds, depending on the temperature. At the end of the Monte Carlo calculation, the energy of the chain is calculated ab initio and compared with the energy of the chain at the end of the Monte Carlo cycles. These two should agree to within the round off error and this forms one of the checks on the correctness of the calculation. Other checks of the program included tracking of all the variables involved in the calculation by printing them out as and when they appeared in the calculations.

Accuracy of the calculations is checked by performing the calculation on a nearest-neighbour antiferromagnetic Ising chain over the temperature range of interest. The exact thermodynamic properties can be easily evaluated from the partition function which can be determined easily. Fig. I.2 gives the Monte Carlo estimation of specific heats and internal energy as well as the exact specific heats and internal energy, over eighteen temperatures in the temperature region of interest. The agreement between

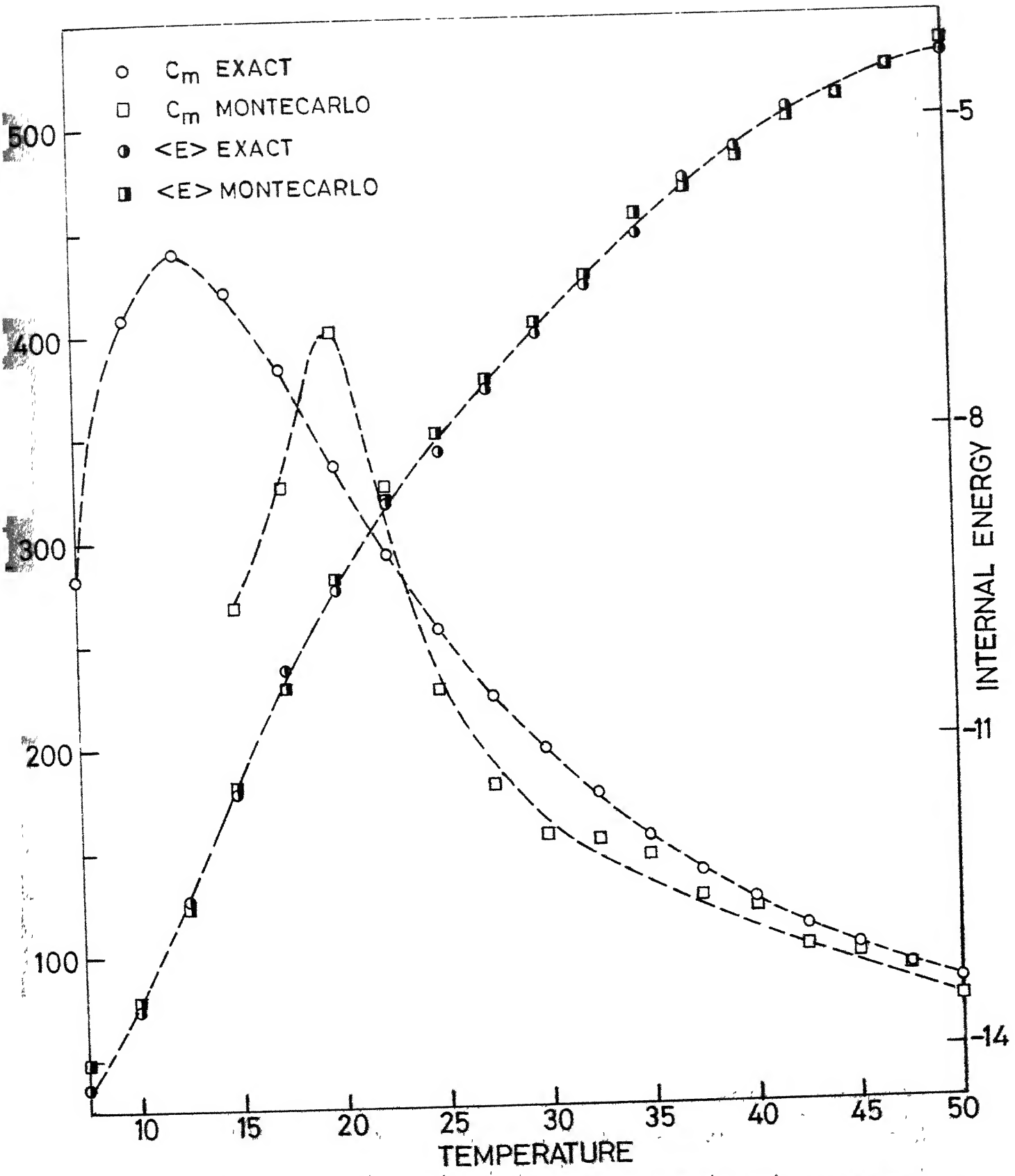

I.2. Specific heat and Internal energy vs temperature plots for a nearest-neighbour antiferromagnetic Ising chain. Nearest-neighbour interaction strength is 15.

Monte Carlo and exact values is good in the higher temperature region. But the peaks in the specific heat curves from the Monte Carlo method and the exact calculation do not appear at the same temperature. This could be due to the presence of large domains, in the Ising chain simulated in our calculations, at low temperatures. The specific heat estimates in the temperature region 0 to $T \simeq 2J/3k$ is not reliable because the number of breaks in the chain ordering are far in excess of the equilibrium number of breaks expected at that temperature. This cannot be got rid of as the number of Monte Carlo cycles required to remove a single break is rather large. This problem may be overcome by using different spin-flip mechanisms, which would make the chain ergodic at these temperatures also. However, from the work of Nagle and Theumann and Høye we know that this temperature region is not of interest. The sublattice magnetization computed in our calculations do not agree with the magnetization from the exact calculations for the same reason, viz. existence of domain structure. Fig. I.3 gives the correlation function of the antiferromagnetic chain at three different temperatures.

We have performed all our calculations by assuming an initially disordered state. In the case of nearest-neighbour antiferromagnetic chain we see that the results in the high temperature region do not depend upon the initial

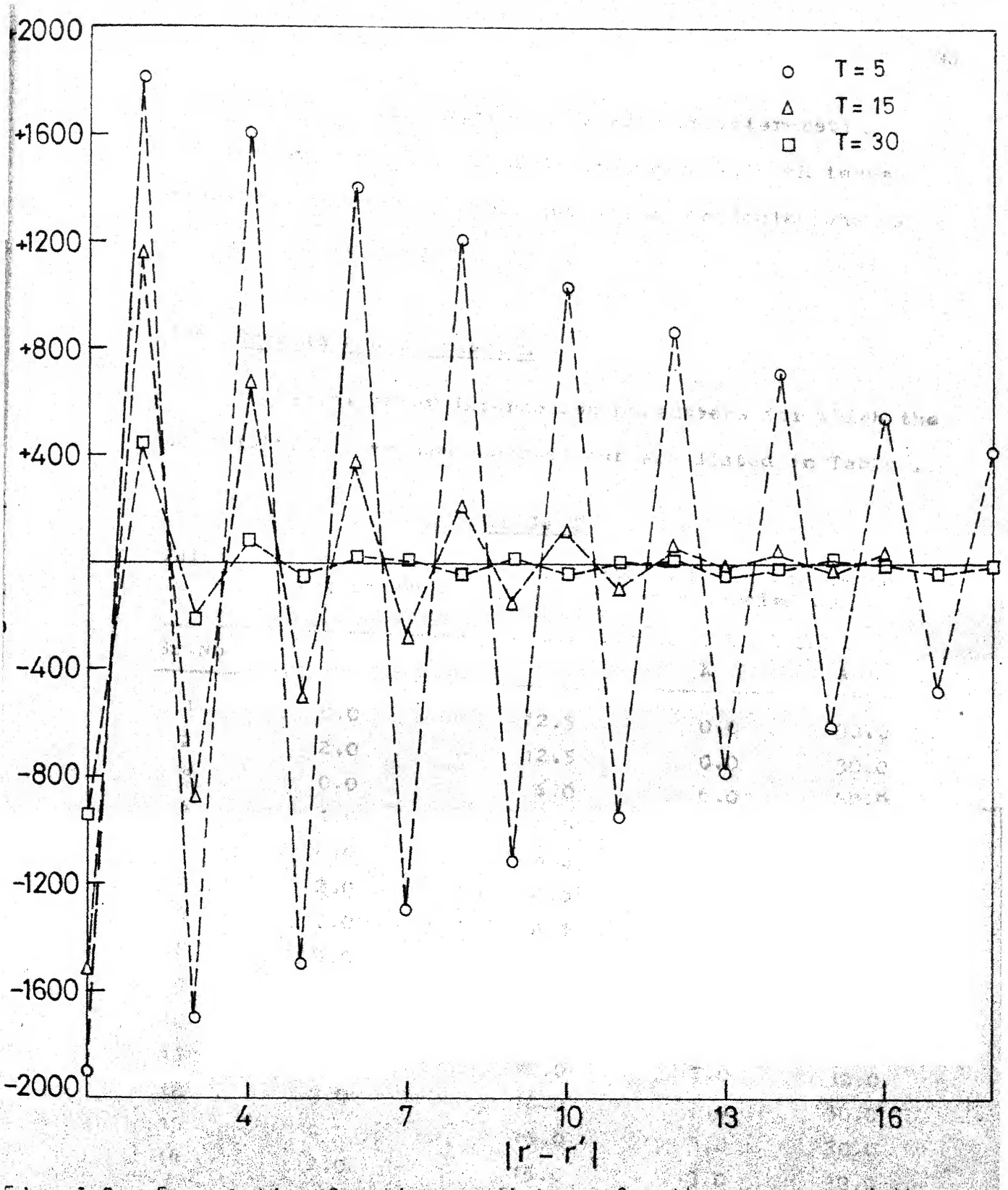

Fig. I.3. Correlation function vs distance for the nearest-neighbour antiferromagnetic Ising chain from Monte Carlo calculation, for three different temperatures.

state. Since our interest lies also in interpreting polytypism where the crystals are grown at high temperatures, we decided to carry out all our calculations using an initially disordered state.

I.5 Results and Discussion

The values of interaction parameters for which the calculations have been carried out are listed in Table I.1.

Table I

Values of interaction strengths and magnetic fields for which the present calculations were carried out.

Sr.No.	H	J	K	A
1	0.0	12.5	0.0	30.0
2	2.0	12.5	0.0	30.0
3	0.0	6.0	6.0	30.0
4	1.0	6.0	6.0	30.0
5	0.0	6.0	12.0	30.0
6	2.0	6.0	12.0	30.0
7	0.0	12.5	12.5	30.0
8	4.0	12.5	12.5	30.0
9	0.0	15.0	9.0	30.0
10	3.0	15.0	9.0	30.0
11	0.0	18.0	7.0	30.0
12	3.0	18.0	7.0	30.0
13	0.0	15.0	3.0	30.0
14	2.0	15.0	3.0	30.0

H = Magnetic field, J = Nearest neighbour interaction strength, K = Next nearest neighbour interaction strength and A/N = A/1000 = Equivalent neighbour interaction strength.

Calculations were performed both in zero field and in the presence of a field. The first two calculations correspond to Nagle's model and the rest are based on Theumann and Høye's model.

The values assumed by the interaction parameters in our study of Nagle's model in zero field correspond to those values for which a first order transition is predicted by Nagle. Our calculations do not show the occurrence of a first order phase transition in specific heat vs temperature plots (Fig. I.4) and the phase is essentially antiferromagnetic at all temperatures. However, in the presence of a field, we observe a first order phase transition from a low-temperature long-range ferromagnetic ordering to a high-temperature short-range antiferromagnetic ordering. We do not see the predicted first order phase transition in zero field apparently due to the fact that the system is in a metastable state below the critical temperature. The low-temperature phase in zero field that we observe is antiferromagnetic while the ground state internal energy is lower for a ferromagnetic phase. Even in our calculations in the presence of a field, the low-temperature phase is antiferromagnetic while once again the ferromagnetic phase is more stable at T=0. In fact,

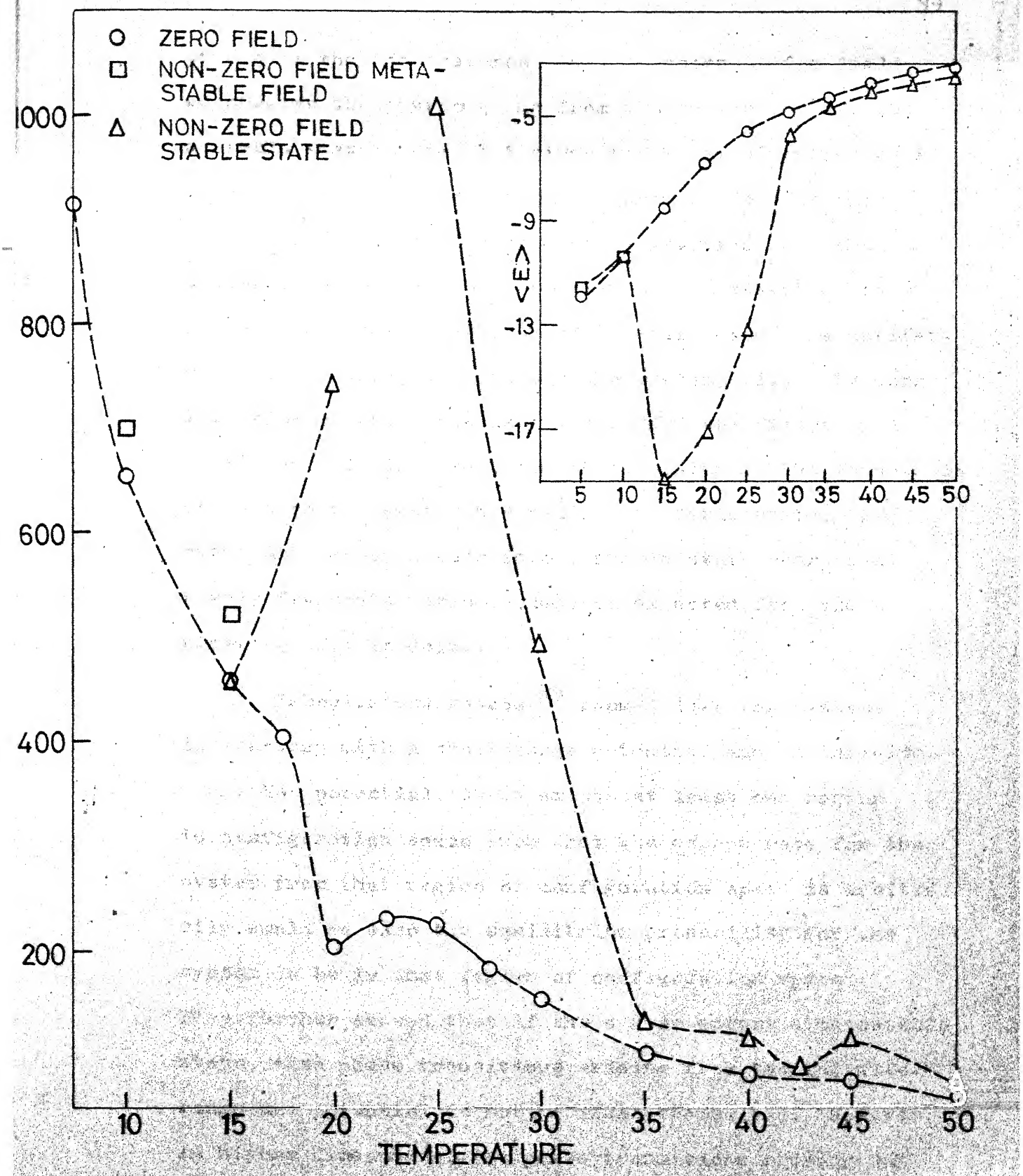

I.4. Specific heat vs temperature plot for Nagle's model in zero field and in the presence of a field. Inset-internal energy vs temperature plot for the same.

at one of the temperatures, in the presence of a field, we observe the system going from a metastable state to a stable state. Fig. I.5 gives the internal energy as a function of the number of Monte Carlo cycles for this case. The antiferromagnetic state satisfies all the criteria that should be satisfied by a metastable state: (i) presence of a single phase (in this case, the antiferromagnetic phase) through out the system, (ii) very long life-time of the state as evident from the figure, and (iii) very little likelihood of returning to the metastable state once the system has reached a stable state. The metastable state decays into a stable state over relatively few Monte Carlo cycles, as expected from the kinetics of this decay.

Lebowitz and Penrose[49] showed that for systems interacting with a short-range potential and an infinite-range Kac potential, there exists at least one region in configuration space such that the escape rate for the system from that region of configuration space is arbitrarily small as also the equilibrium probability for the system to be in that region of configuration space. They further showed that if the system enters a metastable state, then phase transitions arising from the infinite-range Kac potential do not manifest themselves. However, in higher dimensions, the phase transitions arising due

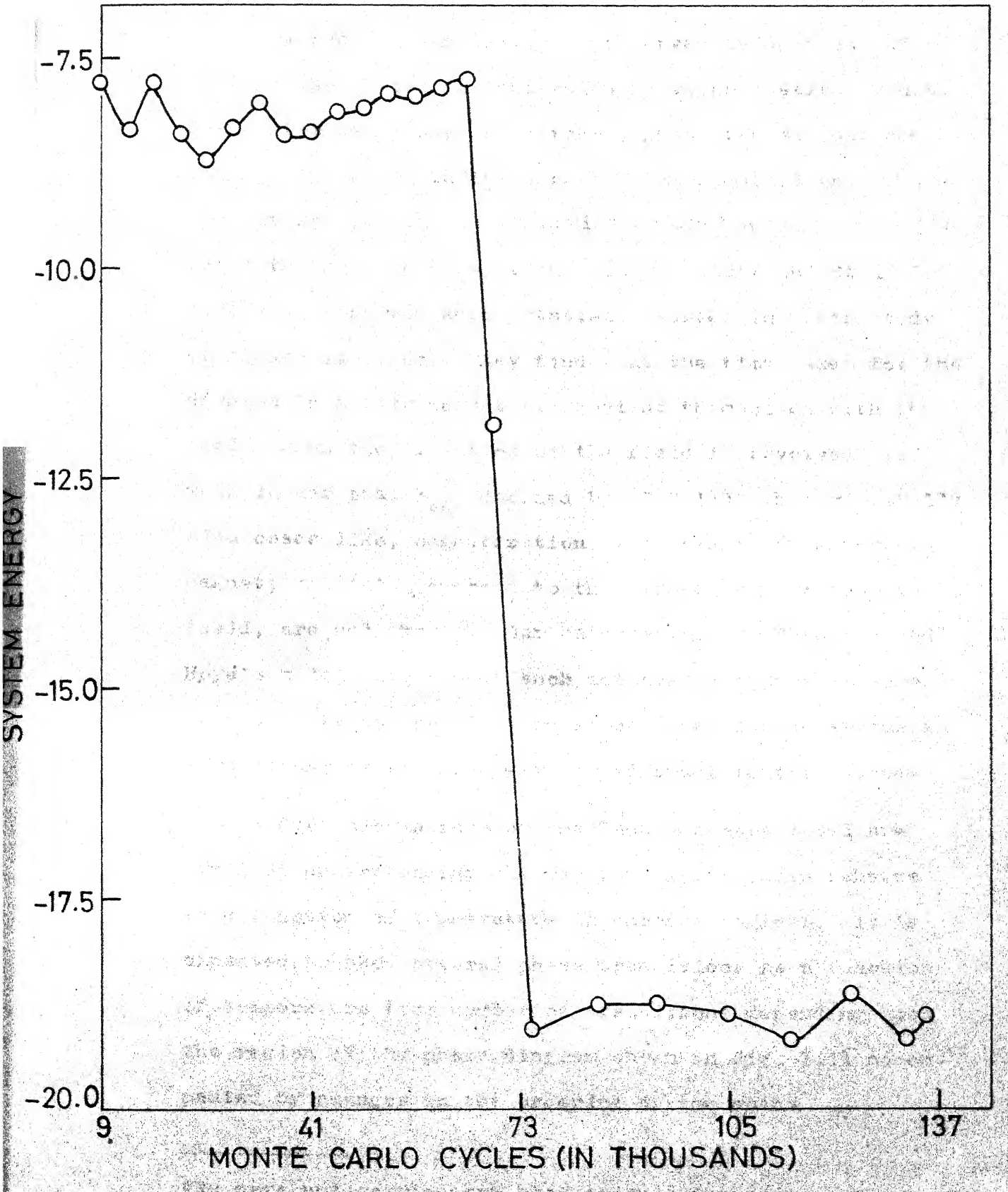

ig. I.5. Internal energy vs number of Monte Carlo cycles for Nagle's Ising chain in a field for T = 15.

to short-range potentials, are observed independent of whether the system has entered a metastable state or not. Our system being one-dimensional, phase transitions can occur only due to infinite-range Kac potential and in the present study, the system having entered a metastable state fails to show the phase transition. Binder and Stoll[50] have also observed such metastable states in their study of square lattices. They find that the time taken for the domains in a ferromagnet to reorient themselves with the field, when the direction of the field is reversed, is much longer than $\tau_{\delta A}^{\Delta e}$ defined by (I.3.14). Experimentally also cases like, magnetization of a domain (in a ferromagnet) remaining opposed to the direction of an applied field, are well known. Our calculations on Theumann and Høye's model also showed such metastable states in some regions. We can possibly avoid such metastable states in simulations by starting with a different initial state*.

Our calculations on the Theumann-Høye model are aimed at understanding the way this Ising chain behaves as a function of temperature in various regions. It is expected to show several phase transitions as a function of temperature (the number of transitions depending upon the region of the phase diagram shown in Fig. I.1) accompanied by changes in the ordering of the spins.

*We have not carried out this calculation since our interest lies mainly in the Theumann-Høye model.

In region I, the system is in a low-temperature ferromagnetic state. With increasing temperature, the chains show a first order transition with a large change in internal energy and a break in specific heat curve (Fig. I.6). The correlation function for various temperatures is shown in Fig. I.7. The high-temperature phase shows a short-range ordering of spins described by a unit cell with 4 lattice sites having the spin configuration ++++ . In the presence of a magnetic field, we observe a metastable state at low-temperatures in which the magnetization of the chain and the applied field are in opposite directions. At higher temperatures, the stable state of the chain is restored and this is observed to undergo a first order phase transition. Once again this first order phase transition is accompanied by breaks in internal energy and specific heat curves (Fig. I.6).

Our calculations in other regions do not show such sharp phase transitions as in region I. Instead, we observe small peaks in specific heat curves. The internal energy curves at these points are no longer smooth. The short-range ordering of the chain in each of these regions does not show any significant change with temperature although the low temperature ordering of the chain is quite different for different regions. For the values of interaction parameter falling in region II, the specific heat versus temperature

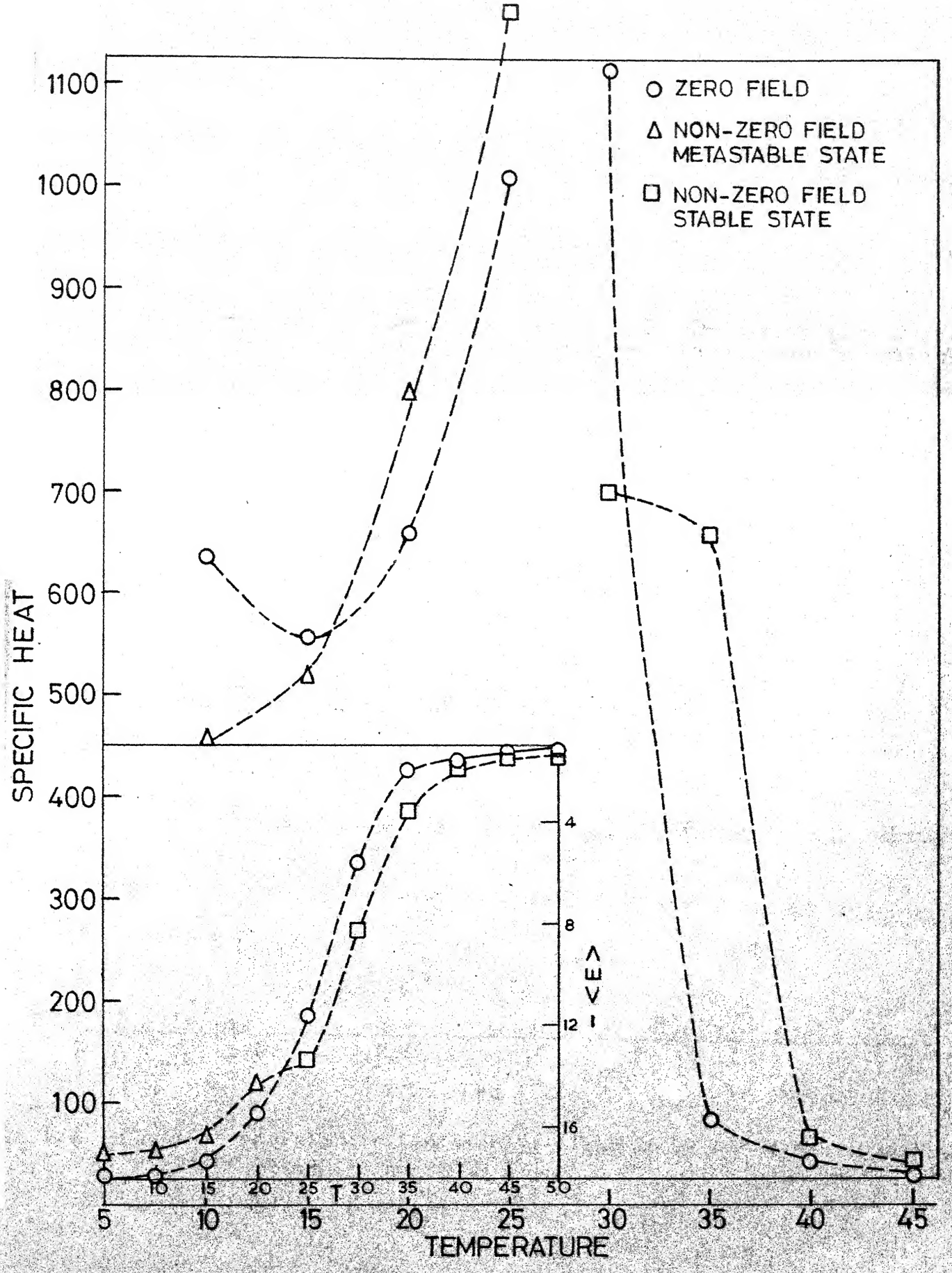

Fig. I.6. Specific heat vs temperature plot of Theumann-Høye model, in region I, in zero field and in the presence of a field. Inset shows internal energy vs temperature plot for the same.

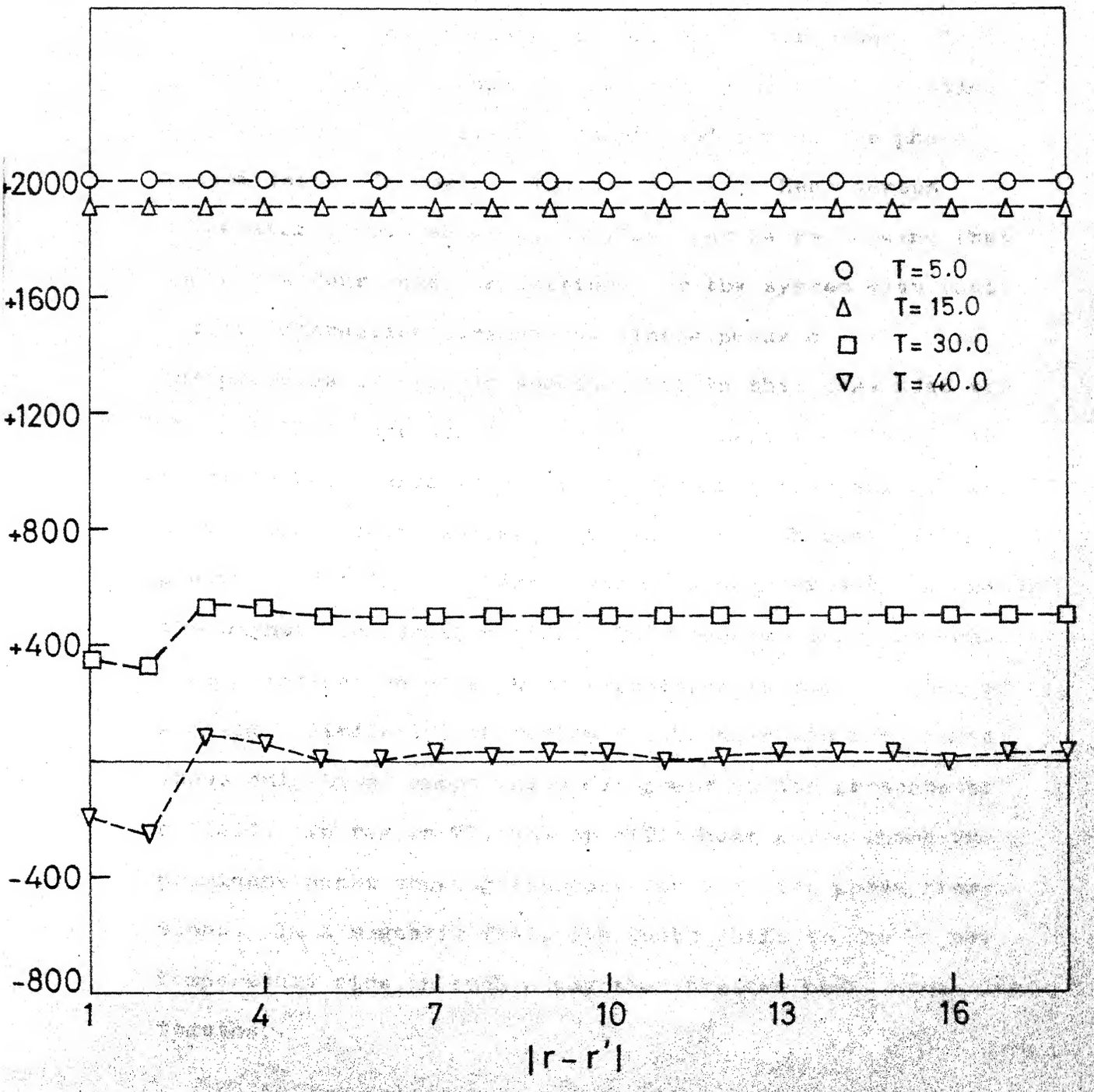

g. I.7. Plots of correlation function vs distance at different temperatures for region I in zero field.

curve (Fig. I.8) shows two peaks indicating the existence of two phase transitions of second or higher order. In the presence of a field, one of the peaks vanishes indicating that the magnetic field has suppressed one of the phase transitions. In region III, the specific heat versus temperature curve shows as many as four peaks showing that there are four phase transitions for the system with that set of interaction parameters. These peaks disappear in the presence of a field showing that in this case also the phase transitions are suppressed by a magnetic field. The specific heat curve in region IV does not have any clear peaks though there appear to be some broad humps. In the presence of a field, these humps disappear except the one in the higher temperature side. This becomes more pronounced giving indication of a phase transition in the presence of a field. Similarly, in region V, the specific heat curve shows only broad humps which disappear in the presence of a field. In region VI, the specific heat curve shows two prominent peaks showing the occurrence of two phase transitions. In a magnetic field the peaks shift to the higher temperature side in such a way that the two peaks come close together.

At low temperatures, the chain exhibits different kinds of ordering in the different regions. The ordering of spins in region II at low temperatures is described by a

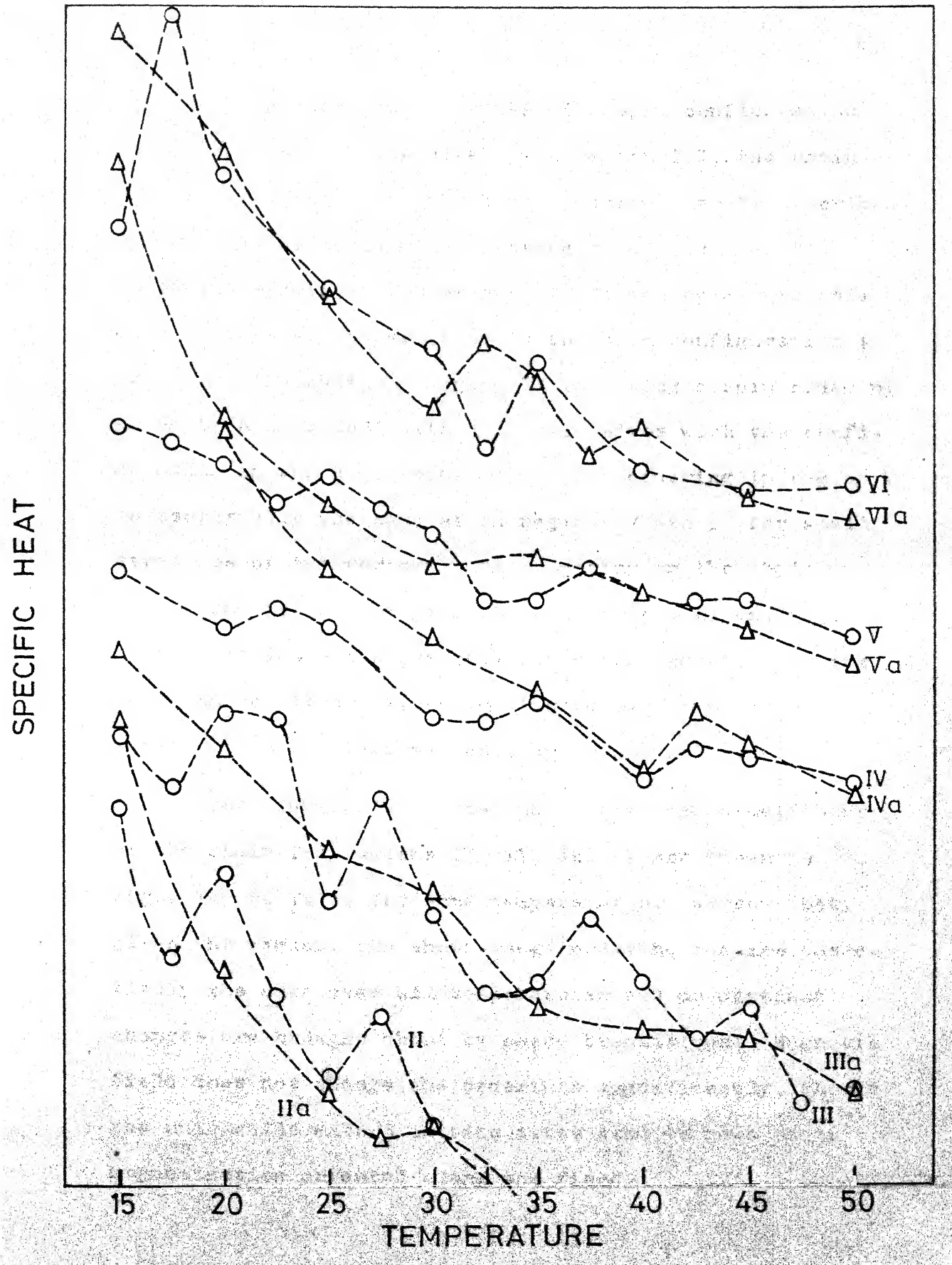

Fig. I.8. Specific heat vs temperature plots for Theumann-Høye model. Roman numerals refer to the region and 'a' implies presence of an applied field. Y-axis is to the same scale as in Fig. I.2.

unit cell of four lattice sites with spin configuration in the unit cell being ↑↑↑↓ . In region III, the chain has some segments over which the ordering can be described by the unit cell with four lattice sites and over the remaining segments, the ordering is given by a unit cell of 3 lattice sites per cell, in the spin configuration ↑↑↓ or ↑↓↑ . The chain in region IV is having a spin ordering given by a unit cell with 3 lattice sites with the configuration in the cell being ↑↓↑. The ordering in region V is essentially the same as in region IV except for small stretches of antiferromagnetic ordering in the chain. The ground state of region VI is described by unit cells with 3 lattice sites per cell (spin configuration in the cell can be either ↑↑↑ or ↓↑↓) extending over short stretches in an otherwise antiferromagnetic chain.

Correlation functions, up to eighteenth neighbour, of the chain for regions II, III and IV are shown in Figs. I.9 to I.11, for some temperatures. We see that, given the region, the short-range ordering remains essentially the same over all temperatures and no distinct changes are brought about by phase transitions. Magnetic field does not change the orderings significantly, though the unit cells with 3 lattice sites tend to have their magnetization oriented along the field.

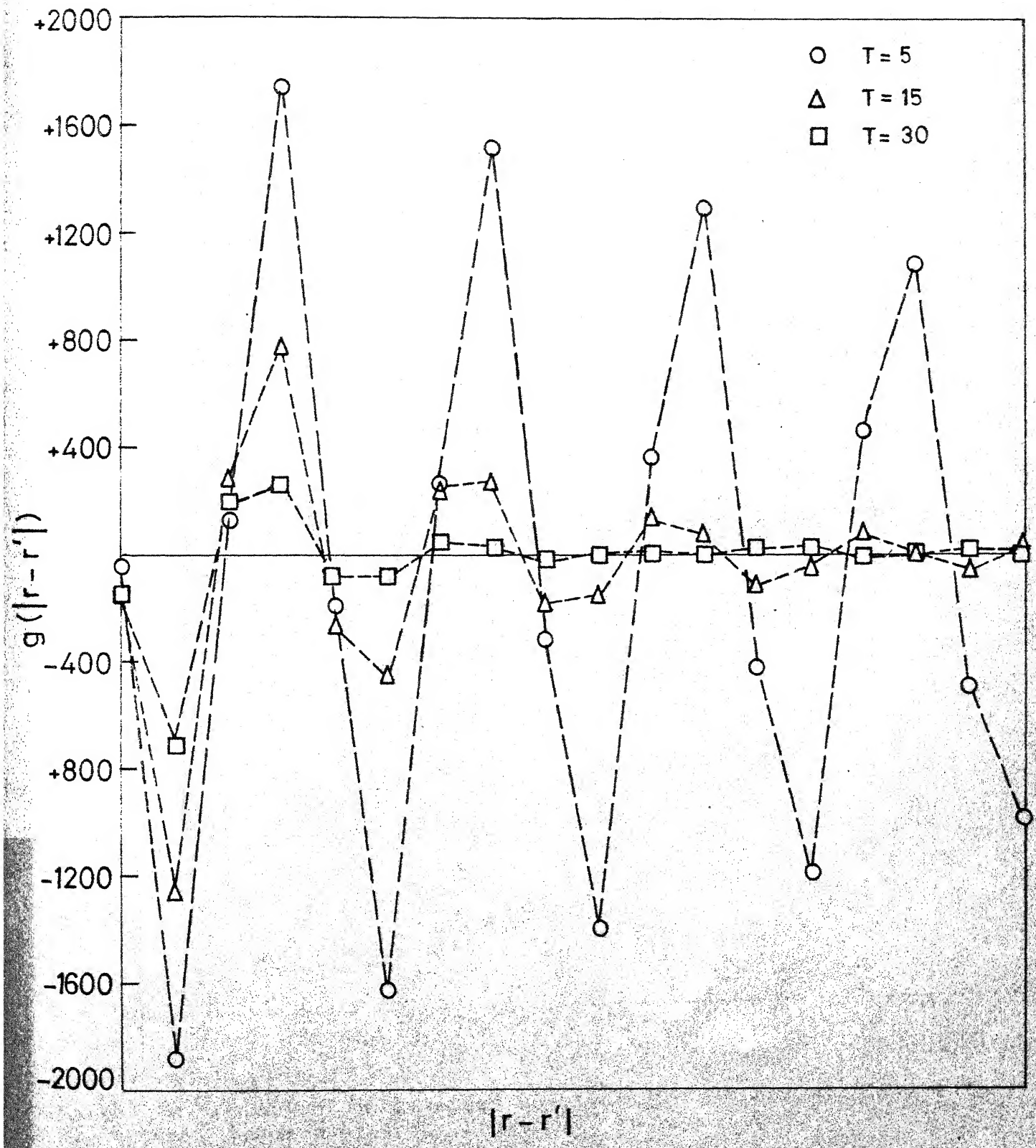

Fig. I.9. Plots of correlation function vs distance at different temperatures for region II in zero field.

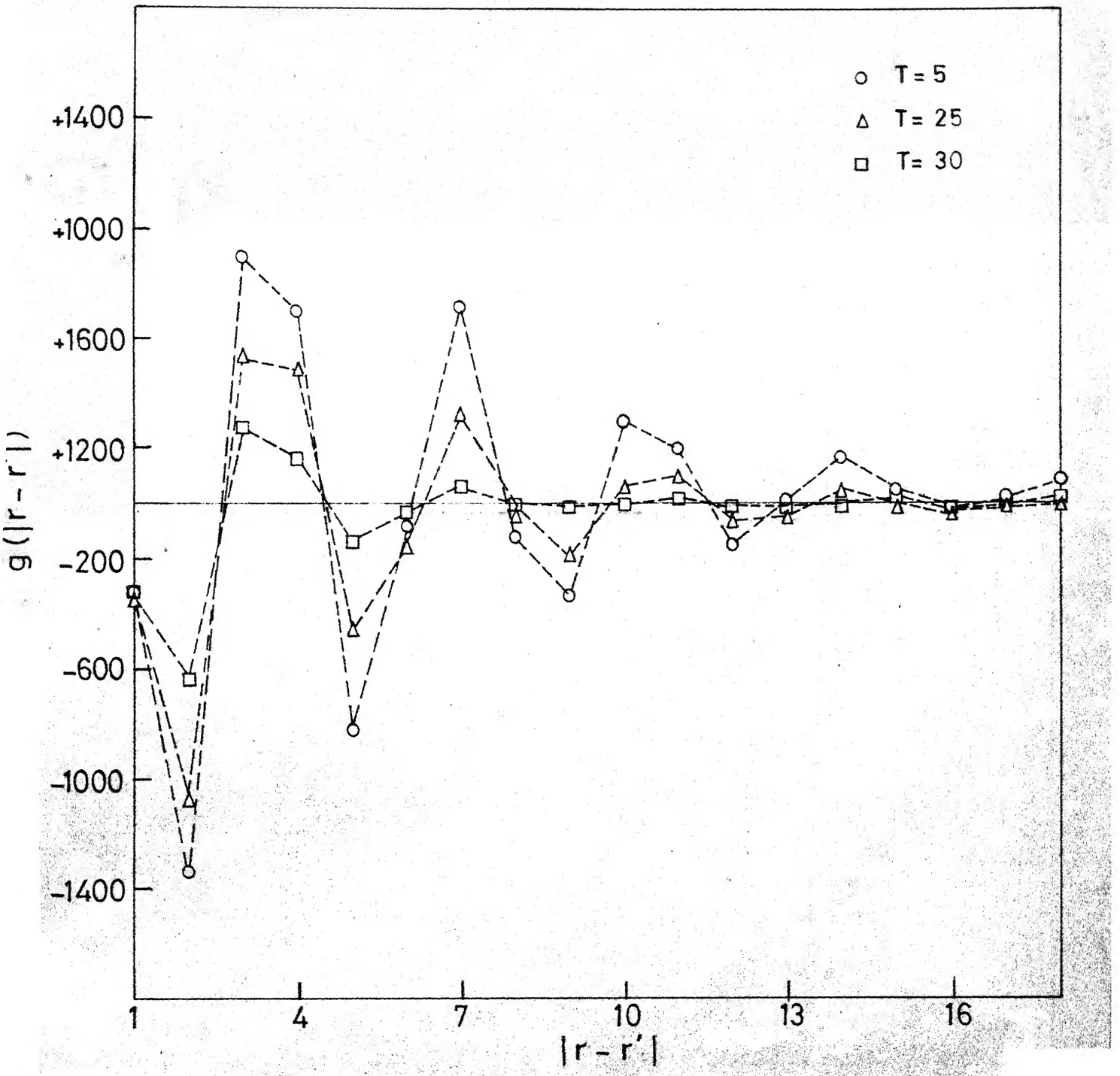

Fig. I.10. Plots of correlation function vs distance at different temperatures for region III in zero field.

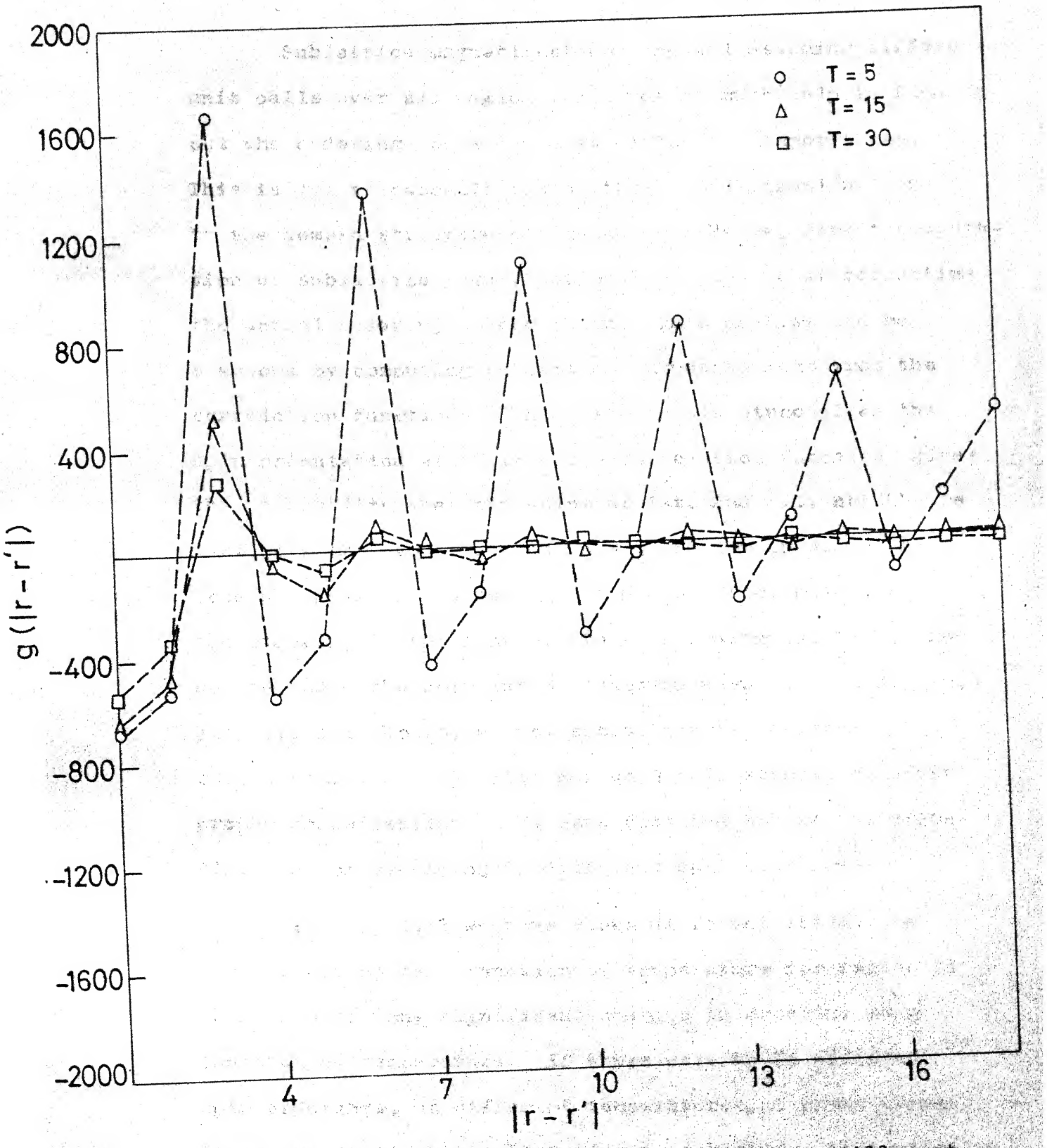

Fig. I.11. Plots of correlation function vs distance at different temperatures for region IV in zero field.

Sublattice magnetizations computed assuming different unit cells over all regions, are not of much help in finding out the orderings of a chain at different temperatures. This is due to cancellation of these magnetizations caused by the domain structure of the chain. Hence, direct computation of sublattice magnetization is incapable of reflecting the actual ordering of the chain. This problem can be overcome by computing sublattice magnetizations from the correlation functions. This is possible since given the spin orientation at a site, the correlation function gives the probability that the spins at 1st, 2nd, ... neighbours also have the same orientation and the domain structure does not mask the correlation function from reflecting the ordering in the system. Thus, for example, by summing up the value the correlation function assumes at 3rd, 6th, 9th, ... neighbours, we get sublattice magnetization corresponding to a 3 sites per unit cell structure, after proper normalizations. We have obtained sublattice magnetization corresponding to different spin orderings.

In Fig. I.12 we have shown different sublattice magnetizations as a function of temperature for region II. We do not see any significant changes in ordering as a function of temperature. If there were to be different spin orderings, at different temperatures, at phase transitions, we should have observed some sublattice magnetization

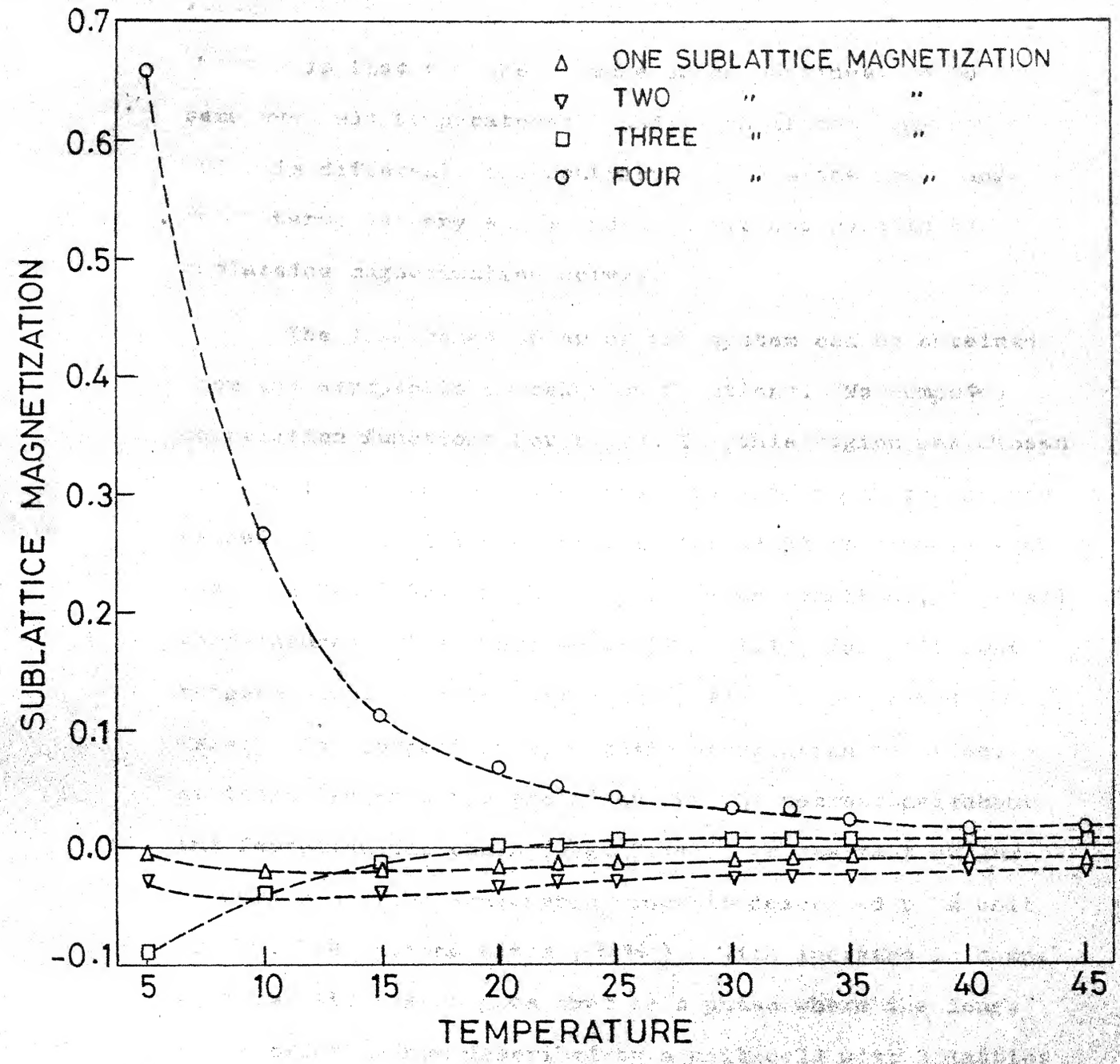

Fig. I.12. Plots of sublattice magnetizations vs temperature for region II in zero field, calculated from the correlation function, assuming existence of one, two, three and four sublattices.

abruptly decreasing while some other sublattice magnetization increase in magnitude. The reason why we fail to see such changes is that the short-range order continues to be the same over all temperatures. And, even if the long-range order is different, the contribution from the long-range order terms is very small and hence is not seen in the sublattice magnetization curves.

The long-range order of the system can be obtained from the asymptotic correlation functions. We computed correlation functions for region II (this region was chosen because there are only two phase transitions in the region as seen in Fig. I.8 and hence is the simplest to deal with) starting from 23rd neighbour up to 40th neighbour, over all temperatures. These are shown (Fig. I.13) for different temperatures, at which different phases are expected to exist. For comparison asymptotic correlation functions at these temperatures are given for the nearest-neighbour antiferromagnetic chain (Fig. I.14). We see that at low temperatures, the long-range order is described by a unit cell with 4 lattice sites (↑↑↓↓). With increase in temperature, the system goes over to a phase where the long-range order is now described by a unit cell with 3 lattice sites (↑↑↓). After the second phase transition, the system tends to have a ferromagnetic alignment, though it is not seen definitely. These results are in keeping with the

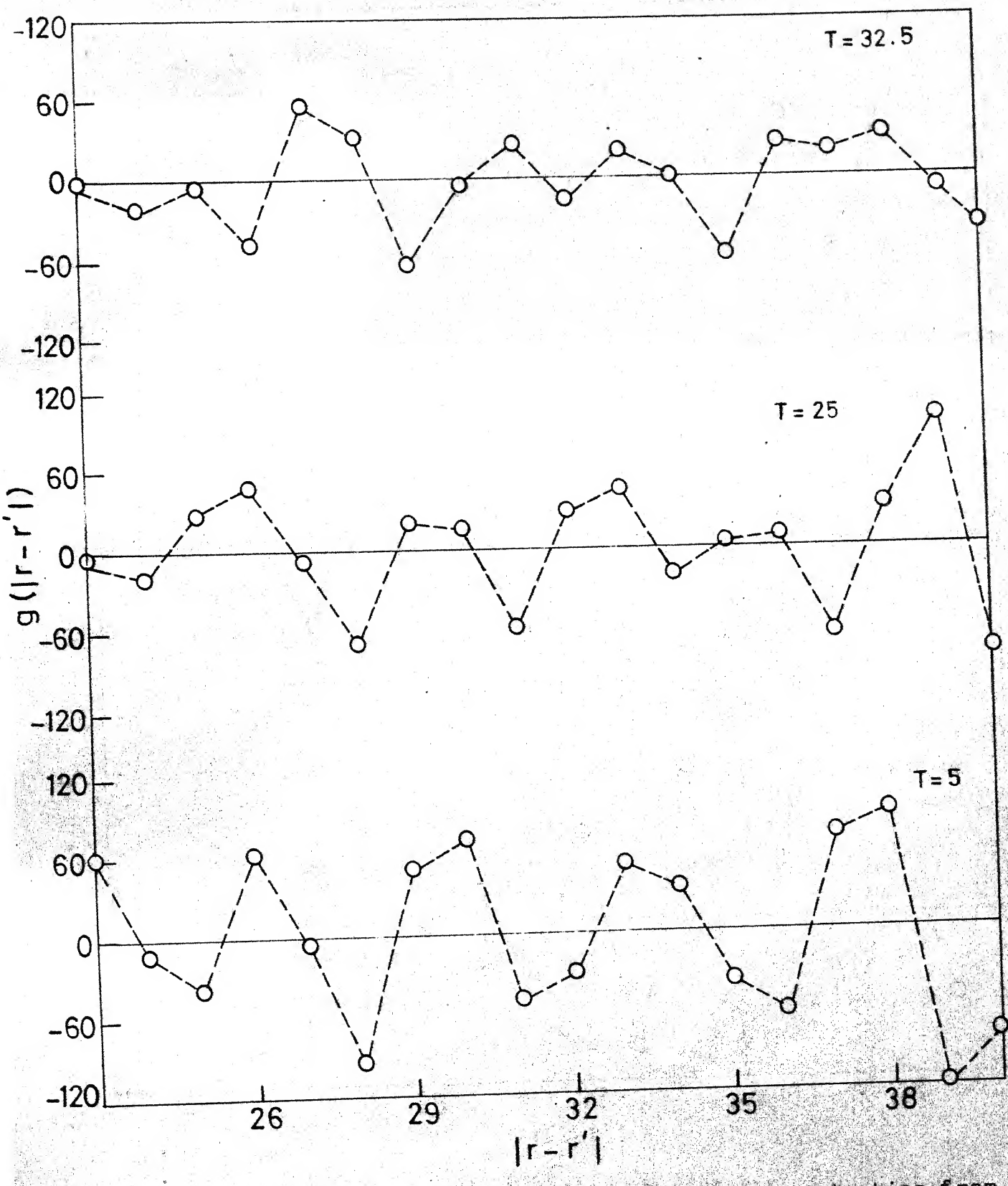

Fig. I.13. Plots of correlation function vs distance, starting from the 23rd neighbour, for region II in zero field at different temperatures.

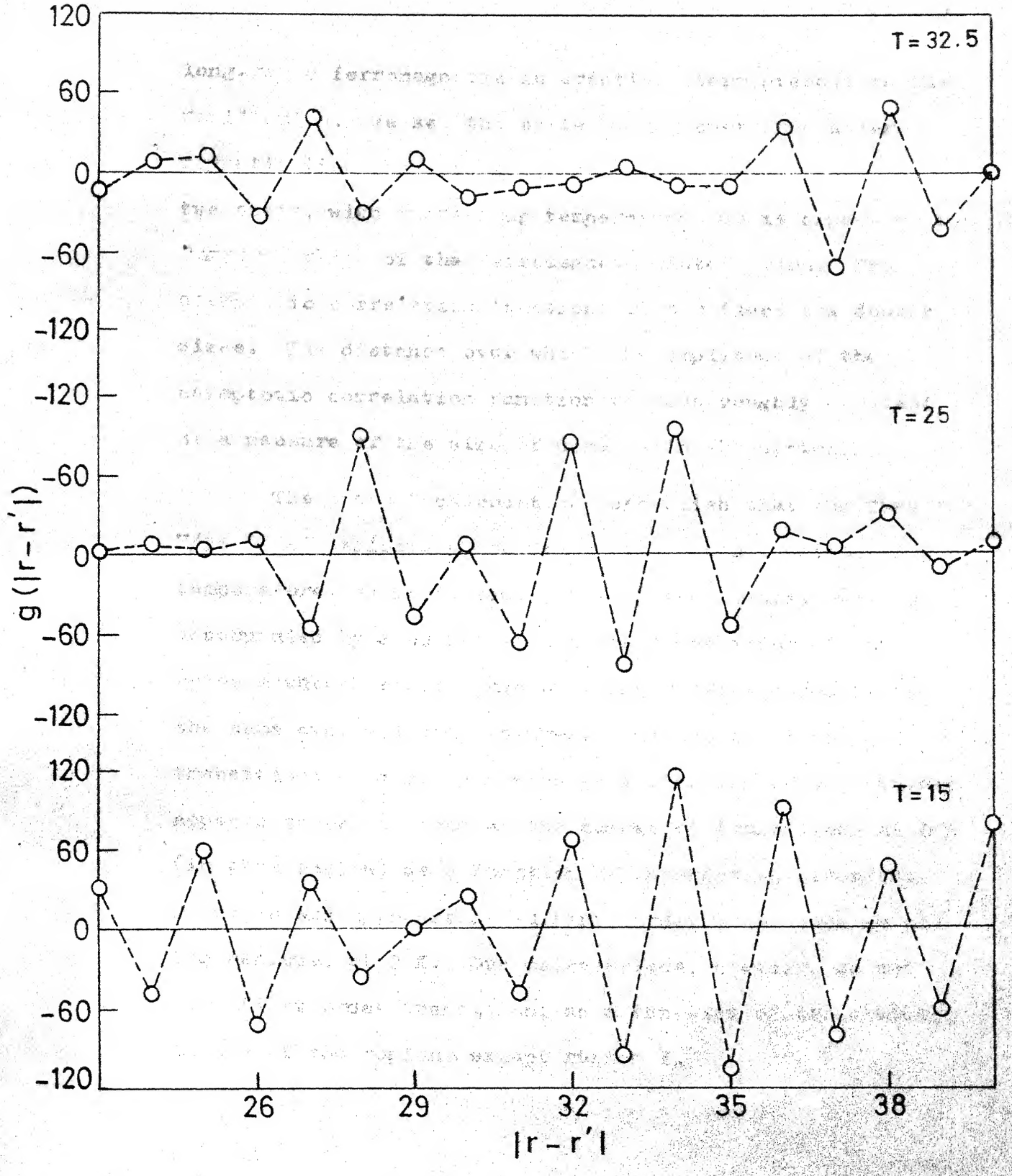

Fig. I.14. Plots of correlation function vs distance, starting from the 23rd neighbour, for the nearest-neighbour antiferromagnetic Ising chain, in zero field, at the same temperatures as in Fig. I.13.

long-range ferromagnetic interaction term present in the Hamiltonian. We see the system moving over from a zero-magnetization phase to a magnetically ordered phase in two steps, with increasing temperature, as is expected from the longer range of the ferromagnetic interaction. The asymptotic correlation functions also reflect the domain sizes. The distance over which the amplitude of the asymptotic correlation function remains roughly constant is a measure of the size of domains in the system.

The present calculations establish that the Theumann-Høye model exhibits phase transitions as a function of temperature, as predicted. These phase transitions are accompanied by a change in long-range ordering of the spins although short-range ordering remains essentially the same over all temperatures. The number of phase transitions in a given region as a function of temperature appears to be the same as the number of transitions at 0 K (in that region) as a function of interaction strengths. Theumann and Høye predicted first order transition in all the regions, at 0 K. Our calculations, however, do not show first order transition, as a function of temperature, in any of the regions except region I.

I.6 Summary

Spin-half Ising chains with short-range antiferromagnetic and infinite-range ferromagnetic interactions are known to exhibit several phase transitions. Nagle observed a first order transition in the presence of a field as well as in zero field as a function of temperature when the short-range interaction was restricted to first neighbour and the infinite range interaction was taken to be an equivalent neighbour interaction. Theumann and Høye extended the short-range interaction up to second neighbour and used infinite-range Kac potential for the long-range part. They obtained a phase diagram with interaction strengths as variables for zero temperature and found that in some regions of this phase diagram, the chain showed as many as four first order phase transitions.

In the present study, we have carried out Monte Carlo calculations on the Ising chains of Nagle and Theumann and Høye. From our calculations we have obtained estimates of specific heats, internal energies and correlation functions, as a function of temperature for various interaction strengths for both the chains. In the case of Nagle's Ising chain, we have observed the predicted first order phase transition in the presence of a field. We did not, however, see the predicted first order transition in zero field and we have attributed this to the formation of a metastable state at

low temperatures. In the case of Theumann-Høye Ising chain, in one of the regions of their phase diagram, we have observed a first order phase transition as a function of temperature, both in the presence and absence of a field. This was accompanied by a change in the short-range ordering of spins. In the other regions of the phase diagram, we did not see such first order phase transitions, as a function of temperature, although the specific heat vs temperature curves showed distinct anomalies indicating occurrence of second or higher order transitions. The low-temperature spin ordering of the chain is found to be different in different regions of the phase diagram. The specific heat anomalies were not accompanied by any perceptible change in the ordering of the spins, as seen from the microstates. Sublattice magnetizations, (computed from the correlation functions) also do not show any characteristic changes as a function of temperature. However, asymptotic correlation functions of region II showed that the long-range ordering of the spins changed when the chain underwent a phase transition. The different long-range ordering of spins in different phases was explained on the basis of longer range of ferromagnetic interactions. In addition to providing support to the models of Nagle and Theumann and Høye, the present Monte Carlo study provides details of the phase transitions and spin orderings as a function of temperature in various regions of their phase diagrams.

Complete characterization of the phases in each region, as a function of temperature, is plausible if a free energy expansion in terms of various order parameters can be worked out. One possible method of arriving at such free energy expansions seems to be the functional integral method. We propose to carry out such calculations in the future to understand the changes in spin ordering accompanying these phase transitions.

References

1. F. Gürsey, Proc. Camb. Phil. Soc., 46, 182 (1950).

2. J. M. Ziman, 'Principles of the Theory of Solids', Cambridge Univ. Press, Cambridge, London (1964).

3. E. W. Elcock, 'Order-Disorder Phenomena', Methuen and Co. Ltd., London (1956).

4. E. W. Montroll, J. Chem. Phys., 10, 61 (1942).

5. D. C. Mattis, 'The Theory of Magnetism', Harper and Row, New York (1965).

6. J. F. Dobson, J. Math. Phys., 10, 40 (1969).

7. M. Kac, Phys. Fluids, 2, 8 (1959).

8. G. A. Baker, Phys. Rev., 122, 1477 (1961).

9. K. Huang, 'Statistical Mechanics', John Wiley and Sons, Inc., New York (1963).

10. M. Kac, G. Uhlenbeck and P. C. Hemmer, J. Math. Phys., 4, 216 (1963).

11. F. J. Dyson, Commun. Math. Phys., 12, 91 (1969).

12. M. E. Fisher, Physics, 3, 255 (1967).

13. G. A. Baker, Phys. Rev., 130, 1406 (1963).

14. M. Suzuki, J. Phys. Soc. (Jap.), 21, 2140 (1966).

15. H. N. V. Temperley, Proc. Phys. Soc., 67, 233 (1954).

16. P. W. Anderson, G. Yuval and D. R. Hamann, Phys. Rev., B1, 4464 (1970).

17. J. F. Nagle, Phys. Rev., A2, 2124 (1970).

18. W. K. Theumann and J. S. Høye, J. Chem. Phys., 55, 4159 (1971).

19. R. Courant and D. Hilbert, 'Methods of Mathematical Physics', Vol. 2, John Wiley and Sons, Inc., New York (1962).

20. L. P. Landau and E. M. Lifshitz, 'Statistical Physics', Pergamon Press, Oxford (1970).

21. G. Stell and P. C. Hemmer, Phys. Rev. Letts., 24, 1284 (1970).

22. J. F. Nagle and J. C. Bonner, J. Chem. Phys., 54, 729 (1971).

23. J. L. Lebowitz and O. Penrose, J. Math. Phys., 7, 98 (1966).

24. W. D. Niven (Ed.), 'The Scientific Papers of James Clark Maxwell', Dover Publ. Inc., New York (1965).

25. G. Stell and P. C. Hemmer, J. Chem. Phys., 56, 4274 (1972).

26. J. M. Hammersley and D. C. Handscomb, 'Monte Carlo Methods', Methuen and Co. Ltd., New York (1964).

27. Yu. A. Shreider (Ed.), 'The Monte Carlo Method: The Method of Statistical Trials', Pergamon Press, Oxford, (1960).

28. H. A. Meyer (Ed.), 'Symposium on Monte Carlo Methods', John Wiley and Sons., Inc., New York (1956).

29. J. Spanier and E. M. Gelbard, 'Monte Carlo Principles and Neutron Transport Problems', Addison-Wesley Publ. Company, London (1969).

30. G. G. Lowry (Ed.), 'Markov Chains and Monte Carlo Calculations in Polymer Science', Marcel Dekker, Inc., New York (1970).

31. O. Taussky and J. Todd in 'Symposium on Monte Carlo Methods', H. A. Meyer (Ed.), John Wiley and Sons, Inc., New York (1956).

32. M. Fluendy in 'Markov Chains and Monte Carlo Calculations in Polymer Science', G. G. Lowry (Ed.), Marcel Dekker, Inc., New York (1970).

33. J. M. Myhre in 'Markov Chains and Monte Carlo Calculations in Polymer Science', G. G. Lowry (Ed.), Marcel Dekker, Inc., New York (1970).

34. W. Feller, 'An Introduction to Probability Theory and Its Applications', Vol. 1, John Wiley and Sons, Inc. New York (1957).

35. N. Metropolis, A. W. Rosenbluth, M. N. Rosenbluth, A. H. Teller and E. Teller, J. Chem. Phys., 21, 1087 (1953).

36. W. W. Wood and F. R. Parker, J. Chem. Phys., 27, 720 (1957).

37. K. Binder, Adv. Phys., 23, 917 (1974).

38. R. Friedberg and J. E. Cameron, J. Chem. Phys., 52, 6049 (1970).

39. A. C. Holt, W. G. Hoover, S. G. Gray and D. R. Shortle, Physica, 49, 61 (1970).

40. P. A. Flinn and G. M. McManus, Phys. Rev., 124, 54 (1961).

41. L. D. Fosdick in 'Methods in Computational Physics', Vol. 1, B. Alder, S. Fernbach and M. Rotenberg (Eds.), Academic Press, New York (1963).

42. T. E. Shirley, Phys. Letts., 42A, 183 (1972).

43. B. D. Metcalf, Phys. Letts., 45A, 1 (1973).

44. L. Guttman, J. Chem. Phys., 34, 1024 (1961).

45. G. E. Norman and V. S. Filinov, High Temp., 7, 216 (1969)

46. D. C. Handscomb, Proc. Camb. Phil. Soc., 58, 594 (1962).

47. L. D. Fosdick, SIAM Rev., 10, 315 (1965).

48. S-k. Ma, Phys. Rev. Letts., 37, 461 (1976).

49. O. Penrose and J. L. Lebowitz, J. Stat. Phys., 3, 211 (1971).

50. K. Binder and E. Stoll, Phys. Rev. Letts., 31, 47 (1973).

APPENDIX

RANDOM NUMBER GENERATION AND TESTING

In this, we outline the method of random number generation and the tests performed to ascertain that they belong to a uniform distribution. Random numbers were generated by the following algorithm. An integer, initially chosen to be 377773 (in octal) was multiplied by $(2^{17}+3)$. If the resulting integer is less than $2^{35}-1$, it is taken as the first random number. If it is greater than $2^{35}-1$ (this number is specific to IBM 7044 on which all our calculations were carried out), the computer truncates the digits of the number from the left till the resulting number is less than $2^{35}-1$. The resulting number is taken as the random number. For the next cycle, the last random number that is generated is multiplied by $(2^{17}+3)$ and the whole process is repeated. Random numbers between 0 and 1 are obtained by dividing the above random numbers by 2^{35}. Only two operations are required to generate a random number by this method.

The first thirty thousand random numbers generated by this method were subjected to the following tests to

ascertain that they belonged to a uniform distribution. (i) Moments test, where up to fourth moment of these numbers were calculated and compared with the expected moments. (ii) Frequency test, where the actual frequency f_i of the random numbers is calculated and compared with expected values. f_i denotes the number of random numbers, from among the thirty thousand generated, that belong to the ith sub-interval defined by the end points (i-1)/10 and i/10. (iii) The correlation tests in which the frequencies $f_{ij}^{(1)}$ are computed. Here i denotes the ith sub-interval to which a random number belongs and j the jth sub-interval to which the next random number belongs. The superscript (1) implies that we are testing for correlation between numbers generated in succession. χ^2-test is not reliable in these cases as the division of the interval (0-1) is arbitrary. However, the χ^2-test for both correlation and distribution show that the random numbers generated belong to a good uniform distribution. Results of the tests (i), (ii) and (iii) are given in Tables IA, IIA and IIIA respectively.

Table IA

Moments Test

(Expected values are calculated for uniform distribution)

Order of the moment	1	2	3	4
Actual value	0.5003	0.3343	0.2513	0.2014
Expected value	0.5000	0.3333	0.2500	0.2000

Table IIA

Frequency Test

Interval	0-.1	.1-.2	.2-.3	.3-.4	.4-.5	.5-.6	.6-.7	.7-.8	.8-.9	.9-1.0
Actual frequency	3106	2935	2977	3021	2937	3045	2918	2875	3189	2996
Expected frequency	3000	3000	3000	3000	3000	3000	3000	3000	3000	3000

Table IIIA

Frequencies for correlation of successive random numbers
(Expected frequency: 300 for all cases)

i→ / j↓	0-.1	.1-.2	.2-.3	.3-.4	.4-.5	.5-.6	.6-.7	.7-.8	.8-.9	.9-1.0
0-.1	356	329	297	322	275	313	317	257	337	303
.1-.2	267	290	314	281	295	310	321	280	300	277
.2-.3	303	288	295	318	311	304	249	287	318	304
.3-.4	316	310	306	274	301	309	280	299	310	316
.4-.5	298	268	284	306	306	292	300	256	325	302
.5-.6	337	295	288	299	311	297	296	307	306	309
.6-.7	319	283	286	278	271	316	288	273	295	309
.7-.8	292	284	273	287	262	288	288	304	337	260
.8-.9	327	287	332	321	315	320	305	336	337	309
.9-1.0	291	301	302	335	289	296	274	276	325	307

CHAPTER II

MONTE CARLO SIMULATION OF POLYTYPES

II.1 Introduction

Close packed structures in solids can be thought of as obtained by packing atomic layers, one above another. Two commonly known close packed structures are the hexagonal close-packed and the cubic close-packed structures. Hexagonal close-packed structures are obtained by packing layers of atoms such that atoms in alternate layers come, exactly, one above another. If we can represent the position of atoms in a layer by the alphabets A and B, in hexagonal close packing the layers are stacked in the sequence ...ABABAB..... In cubic close packing, the atoms of every first and fourth layer are superposed on one another. In the above notation, the layer sequence would be ...ABCABC... This is because, after the first two layers are packed one above another, we are left with only two options - one leading to a cubic close packing and the other to a hexagonal close packing. A given

atomic layer is said to be in a hexagonal close-packed configuration (h) if atoms in its neighbouring layers are exactly superposed on one another (e.g., layer 'B' in the sequence ...ABA...). Otherwise, the layer is said to be in a cubic close-packed configuration, k (e.g., layer 'B' in the sequence ...ABC...). Some substances, in addition to existing in pure cubic or pure hexagonal close packed structures, also exist in structures resulting from a repeating sequence of layers in which a layer within each repeat unit is in either 'h' or 'k' configuration (e.g., the sequence ...ABCBABCB... in which a repeat unit consists of 4 layers in the configuration hkhk). The different crystal structure modifications thus obtained are known as polytypes. Unit cells of polytypes of a substance have the same a and b dimensions but differ in the c dimension. The c dimension of the unit cells depends upon the number of layers in each repeat unit and examples where the c dimension of a unit cell is as large as a few thousand Angstroms are known. Typical substances exhibiting polytypism are SiC, CdI_2, ZnS and TaS_2. Cadmium Iodide alone has as many as two hundred and ten known polytypic modifications and a polytype of SiC with a repeat sequence of 4680 layers (c dimension 12000 Å) is also reported. Polytypism in various substances has been reviewed by Verma and Others.[1-3]

Polytypism can be considered as a one-dimensional phenomenon since the only difference between any two polytypic modifications of a substance lies in the sequence in which the layers are stacked along the c-axis. This appears difficult to comprehend since truly one-dimensional systems normally do not have ordered phases at non-zero temperatures.

A polytype is completely characterized by its ABC layer sequence. For many polytypes, the full ABC layer sequence happens to be rather long and hence it is often inconvenient to characterize a polytype by giving the full ABC sequence. Pauling, Wyckoff and Jagodzinski evolved a notation by using which the length of the layer sequence that need be specified is reduced to 1/2 or 1/3 (compared to the ABC sequence) depending upon whether the polytype belongs to a hexagonal system or a rhombohedral system, respectively. In this system, each layer is characterized by 'h' or 'k' depending upon whether the layer is in a hexagonal close-packed configuration or a cubic close-packed configuration respectively. The hk sequence now will characterize the polytype. Another common notation is due to Zhdanov.[1] In this notation a number is used to characterize a polytype. The digits of the number from the left, give the number of successive cyclic and anti-cyclic changes (A→B→C and A→C→B, respectively) in the layer orientation.

Polytypic modifications of a substance form under almost identical conditions of growth. Often, a substance shows different polytypic modifications in different parts of a single specimen. Frequently, polytypic modifications show growth spirals on the faces of their crystals. Many polytypic substances exhibit random disorder of layers to varying extents. Interpolytypic phase transitions have been observed in some cases, though rarely.

The periodicity of layer stackings in polytypes are often much larger than the range of commonly known atomic forces and this renders the explanation of this phenomenon difficult. Most polytypes are known to be quite stable and temperature or pressure does not apparently affect their relative stabilities. However, temperature in some cases has the effect of increasing the randomness in layer stackings. The number of polytypic phases existing for a substance, often far exceeds the maximum number of phases that can exist for a single component system according to Gibbs' phase rule.

We mentioned earlier that polytypism can be considered as a one-dimensional phenomenon. In fact, we can consider polytypes as different ordered states of a spin-half Ising chain. The two states of the spin can be taken to represent the two lowest energy configurations

of a layer in a polytype viz., the cubic and hexagonal configurations. All other configurations of layers (like AAB, ABB etc.) are of very high energies and are not observed experimentally, even at high temperatures. Hence there should be one to one correspondence between the thermodynamic properties of a polytype and the thermodynamic properties of an appropriate Ising chain.

To have ordered arrangement of spins in an Ising chain, it is necessary to have an infinite-range interaction among spins (see section 1, Chapter I). The form of infinite-range interaction most suitable for Monte Carlo simulations is the equivalent-neighbour interaction. The contribution to internal energy from this form of infinite-range interaction is given by $-J_{lr} M^2$. This form of infinite-range interaction is to some extent justified, since such forces do exist in Nature. Friedel[4,5] has shown that the major component of elastic interaction between atoms of different sizes, in an elastic medium, has the following properties: (i) the interaction between like defects is necessarily attractive and (ii) this force is the only interaction known, which is truly infinitely long-range. The contribution to the elastic energy is given by $-C(x_1-x_2)^2$, where x_1 and x_2 are mole fractions of the atoms of two different sizes and C is a constant. We see that this form is

identical to the contribution coming from an equivalent-neighbour interaction term in the magnetic Ising chain. If we postulate that the layers in the hexagonal and cubic configurations have different thicknesses*, we would have justified the use of the equivalent-neighbour interaction term in the Ising chain that describes polytypism.

If we should have different spin orderings in the Ising chain in order that the chain describes polytypism it would be necessary to add a competing short-range interaction term, to the equivalent-neighbour interaction term. Since the Theumann-Høye[7] Ising chain described in Chapter I exhibits different spin orderings, we considered it appropriate to employ this for the study of polytypism as well. Thuemann-Høye Ising chain shows coexistence of as many as five phases for some interaction strengths. This property of the Ising chain can then be extended to polytypes to explain the coexistence of several polytypic phases under identical conditions of temperature and pressure, without violation of Gibbs' phase rule.

---

*It is known, for example, that ionic crystals of the formula AB crystallize in cubic close-packed structures and covalent crystals crystallize in hexagonal close-packed structures.[6] Since ionic and covalent radii of an atom are different, our postulate is not entirely without meaning.

While we could justify the equivalent-neighbour interaction term to some extent it is not easy to visualize the origin of short-range interaction terms in polytypes. The strengths of different short-range interactions (J and K of II.3.1) in polytypes could possibly be related to the growth conditions. This would imply that corresponding to a given set of growth conditions, a particular set of polytypes would be formed.

In the present study, our primary interest was in the Monte Carlo simulation of polytypes by analogy to our studies on the Ising chain reported in Chapter I. The mechanism for going from one system of the ensemble to another, in the case of the Ising chain, was a simple spin-flip mechanism. This mechanism loses meaning in the context of polytypes. To arrive at thermodynamic states of a polytype, from given initial state, we have to devise different mechanisms for layer rearrangements. These are discussed in section II.3, together with the programs. In section II.4 we present results and discussion of our simulation studies. We shall briefly survey theories of polytypism in the next section, since this may be relevant to understanding the present study in the context of the existing knowledge in this field.

II.2. A Brief Review of the Theories of Polytypism

Early theories of polytypism attempted to explain the phenomenon by correlating aspects such as impurity content, rate of crystallization and orientations of neighbouring crystals during growth, with the observed polytypic modifications.[1-3] It was seen that the range of impurity content in 6H, 15R and 4H SiC polytypes differed distinctly. Similarly, evidence for correlation between the polytype modification formed and the rate of crystallization, was found for some polytypic modifications of CdI_2. Attempts to attribute a definite range of growth temperature for each polytype also met with some success. However, as more and more polytypic modifications of substances were discovered, these correlations became increasingly difficult, prompting a search for a more basic theory of polytypism.

Ramsdell and Kohn[8] suggested that different polytypic modifications were formed by stacking basic polymeric unit(s) of the substance. They proposed seven basic polymeric units for SiC, with Zhdanov symbols 33, 32, 23, 22, 34, 43 and 44. These basic polymeric units were arrived at from a knowledge of the stacking sequences in the known polytypic modifications of SiC. It was assumed that each polymer had a range of temperature

over which it was stable. These stability ranges sometimes overlapped, to give rise to two different polymeric units in different concentrations, resulting in the formation of long-ordered polytypes. This theory was useful in solving the crystal structures of newer polytypes. However, there is no experimental evidence for the existence of such polymeric units. Also it does not attempt to explain the origin of the ordered stacking of different polymeric units in long-ordered polytypes.

Verma,[9] while studying SiC crystals, to render support to Frank's screw-dislocation theory of crystal growth, observed growth spirals on the crystal faces. The measured step height of the growth spiral of 6H SiC was found to be equal to the unit cell c-dimension. This led Frank[10] to suggest that polytypism in SiC is brought about by the spiral growth of crystals around screw dislocations of different Burgers vectors. Frank proposed that SiC crystals initially grow into thin plates. These plates then become self-stressed through nonuniform distribution of impurities or thermal stresses and buckle, resulting in the formation of a screw dislocation, exposing a ledge on the surface. Subsequent growth of the crystal will have a structure corresponding to that of the ledge and will repeat with a period equal to the pitch of the screw. Screw dislocations, with Burgers vectors whose

magnitudes are not integral multiples of the height of the parent unit cell, will thus give rise to polytypic modifications different from the parent crystal. Support for Frank's screw-dislocation theory of polytypism has come from the observation and measurements on screw dislocations in polytypes. Direct correlation between step-heights of growth spirals and unit cell heights of the corresponding polytypes have been demonstrated in many cases. Another important experimental support of this theory comes from the observation of syntactic coalescence (two different polytypes growing on the same specimen). Syntactic coalescence is expected since this theory provides for the growth of one structure from a screw dislocation in another. Different mechanisms have been proposed for the formation of screw dislocations (with Burgers vectors whose magnitudes are non-integral multiples of the parent unit cell height) in different substances,[11,12] e.g., impurity mechanism is favoured for the formation of such a screw dislocation in ZnS.

Jagodzinski[13,14] raised the following objections to Frank's screw-dislocation theory: (i) In close-packed structures, edge dislocations are energetically favoured over screw dislocations and the former would completely destroy any order created by the latter. (ii) The high strain energy required for creating a screw dislocation

can come only when the crystal has grown to a considerable volume by which time it would have already settled down to a certain structure. (iii) While the screw dislocation mechanism requires the resulting structure to be perfectly ordered examples of structures with superposed random disorder are not uncommon. (iv) The screw dislocation mechanism does not account for the thermal stability of polytypic structures. (v) A large number of polytypes are known, where correlation between step-height of growth spiral and the unit cell height, is not found. Objections (ii) and (v) have been refuted by Vand and Hanoka[13] on the following basis. The greatly strained regions in a real crystal are not occupied by atoms, thus giving rise to a cylindrical hole (as observed in CdI_2) around the dislocation. Absence of syntactic coalescence was not confirmed in the crystals (under (v)) and the observed lack of correlation may well be due to this.

Jagodzinski proposed a thermodynamic theory of polytypism. He assumed that the internal energy contribution to free energy differences, among various polytypes, is negligible. Thus the stability of different polytypes should be determined from the entropy contributions. While configurational entropy favours a disordered arrangement of layers, the vibrational entropy of the

system favours ordering. The total entropy, estimated by Jagodzinski, as a function of the degree of disorder, α, showed two maxima, one at $\alpha = 0$ (corresponding to a stable state) and the other at $\alpha \sim 0.12$ (corresponding to a metastable state). This implies formation of perfectly ordered polytypes as well as polytypes with a certain degree of randomness. Sixtytwo of the one hundred and fifty crystals of SiC (the hundred and fifty crystals were picked at random) showed existence of one-dimensional disorder, rendering support to the thermodynamic theory. However, this theory is not without drawbacks. Long-ordered polytypes without faults have been observed, while it is known that the contribution to vibrational entropy decreases with increasing periodicity. The existence of maxima on the entropy versus disorder curve is based on purely qualitative arguments.

Schneer[15] proposed a theory of polytypism, similar to Bragg-Williams order-disorder theory of alloys. The two possible layer configurations 'h' and 'k' are represented by the two states of a half-integral Ising spin. Assuming that there is an energy difference between the layer in 'h' and 'k' configurations, Schneer obtained an equilibrium ratio (D) of layers in 'h' configuration to layers in 'k' configuration. Once this ratio is determined, interaction between the layers in different configurations is switched on and the arrangement of layers for

which the interaction energy is a minimum is the equilibrium arrangement of the layers at the given temperature. Schneer proposed that different polytypes were obtained from a quenching of such equilibrium arrangements of layers. Thus polytypes, according to this theory, are metastable states formed on quenching the layer system, when the layer system is undergoing a second order phase transition from a cubic to a hexagonal (4H) state. However, there is little experimental evidence to support this theory. It has not been possible to associate definite polytypes with specific temperatures and interpolytypic transformations are not very common. The high temperature modification of SiC and ZnS are not characterized by $D = 1/2$, contrary to the prediction of the theory.

Peibst[1,2] proposed a theory of polytypism according to which different polytypes are formed under different conditions of crystal growth. He postulated that thermal vibrations, under specified growth conditions, can bring about a periodic introduction of stacking faults in the basic structure, resulting in the generation of polytypes. The observation of spiral growth, according to him, is associated with circularly polarized transverse elastic waves which may exist at the time of growth. However, his theory is very qualitative in nature and offers little scope for experimental verification.

We see that none of the above theories (barring Frank's screw-dislocation theory to some extent) explains all the basic features of polytypism viz., (i) existence of different types of unidimensional order while one-dimensional systems, usually, should not show any long-range ordering, (ii) seeming violation of Gibbs' phase rule due to the coexistence of various thermodynamically stable phases under identical conditions, (iii) syntactic coalescence and (iv) existence of differing amounts of disorder in many polytypes. Since Theumann-Høye Ising chain shows the above behaviour, we have attempted to simulate polytypes based on the interactions of this Ising chain. We shall discuss the mechanisms for layer rearrangements and also the simulation procedure in the next section.

II.3 Programs and Mechanisms for Layer Rearrangements

Monte Carlo simulation is carried out on a chain of one thousand layers. The calculational procedure involves generation of a random initial chain. Changes in configurations of layers are then carried out to bring the chain to equilibrium at the given temperature. Once the chain is brought to equilibrium, estimates of thermodynamic properties are carried out. At the end of the

calculations an output of the microstates is obtained. This is further processed to check for the type of ordering existing in the system at the given temperature. The input parameters are, values of short-range and long-range interaction strengths, temperature and a parameter, Δ; Δ gives the energy separation (in the absence of any interaction) between layers in 'h' or 'k' configuration and all other high energy configurations (corresponding to $\Delta\Delta B$, ΔBB etc.) whose energies are all taken to be zero. The value of Δ should be large enough to avoid occurrence of higher energy states at equilibrium even at high temperatures. The initial state of the chain is always taken to be random assuming that the polytypes are grown from melt.*

The disordered chain is created using random numbers between 0 and 1. Numbers '1', '2' and '3' are used to designate A, B and C layers respectively. We begin with the first site and call a random number between 0 and 1. If the random number belongs to the interval 0-1/3, '1' is assigned to the site. If the random number belongs to

* One can, in principle, study the formation of polytypes under different growth conditions by either starting with a different initial state or by building a chain at equilibrium such that the chain approaches equilibrium at each instant. The former would correspond to growth of polytypes from an already existing polytypic phase and the latter to a simulation of growth of polytypes from solution or vapour deposition.

the interval 1/3-2/3, '2' is assigned to the site, otherwise '3' is assigned to the site. This process is continued till a number is assigned to each site. The initial hk sequence is extracted from the random ABC sequence. The configuration 'h' is designated by '1' and the configuration 'k' by '2'. All higher energy configurations are designated by 'C'.

The initial energy is calculated using the hk sequence. The configuration 'h' corresponds to a down-spin ($S_i = -1$) state and the configuration 'k' corresponds to an up-spin ($S_i = +1$) state while all other configurations correspond to $S_i = 0$. The initial energy is calculated from the following expression:

$$E_i = (H - \Delta) H \sum_{i=1}^{1000} S_i + J \sum_{i=1}^{1000} S_i S_{i+1} + K \sum_{i=1}^{1000} S_i S_{i+2} - AM^2 - \Delta \sum_{i=1}^{1000} |S_i| \qquad \text{(II.3.1)}$$

Here, H is the separation between 'h' and 'k' configurations (equivalent of the magnetic field) in the absence of interactions, Δ is the parameter already defined, J and K are short-range interaction parameters, A is the long-range interaction parameter and M the difference between the number of layers in 'h' state and the number of layers in 'k' state. A cyclic boundary condition is used in our calculations.

To bring the chain to equilibrium at a given temperature, we have to rearrange the layers. There is no straight-forward mechanism, like the spin-flip mechanism in the magnetic Ising chains, for bringing about the rearrangement of layers. Although we are tempted to deal with the hk sequence and use the mechanism in which states h and k flip to each other (in analogy to the spin-flip in magnetic Ising chains), a closer scrutiny points to the fact that such flips are not physically meaningful. This is because a flip in the configuration of a layer changes the configuration of the neighbouring layers in such a way as to result in high energy configurations (e.g., flipping the state of the underlined layer in the sequence ABC ACB ABC leads to ABC ABB ABC). It would, therefore, be best to deal with the ABC sequence directly and evolve physically reasonable mechanisms for changing the configurations of layers. Our aim is to demonstrate that there exists a physically meaningful mechanism for rearranging the layers in a polytype, which is as efficient as the spin-flip mechanism of magnetic Ising chains. Once this is done, we can transfer all our results of the magnetic Ising chains of Chapter I to the case of polytypes*.

*The results of magnetic Ising chain cannot be transferred to polytypes, if no physically meaningful mechanism, as efficient as the spin-flip mechanism of magnetic Ising chains, exists because this would imply that changes in configuration allowed in a magnetic Ising chain are no longer allowed in polytypes. There is really no one to one correspondence between the states of the polytype chain and the states of magnetic Ising chain, over which thermodynamic averaging is carried out.

Having known the mechanism by which changes in configuration of the layers can be effected, we can bring the chain to equilibrium at the given temperature.by the probability prescription given in section 4 of Chapter I. Thermodynamic properties of the chain are estimated, as in the case of magnetic Ising chains, by averaging over a large number of states of the chain at equilibrium.

We have examined three different mechanisms for rearranging the layers in the polytypic chain. The simplest of these, was the single layer mechanism. In this mechanism, a layer can change from its initial state (given by A, B or C) to any of the two other states, e.g., ABCAAC → ABCABC. This is physically meaningful and implies that the layer in question changes its state by shearing with respect to its neighbours. However, this mechanism failed to give different states of the chain, starting from a given state, since any two low energy states of the chain were invariably connected only through high energy states. This made low energy states inaccessible to one another. The low temperature state of the chain for negative H and zero J, K and A (eq. II.3.1) contained 'h' configurations far in excess of the number expected at equilibrium. (In one case the expected number was around 0% while the observed number was ∿16%.) The chain seemed

to be locked in a particular state, far from equilibrium. Hence this mechanism was discarded.

The second mechanism that we experimented with was the layer transposition mechanism due to Jagodzinski.[13] In this mechanism, two adjacent layers in the chain interchange their ABC configuration, e.g., ABC ACB ABC → ABC ABC ABC. This mechanism is also physically reasonable since it involves a shearing of the two layers in question. This mechanism was proposed by Jagodzinski to explain formation of different polytypic modifications from an ordered phase. We carried out a simulation using this mechanism for J > 0 and H, K and A equal to zero (Eq.II.3.1). We found that the number of like neighbours (hh or kk) was far larger than the number expected at equilibrium. A closer look at the microstates showed that we were led to configurations from which we cannot come out, except via high energy states (e.g., for J > 0 & A, K & H=0, we observed states like ...ACBCABCBC, which can never go to ACBCACBCA by layer transposition mechanism, though the latter is a lower energy state). Jagodzinski's mechanism thus failed to yield a polytypic modification, starting from a disordered state. A combination of the single layer mechanism and the layer transposition mechanism also similarly failed. To overcome these difficulties, we

brought the higher energy states slightly lower and carried out a gradual cooling experiment*. We were once again faced with the same problem viz., locking of the chain in non-equilibrium configurations unless the higher energy states were brought sufficiently low so as to be accessible at low temperatures, a situation in contradiction to experimental observations. Using these mechanisms, in the case of A, K and J equal to zero and H less than zero, the observed number of 'h' states was 3.5% while the expected number was ~0%.

A successful mechanism of layer rearrangement should be capable of connecting two low energy configurations directly (i.e., without an intermediate high energy configuration). This can be achieved by a general two-layer mechanism. In this mechanism, two adjacent layers are allowed to change their layer configurations arbitrarily (e.g., ABCACB → ABCBCB or ABABCB and other high energy configurations). Changes to high energy configuration are highly improbable and changes from one low energy configuration to another low energy configuration alone occur at the temperatures of interest. This mechanism is physically meaningful since such changes can

* Here, we start from an arbitrary high temperature state and lower the temperature in convenient steps, till the desired low temperature is reached. At each temperature, we take the chain through a sufficiently large number of Monte Carlo cycles so that the chain comes to equilibrium at each of these temperatures.

be brought about by shearing the layers such that the atoms in the layer move, always keeping to the hollow space formed by the atoms in the neighbouring layers (during the whole process these atoms in adjacent layers never come one above the other while going from one low energy configuration to another)*. This mechanism gave nearly equilibrium number of hh and kk configurations, for $J > 0$ and H, K and A all zero (eq. II.3.1), in a reasonable number of Monte Carlo cycles. Using this mechanism, the computer time taken (on IBM 7044/1401 system) for carrying out 120,000 Monte Carlo cycles was about 20 minutes. A display of a section of the chain at different stages in its approach to equilibrium via the double layer mechanism is given on the next page (Fig. II.1).

It is difficult to see the existing order in the chain, in any given state, just by looking at the chain. The order parameters in the form of correlation functions are obtained by an averaging of the same over a large number of states of the chain and hence do not give the ordering of just a single state of the chain. To search for order in a given state of the chain, we have employed a display program. In the display program, we start with a unit of a given number of layers, at the beginning

*This implies that a high activation energy barrier that was separating any two low energy states in our calculations has been overcome. Thus, we can achieve equilibrium configurations in much fewer Monte Carlo cycles. Physically, this means that equilibrium is achieved in shorter times and the changes in configurations are no longer kinetically controlled but are controlled by thermodynamic probabilities.

Figure II.1. Growth of 4H Polytype Using the General Two Layer Mechanism: (a) After 45000 Monte Carlo Cycles (b) After 95000 Monte Carlo Cycles (c) After 145000 Monte Carlo Cycles (d) After 195000 Monte Carlo Cycles.

(a)

A C A . C B A B C B A . A C A B A C A B A C A B . B C B A B C . C A C B C A C B C A C B C A C B . B
A B C B A B C B A B C B A B C B A B C B A B C B A B C B A B C B . . A C B C A C B C A C B C A C B .
B A B C B A B C B A B C . C A C B C A C B C A C B C A . A B A C A . C B A B C B A B C B A B C B A B
. A C B C . B A C A B . B C B A B C B A B . A C B C A C B C A . . . . . C A B A C A B A . B A B C B
A B C B A B C B A B C B A . . . . . A C A B A C A B A C A . C A C B C A C B C A . A B A C . C B C

(b)

B C A C B C A C B C A . . . . . A C A B . B C B A B C B A B C . C A C B . B A B C B A B C B A B C B
A B C B A B C B A B C B A B C B A B C B A B C B A B C B A B C B . C A B A C . C B C A C B C A C B C A C B .
B A B C B A B C B A B C B A B C . C A C B . B C A C B C . B A C A . C B A B C B A B C . . . C A B A
C A B A C A B A C A . C B A B C B A B . . C A B A C A B A C A B . B C B A B C B A B C B A B C B A B
C B A B C B A . . . A C B C A C B C . B A C A B A . B C A C B C A C B C A C B C . . . C B C A C B C

(c)

B C . B A C A B . B C B A B C B A B C B A B C B A B C B A B C B A B C . C A C B . B A B C B A B C B
A B C B A B C B A B C B . C A B A C A B A C A B A C A B A C A B A C . C B C A C B C A C B C A C B C A C B .
B A B C B A B C B A B C B A B C B A B C B A B C B A . . C B C A C B C A C B . B A B C B A B C B A B
C B A B C B . C A B A C A B A C A . C B A B C B A B C B A B C B A B C B A B C B A B C B A B C B A B
C B A B C B A B C B . . A C B C A C B C A C B C A C B C A . A C B C A C B C A C B C A C B C A C B C

(d)

A B A C A B A C A B A C A B A C A B A C A B A C A . C B A B C B A . A B C B A B C B A B C B A B C B
A B C B A B C B A B C B A B C B A B C B A B C B A B C B . . A C B C A C B C A C B C A C B C A C B C A C . A
B C B A B C B A B C B A B C B . C A B A C A B A C A B A C A B A C A B A C A B A C . . B A B C B A B
C B . C A B A C A B A C A B A C A B A C A B A C A B A C A . C B A B C B A B C B A B C B A B C B A B
C B . C A B A C A B A C . C B C A C B C . B A C A B A C A B A C A B A C A B A . B C A C B C A C B C

of the chain and see if it repeats itself. If it does, then we continue till there is a mismatch (stacking fault). At the mismatch a blank (or a dot) is stored and we proceed with the comparison using the same number of layers, beginning immediately after the mismatch. If there is a mismatch, even before the set of layers has repeated once, we store a blank (or a dot) in the first layer of the initial set and start afresh with a set of layers (containing the given number of layers) immediately after the mismatch and proceed in the same fashion till we reach the end of the chain. We can search for order of any periodicity in a polytype chain (or a magnetic Ising chain) by employing this program. In our displays, we have searched for order in hk sequence and have later converted them into the ABC sequence.

II.4 Results and Discussion

The Monte Carlo simulation of polytypes reported here is based on the Theumann-Høye Ising chain. The interaction strengths are so chosen as to cover all regions of Theumann-Høye phase diagram (Fig. I.1), with one set of interaction strengths per region (actual values are the same as in Table I.1). We find that the actual numerical value of Δ (defined in the previous

section) does not alter the results of our calculations, as long as its absolute value is much larger than the absolute values of interaction strengths. In each region of the Theumann-Høye phase diagram, we have carried out a Monte Carlo simulation for a single temperature, this temperature corresponding to the lowest temperature in our calculations on the magnetic Ising chain (Chapter I). In all our calculations, H (Eqn. II.3.1) is taken to be zero; non-zero H would imply that, in the absence of interactions, the layers in the hexagonal and cubic configurations differ in stability.

In region I, the polytypic modification obtained was 3C (cubic close-packed structure). The 2H modification (hexagonal close-packed structure)* is also equally likely since for zero H, there is no preference between 'h' and 'k' configurations. By starting with a different random chain, we could well have obtained a 2H polytype. We would have expected these polytypic modifications, from our results on the magnetic Ising chain, for this region. A display of the actual polytype is given in Fig. II.2. We should also expect this polytype to show a first order phase transition. The high temperature

* 2H and 3C are the two extreme polytypic modifications of a substance.

Figure II.2. Display of Polytype Formed in Region I

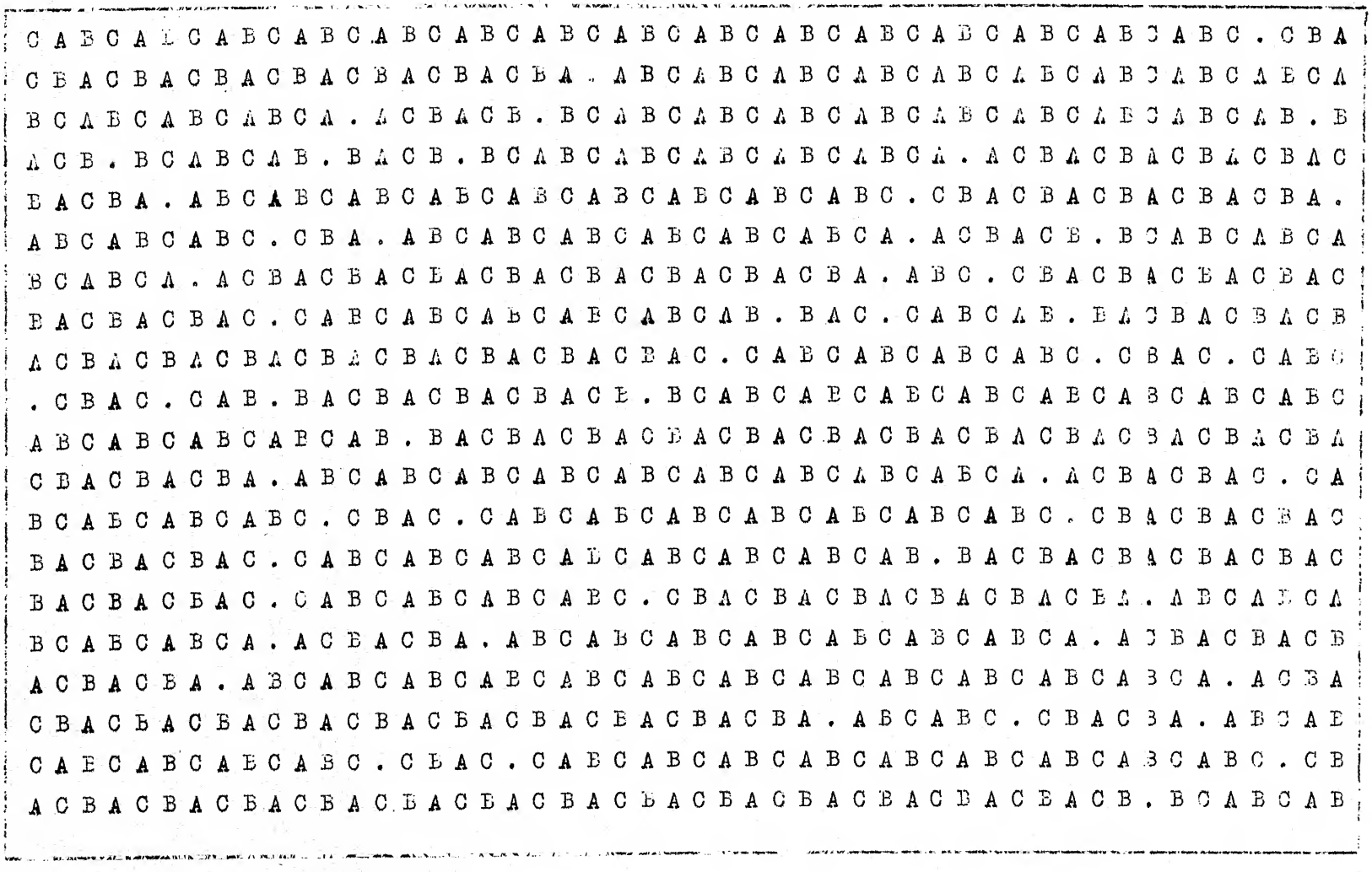

phase would have a short-range ordering of the type hhkk while the long-range order still remains the same (Fig. I.7).

In region II, the low temperature ordering of the layers corresponds to a 12R polytype (ABACBCBACACB). This is what we should expect from our studies of the magnetic Ising chain, since ↑↑↓↓ spin configuration corresponds to hh kk or kk hh layer configuration; both these lead to the same 12R polytype. A display of this polytype, obtained from our Monte Carlo simulation, is given in Fig. II.3. In this region, the magnetic Ising chain showed two phase transitions and the same would be expected of the polytype chain. We showed that, for the magnetic Ising chain, the short-range order remains essentially the same, while the long-range order changes, as the chain undergoes a phase transition. The same should be true in the case of the polytype as well. From Fig. I.13, we see that this transition implies a change in long-range ordering from 12R to 9R (ABCBCACAB) in the case of the polytype.

In region III, the polytype does not have a single ordering of layers throughout the chain. In some parts of the chain, the polytypic modification is 12R while in other parts, the polytypic modification is either 6H (BACBCA) or 9R (ABCBCACAB). Presence of different polytypic modifications in the same specimen has indeed

Figure II.3. Display of Polytype Formed in Region II

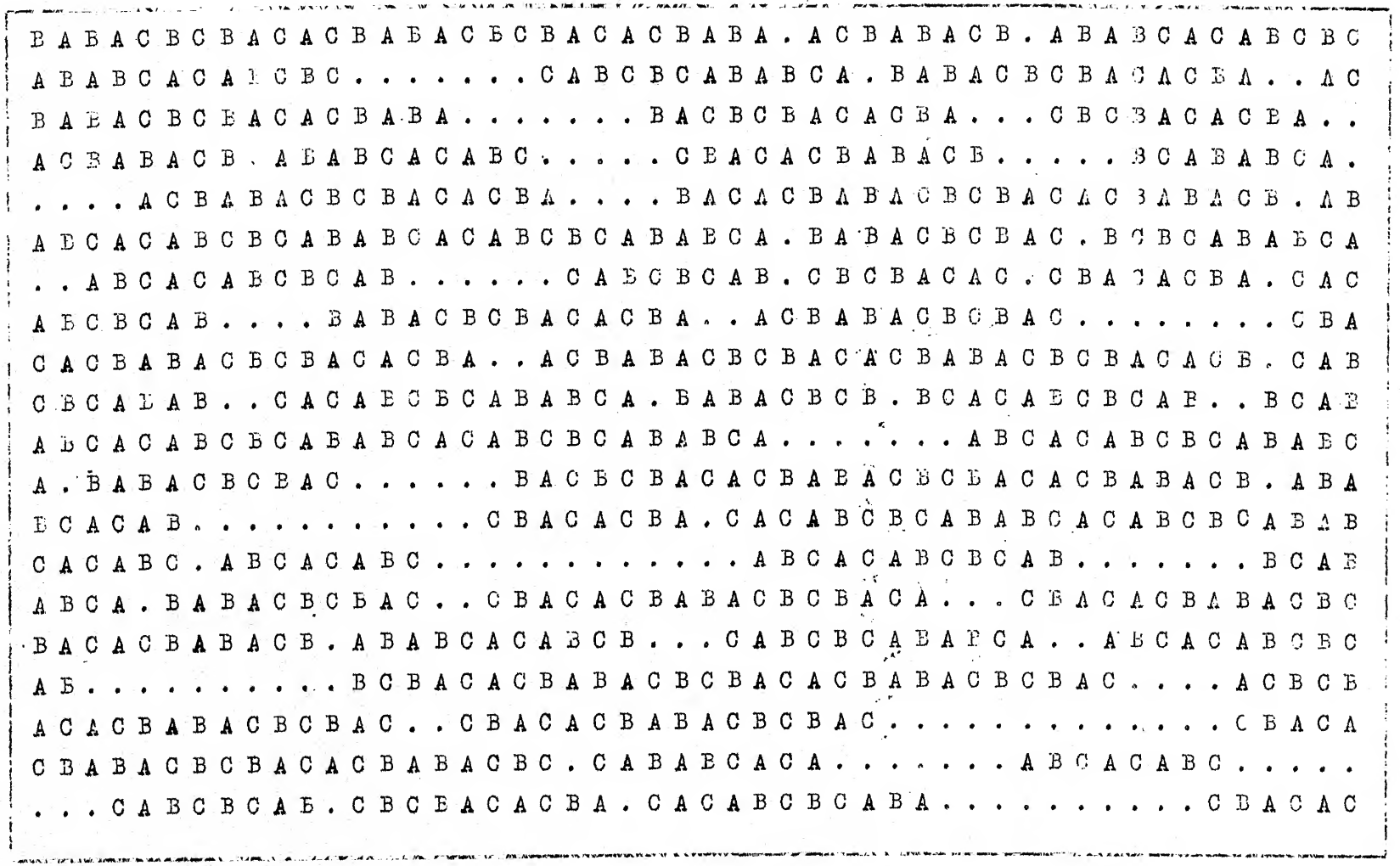

been observed experimentally in many systems. From our results on magnetic Ising chain, we should expect to see several second-order phase transitions in this region (though we are not in a position to comment on the changes in ordering).

The polytype obtained from region IV belongs to the 9R modification. Once again, like in region I, we could have instead obtained a 6H polytype. The 9R and 6H polytypes correspond to the +++ and ++- spin configurations, respectively. Display of the polytype formed in this region is given in Fig. II.4. The polytype formed in region V could be considered as a 9R modification with a large number of stacking faults. Similarly, the polytype from region VI was a 4H (ABAC) modification with a large number of stacking faults. Experimentally, such polytypes with a large amount of stacking faults are known to exist. Polytypes in these regions (IV, V and VI) are again expected to undergo several phase transitions. An increase in temperature will have the effect of increasing the concentration of stacking faults (as can be seen from the correlation functions in Chapter I) in conformity with experimental observations on polytypes.

We extended the range of short-range interactions up to fifth neighbour, in an attempt to generate longer period polytypes in our simulations. In this attempt,

Figure II.4. Display of Polytype in Region IV, in Field

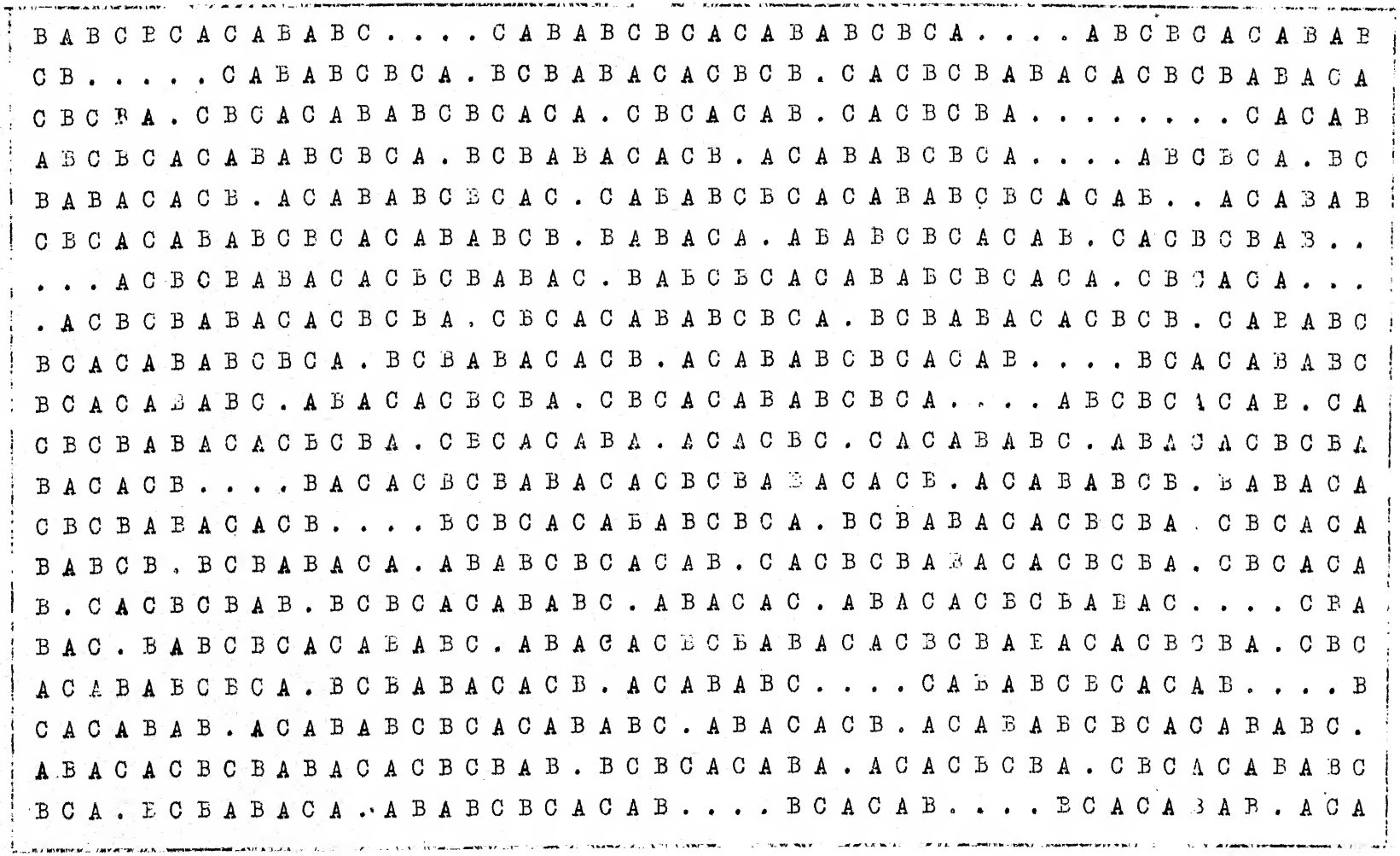

we experimented with different forms of short-range interaction potentials. These are shown in Fig. II.5. Simulations with interactions of the form 'a' and 'b' (given in the figure) resulted in 4H polytypes with varying amounts of disorder. It, therefore, appears that short-range interaction similar to these forms (potentials gradually decreasing with distance) are not responsible for formation of long-ordered polytypes. Simulation with the short-range interaction potential given by Fig. II.5c resulted in the formation of 12H polytypic modification (hhhkkk). A display of this polytype is given in Fig. II.6. Contrary to our expectations, an increase in the range of short-range interactions did not result in the formation of polytypes with longer periodicities (compared to the Theumann-Høye chain). The longest polytypes found by us were the 12R and 12H polytypes corresponding to a c-dimension of about 30 Å. This in itself is quite encouraging considering that we have not really focussed on carrying out calculations with various possible combinations of interaction parameters. It may be worthwhile to examine whether there are other forms of short-range interactions (together with equivalent-neighbour interaction) which give rise to polytypes with very large periodicities compared to those encountered in the present study.

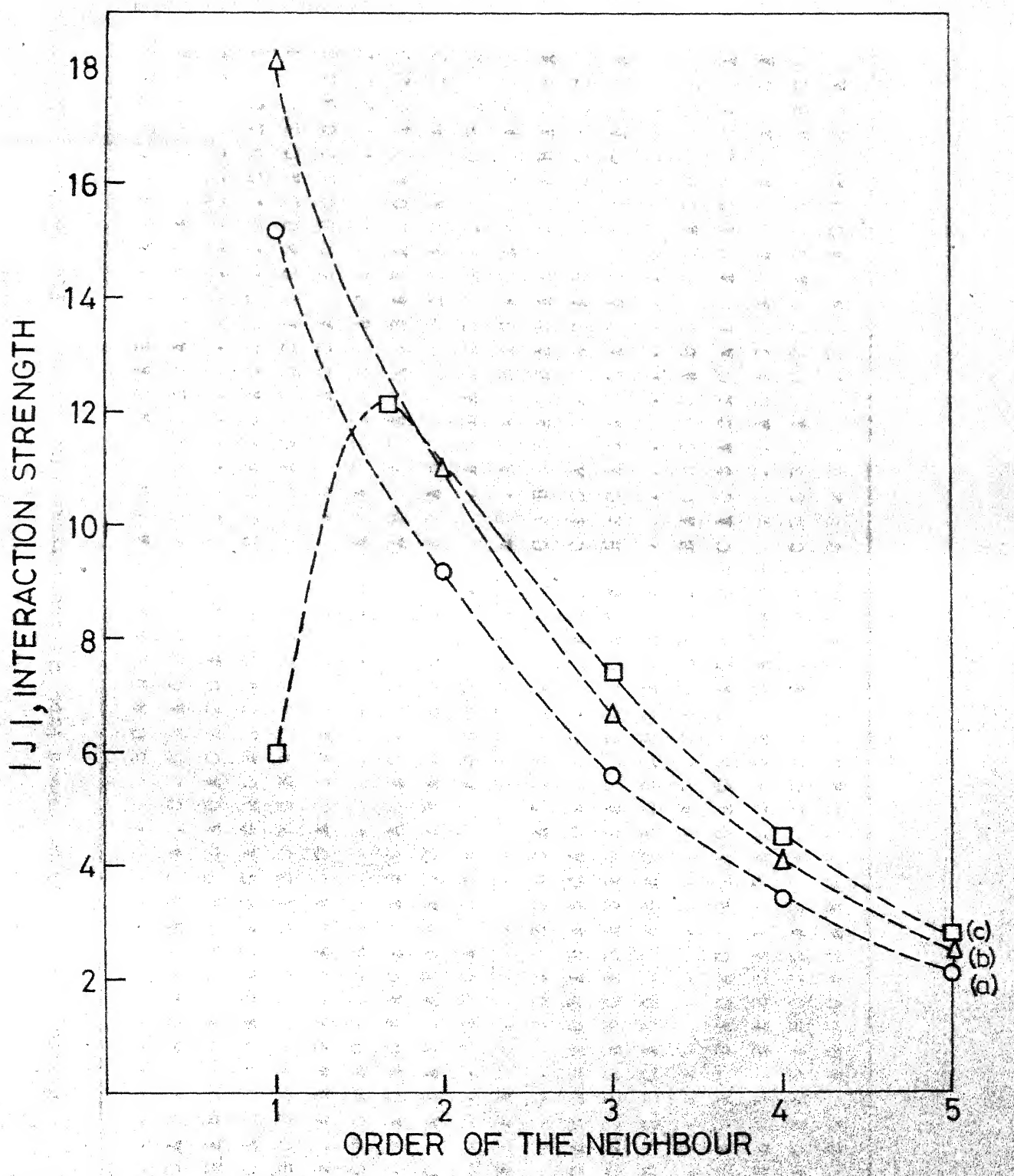

Fig. II.5. Different forms of short-range interactions used in our attempt to generate long period polytypes.

Figure II.6. Polytype Formed From the Short-range Interaction of Fig. II.5c

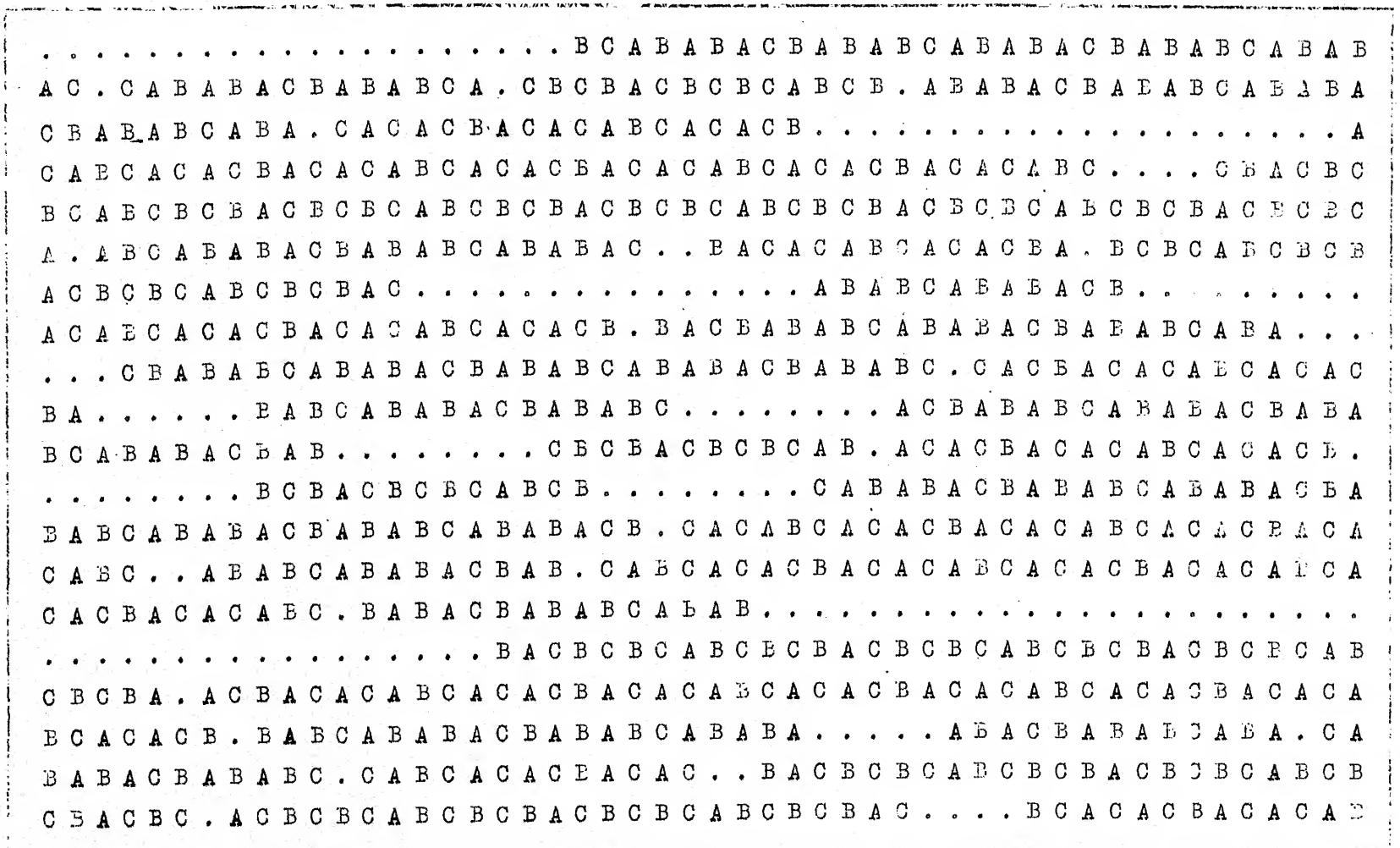

II.5 Summary

Since polytypic modifications of a substance differ from one another in the stacking sequence of layers in one direction (c), we can treat them essentially as one-dimensional systems. A polytype can, in fact, be considered as a spin-half Ising chain since only two possible configurations for a layer exist, viz., the hexagonal and the cubic. Existence of polytypes seems to contradict Gibbs' phase rule because polytypes far in excess of the maximum number of phases allowed by the phase rule are known to be stable under identical conditions of temperature and pressure. Furthermore, in one-dimensional systems, unless there is an infinite-range interaction, there does not exist any long-range order above absolute zero. Thus, polytypes seem to have a behaviour similar to that exhibited by the Theumann-Høye Ising chain studied in Chapter I. The long-range interaction term used in the Theumann-Høye Ising chain is justified for polytypes, if we assume that the layers in the two configurations 'h' and 'k' have different thicknesses. Although we do not have any real justification for using the short-range interaction terms of Chapter I, we feel that this may be related to growth conditions.

To carry out a Monte Carlo simulation of polytypes, we must have a mechanism for rearranging the layers in analogy to the spin-flip mechanism used in magnetic Ising chains. To extend our results of magnetic Ising chains to polytypes, we should arrive at a physically meaningful mechanism capable of connecting any two states of a polytype, with a probability which is about the same as the probability with which spin-flip mechanism connects the two corresponding states of a magnetic Ising chain. We have studied three different layer rearrangement mechanisms, viz., (i) single layer mechanisms (e.g., ABBABC → ABCABC), (ii) layer transposition mechanism (e.g., ABCACB → ACBACB) and (iii) general two layer mechanism (e.g., ABCACB → ABCBCB or ABABCB). We find that the general two layer mechanism satisfies the criteria set forth viz., it is physically meaningful and ergodic.

We have carried out a direct simulation of polytypes for one value of temperature and for interaction strengths corresponding to different regions of Theumann-Høye phase diagram (Fig. I.1). We observe different polytypes in different regions as expected. The various polytypes observed are 4H, 6H, 9R and 12R, in addition to the basic 2H and 3C polytypes. In region III, the polytypic chain showed 12R ordering in some sections (of the chain) and 9R or 6H in some others, an observation supported by experiments (syntactic coalescence). To effectively generate

different polytypes on different parts of a chain, we should deal with longer chains and take them through larger number of Monte Carlo cycles. These are expected to undergo phase transitions by analogy with the magnetic Ising chain. Associated with these phase transitions, we should observe changes in long-range order. We also simulated polytypes with different forms of short-range interaction, extended upto fifth neighbour, in an attempt to generate polytypes with longer periodicities. This was not very successful and the longest polytype observed in this study was a 12H polytype.

The origin of short-range interaction terms used in the present study is still to be understood. However, an understanding of the mechanism of layer rearrangements together with Monte Carlo simulations provides a means of directly verifying the formation of polytypes from a proposed interaction model. We can also use this method to simulate different sets of growth conditions and study the formation of polytypes under any given set of growth conditions. In the present stage of our study, we have not concerned ourselves with the formation of growth spirals on the crystal faces of most of the polytypes.

References

1. A. R. Verma and P. Krishna, 'Polymorphism and Polytypism in Crystals', John Wiley, New York (1966).

2. A. R. Verma and G. C. Trigunayat, in 'Solid State Chemistry', C. N. R. Rao (Ed.), Marcel Dekker, Inc., New York (1974).

3. W. F. Knippenberg, Philips Res. Repts., 18, 161 (1963).

4. J. Friedel, in 'Solid State Physics', Vol. 3, F. Seitz, D. Turnbull and H. Ehrenreich (Eds.), Academic Press, New York (1956).

5. P. W. Anderson and S. T. Chui, Phys. Rev., B9, 3229 (1974).

6. J. C. Phillips, Rev. Mod. Phys., 42, 317 (1970).

7. W. K. Theumann and J. S. Høye, J. Chem. Phys., 55, 4159 (1971).

8. L. S. Ramsdell and J. A. Kohn, Acta Cryst., 5, 215 (1952).

9. A. R. Verma, Phil. Mag., 42, 1005 (1951).

10. F. C. Frank, Phil. Mag., 42, 1014 (1951).

11. V. Vand and J. I. Hanoka, Mat. Res. Bull., 2, 241 (1967).

12. E. Alexander, Z. H. Kalman, S. Mardix and I. T. Steinberger, Phil. Mag., 21, 1237 (1970).

13. H. Jagodzinski, Acta Cryst., 7, 300 (1954).

14. H. Jagodzinski, Neues Jahrb. Mineralk., 3, 49 (1954).

15. C. J. Schneer, Acta Cryst., 8, 279 (1955).

CHAPTER III

MODELS FOR LOW SPIN-HIGH SPIN TRANSITIONS IN SOLIDS

III.1 Introduction

When a transition metal ion is placed in a crystal field, the shift in energies of the various terms, with changes in crystal field strength is given by the Tanabe-Sugano[1-3] diagrams. For some configurations (d^4, d^5, d^6 and d^7), the diagram predicts a crossover in the ground state from a spin state with a lower multiplicity to a spin state with a higher multiplicity, with change in crystal field strength. In systems where the crystal field strength lies close to the crossover points, a thermal equilibrium may be established between the low-spin states and the high-spin states. Such a spin-state equilibrium in a system gives rise to interesting magnetic behaviour. Existence of a spin-state equilibrium was first established in the iron (III) complex, Fe (dimethyl dithiocarbamate)$_3$.[2]

Recently, some coordination compounds of iron (II) (d^6 configuration) have been studied in detail in the solid state.[4-7] These complexes seem to undergo gradual or abrupt changes in the spin-state populations, often accompanied by a phase transition. The nature of this phase transition is, however, not well understood. Spin-state transitions have also been observed in inorganic solids such as MnAs and MnP,[8,9] Co_2O_3,[10] $LaCoO_3$,[11,12] $HoCoO_3$[13] and other rare earth orthocobaltites. Spin-state transitions in some of these inorganic solids, unlike in the case of the coordination complexes, are associated with structural phase transitions. Particularly interesting are the spin-state transitions in $LaCoO_3$ and $HoCoO_3$. The transitions in these two systems are associated with an unusual structural phase transition[14] in which the high-temperature phase is of lower symmetry than the low-temperature phase.* The low-temperature phase in the case of these cobaltites, has a residual high-spin population. The spin-state transition in these cases is either gradual or abrupt and in the high-temperature region, the populations of the low-spin and high-spin states are found to be nearly equal. The spin-state transition in the cobaltites is followed by an ordering transition resulting in the symmetry change. In the ordering region of MnAs, MnP and the rare

*$PrAlO_3$[15] is another system in which the high-temperature phase has a lower symmetry than the low-temperature phase.

earth cobaltites a plateau is observed in the inverse magnetic susceptibility versus temperature curve.

Although some macroscopic approaches have been employed to explain spin-state transitions in solids with some reasonable success, particularly in the case of coordination compounds, a satisfactory microscopic model for these phase transitions is still lacking. To explain the phase transition in $LaCoO_3$, Bari and Sovardiere[16] extended Chestnut's theory[17] for first order singlet-triplet transitions in radical salts of TCNQ. Bari[18] also proposed a two-sublattice model to explain the change in symmetry following the change in spin-state population. However, these models are not successful in explaining the observed behaviour near the transitions in $LaCoO_3$, $HoCoO_3$ and related systems. A successful model for spin-state transition should be able to explain the following observations: (i) smooth as well as abrupt changes in the spin-state population ratio with temperature, (ii) the occurrence of thermodynamically first or second order structural transitions in the system and (iii) non-zero population of high-spin states at low temperatures, found in some systems. Besides in the rare earth cobaltite systems, plateau in the inverse magnetic susceptibility versus temperature curve as well as the unusual structural transition resulting in a lower symmetry high-temperature phase also need be explained.

Because of considerable experimental interest in this laboratory in spin-state transitions, we decided to examine some models to explain such a transition. In this chapter, we present results of our investigations of some new models for high-spin-low-spin transition in solids. We have been able to show that the coupling assumed in Bari's model is incapable of producing a phase transition if we consider the dynamics of the lattice. To explain residual population of the high-spin state at low temperatures, we have studied a model in which the crystal field strength is quadratically coupled to the lattice displacement, with the coupling capable of mixing the spin states. This model predicts a residual high-spin population at low temperatures, although, like in the previous case, it does not exhibit any phase transition and only shows a gradual variation of the ratio of the two spin-state populations with temperature. Since a structural transition is associated with the spin-state transition in systems of our interest, we have obtained a free energy expansion in terms of displacement by employing the path integral method to evaluate the partition function. (Details of the method are given in the Appendix.) In the two-sublattice case with linear coupling, we observe a second order phase transition with a gradual change in high-spin-low-spin population ratio, as a function of the order parameter over each sublattice. We have studied a two-sublattice model with cubic

coupling of the spin states to the lattice and we find that this system is capable of giving a thermodynamically first order structural transition. A two phonon model has also been studied by us. In this model the spin-states are coupled linearly to the breathing mode and quadratically, with mixing, to the optical (ion versus octahedral cage) mode. This model shows a phase transition and the ratio of spin-state populations depends upon the order parameter. Further it also shows a non-zero high-spin state population at absolute zero.

In the next section, we give brief review of the experimental situation in spin-state transition in solids.

III.2 Spin-State Transitions in Solids - The Experimental Situation

Spin-state transitions in coordination complexes of iron (II) have been studied extensively. Sorai and Seki[7] observed heat capacity anomalies in the iron (II) complexes $[Fe(Phen)_2(NCS)_2]$ and $[Fe(Phen)_2(NCSe)_2]$ at 176 K and 231 K respectively. The inverse susceptibility versus temperature plots show a plateau around the temperatures at which the heat capacity anomalies are observed. The respective effective magnetic moments show abrupt jumps at these temperatures. The infrared spectra of these compounds show interesting variations with temperature. The spectra of the sulphur

complex show a doublet (ν_{C-N}) centred around 2068 cm^{-1} at low temperatures. As the temperature is increased, another doublet centred around 2110 cm^{-1} appears. The intensity of the low-temperature doublet decreases with increasing temperature while the high-temperature doublet shows the opposite trend. The positions of the doublets remain unchanged with temperature. The results are explained on the basis of a spin-state transition in these systems. The infrared studies indicate that the energy separation between the two spin states remains the same at all temperatures.

Direct evidence of spin-state transitions have been obtained by Mössbauer studies.[4,5] Low-spin and high-spin Fe(II) ions have different isomer shifts thus making possible, separate quantitative study of the individual spin states. The iron (II) complex $[Fe(4,7\text{-}(CH_3)_2\text{-Phen})_2(NCS)_2]$ and $[Fe(Papt)_2]$ (Papt = 2-(2-pyradilamino)-4-(2-pyridyl)thiazolate) have been studied employing Mössbauer spectroscopy. The studies reveal that $[Fe(4,7\text{-}(CH_3)_2\text{-Phen})_2(NCS)_2]$ undergoes an abrupt low-spin-high-spin transition while $[Fe(Papt)_2]$ undergoes a smooth spin-state transition. $[Fe(Papt)_2]$ also shows a residual population of the high-spin state at low temperatures. The spin-state population in $[Fe(4,7\text{-}(CH_3)_2\text{-Phen})_2(NCS)_2]$ is known to show hysteresis behaviour with temperature[6] (indicative of a structural transition). However, no definitive structural transition appears to have been reported to accompany a spin-state transition in any of the coordination complexes.

Among simple inorganic solids, MnAs and MnP[8,9] are the first solids in which spin-state transitions were observed. MnAs exhibits two structural phase transitions which are also associated with changes in magnetic properties. The phase transition around 315 K is a first order transition with a change in structure from $B8_1$ to B31. The second phase transition occurs around 400 K and the structure changes from B31 to $B8_1$. The low-temperature $B8_1$ phase is ferromagnetic ($\mu_{Mn} = 3.4\ \mu_B$) and the high-temperature $B8_1$ phase is paramagnetic ($\mu_{eff} = 4.95\ \mu_B$). The B31 phase does not exhibit any magnetic ordering and in this region the inverse susceptibility versus temperature curve has a negative slope. These results have been qualitatively explained by Goodenough, Ridgley and Neuman,[9] on the basis of a spin-state transition brought about when the energy parameters occurring in the band diagrams (of MnAs in $B8_1$ and B31 phases) satisfy certain inequalities.

Cobalt sesquioxide, Co_2O_3, is another system where a spin-state transition has been observed. The ionic radius of high-spin cobalt (III) is significantly larger than the ionic radius of low-spin cobalt (III). Co_2O_3 synthesised at high pressure[10] thus has all the cobalt ions in a low-spin state. On annealing Co_2O_3 at 673 K, the crystal changes from a hexagonal structure to a corundum structure with 6.7% increase in volume. Comparison with X-ray pattern of α-Fe_2O_3

indicates that all the cobalt ions in the corundum structure are in the high-spin state. Although this transformation has not been reversed or fully characterized, it appears that this transition in Co_2O_3 represents a first order spin-state transition.

The rare earth cobaltites that have been studied so far can be classified into two categories. The first category in which the low-spin Co^{3+} ions first transform to the high-spin state upto a temperature, followed by formation of 2^+ and 4^+ oxidation states of cobalt arising from charge-transfer between the two spin states of trivalent cobalt and the second category where low-spin Co^{3+} ions transform to the high-spin state upto a temperature and then exhibit a constant proportion of the two spin states upto high temperatures. The cobaltites belonging to the first category are $LaCoO_3$,[11,12,24] $NdCoO_3$,[19,24] $EuCoO_3$,[20,25] $GdCoO_3$[19,24] and $YCoO_3$.[21,24] The cobaltites that belong to the second category are $HoCoO_3$,[13,24] $ErCoO_3$,[21,24] $YbCoO_3$[22] and $LuCoO_3$.[22,23] In addition to these, cobaltites of praseodymium and Dysprosium have also been studied.[24] In Table III.1 we have given a brief summary of spin-state transition studies carried out on the various rare earth cobaltites (including $YCoO_3$). Only cobaltites belonging to first category show thermal anomalies (e.g., differential thermal analysis curves) around the spin-state transitions implying that the spin-state transition is followed

Table III.1

Spin-State Transitions in Rare Earth Cobaltates
Transition temperatures, K from

	DTA	X-ray[a]	Magnetic susceptibility[b]	L-M factor[c]	Center shift[d]	$[Co^{3+}]$[e]	ΔH[f], Kcal mol^{-1}
$LaCoO_3$ [12,24]	680	500	620	650	650	1.0	0.2 or much greater[g]
$NdCoO_3$ [19,24]	600	580	600	-	400	0.8	≤ 0.2
$EuCoO_3$ [20,25]	-	600	600	600	600	0.8-0.9	< 0.1
$GdCoO_3$ [19,24]	530	450	550	500	600	1.3	0.1-0.2
$YCoO_3$ [21,24]	650	700	520		650	0.8	0.2
$HoCoO_3$ [13,24]	-	325	300	300	300	1.0 (rises from a non-zero value)	<0.1
$ErCoO_3$ [21,24]	600	600	600	-	550	1.0 (rises from a non-zero value)	<0.2
$LuCoO_3$ [22,23]	-	540	450	-	-	1.0 (rises from a non-zero value)	<0.1

[a] From Debye-Waller factor data; [b] Temperature corresponding to the beginning or end of plateau region in the $1/\chi$-temperature curve; [c] from Lamb-Mössbauer factor data; [d] Temperature where the Mössbauer centre shift decreases markedly; [e] Relative proportion of high-spin Co^{3+} at DTA transition temperature; [f] values from DTA; [g] ΔH seems to depend on method of preparation. The transition could indeed be thermodynamically first order, particularly in $LaCoO_3$ prepared by cobalticyanide decomposition.

by a phase transition. The ΔH values of the endothermic transitions (when observed) are generally small (Table III.1); such ΔH values could imply occurrence of second order transitions. Another general feature of the spin-state transitions in the cobaltites is that around the transition temperature, the ratio of high-spin population to the population of other spin states is unity[26] (Table III.1). In the rest of this section we shall confine ourselves to a discussion of relevant studies on $LaCoO_3$ and $HoCoO_3$ as these are representative of the two typical categories mentioned earlier.

Systematic studies on $LaCoO_3$ were first carried out by Raccah and Goodenough[11] and later by Bhide, Rajoria, Rao and Rao.[12] These investigators found a plateau in the inverse susceptibility versus temperature curve in the region $400\ K < T < 650\ K$. The variation of inverse susceptibility with temperature is found to be linear in the regions $4.2\ K < T < 400\ K$ and $650\ K < T < 1200\ K$, although the slopes in the two regions differ. The unusual magnetic behaviour suggested the existence of two different spin states of cobalt ion in equilibrium. The DTA curve shows a broad endothermic peak around 680 K indicating a phase transition in the system. X-ray diffraction studies[11] show that the space group symmetry of $LaCoO_3$ changes at 650 K from $R\bar{3}C$ (below 650 K) to $R\bar{3}$ (above 650 K). Below 650 K, there is only a single O-Co distance while at 650 K the O-Co distance

versus temperature curve branches, indicating two distinct O-Co distances, above 650 K. The volume of the unit cell does not show any significant change at this temperature though the volume versus temperature plot shows changes in slope at 400 and 650 K. Debye-Waller factor (from X-ray measurements) shows abrupt changes at 400 K and 650 K. In the temperature region 400 K < T < 650 K, short-range ordering of two different types of cobalt ions is suggested based on the Debye-Waller factor studies.

The variation in spin-state equilibrium as a function of temperature was studied by Bhide et al.,[12] employing Mössbauer spectroscopy taking ^{57}Co diffused $LaCoO_3$ as the Mössbauer source and $K_4Fe(CN)_6.3H_2O$ as the absorber. It is assumed that the decay does not affect the spin-state of the ion i.e. a high-spin Co^{3+}, on decay, gives a high-spin Fe^{3+} and similarly a low-spin Co^{3+} gives a low-spin Fe^{3+}. Mössbauer spectra of $LaCoO_3$ show a doublet with isomer shifts 0.0 ± 0.04 mm/sec and 0,45 ± 0.04 mm/sec and can be safely assigned to the two spin states of Co^{3+} ion. The ratio of the high-spin population to low-spin population has been obtained from intensity measurements in the temperature region 4.2 K < T < 1200 K. This ratio is also calculated from the susceptibility data and these are shown in Fig. III.1a. The susceptibility studies indicate that the high-spin ion population increases with temperature upto 1200 K while Mössbauer

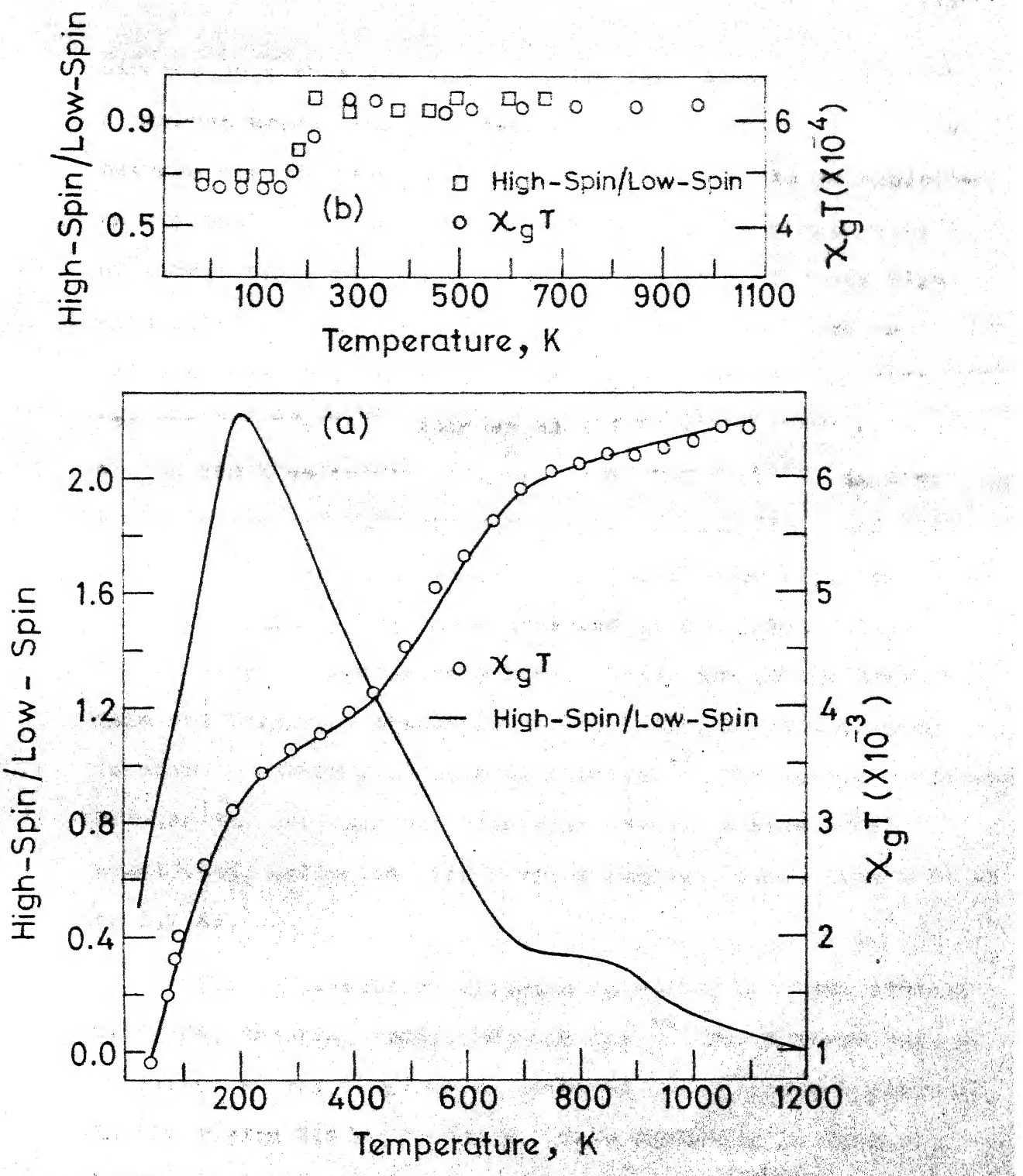

Fig. III.1. Comparison of the variation of high-spin-low-spin population ratio with temperature, obtained from Mössbauer and susceptibility data ($\chi_g T$ is related to the population ratio), in the case of (a) $LaCoO_3$ and (b) $HoCoO_3$.

studies show that the high-spin ion population goes through a maximum around 200 K to zero at 1200 K. This discrepancy between the Mössbauer and susceptibility results is explained on the basis of charge transfer between the two spin states of cobalt (III) resulting in low-spin cobalt (II) and high-spin cobalt (IV). The latter pair of ions also have an isomer shift of nearly 0 mm/sec and overlap with low-spin cobalt (III) resonance. Mössbauer studies also indicate a phase transition around 650 K as evidenced by (i) a marked decrease in the centre shifts of both the spin states around 650 K and (ii) dips in Lamb-Mössbauer factor-temperature curves at 400 K and 650 K, similar to those observed in the Debye-Waller factor versus temperature curves. Existence of the low-spin and high-spin states of cobalt (III), in equilibrium, is also confirmed from optical studies.[27] The energy difference between the low-spin and high-spin states in rare earth cobaltites, estimated from various studies, range from 0.01 eV to 0.2 eV.

The spin-state equilibrium in $HoCoO_3$ has been studied by Bhide, Rajoria, Reddy, Rao and Rao.[13] The inverse susceptibility versus temperature curve of $HoCoO_3$ shows a plateau in the region 250 K < T < 300 K. This variation is linear, below 250 K and above 300 K, although the slopes in these two regions are different. This behaviour suggests a spin-state equilibrium in the system. The DTA curve of $HoCoO_3$ does not

show any peak around the plateau region and hence no definite phase transition is associated with the spin-state transition. Detailed X-ray investigations have not been carried out on $HoCoO_3$ and so no definite structural transition has been established, unlike in the case of $LaCoO_3$. However, Debye-Waller factor versus temperature curve exhibits breaks around 300 K and 600 K, although the X-ray unit cell volume varies smoothly with temperature in the interval 300 K < T < 1200 K.

Mössbauer spectra of $HoCoO_3$ show doublets, corresponding to the high-spin and low-spin states of trivalent cobalt, in the region 78 K < T < 800 K. From intensity measurements, it was found that the ratio of high-spin population to low-spin population is constant at ~0.7, below 300K. Around 300 K, this ratio shows an abrupt jump to a value ~1.0 and above 300 K, the ratio remains constant at this value. The spin-state population ratio obtained from susceptibility measurements agrees with the Mössbauer data (Fig. III.1b). Thus, unlike in the case of $LaCoO_3$, we need not postulate charge transfer between different spin states of cobalt (III), in $HoCoO_3$. Center shifts of the two spin states of $HoCoO_3$ show a marked decrease around 250 K and Lamb-Mössbauer factor variation with temperature closely follows the temperature variation of X-ray Debye-Waller factor. These results point to an ordering transition in $HoCoO_3$, similar to that observed in $LaCoO_3$.

Temperature dependent resistivity and Seebeck coefficient measurements have been carried out on rare earth cobaltites. The variations of these properties with temperature reflect the changes in the nature of cobalt states found by Mössbauer and susceptibility measurements. The rare earth cobaltites are p-type semiconductors at room temperature and undergo a semiconductor ⇄ metal transition at high temperatures (~1200 K), an aspect of considerable interest but not of direct relevance to the present discussion. In the next section we give a brief introduction to the models of Chestnut,[17] Bari and Sivardiere.[16,18]

III.3 Earlier Models for Low-Spin-High-Spin Transition in Solids

In order to explain the first-order transition between singlet and triplet states of radical salts of TCNQ, Chestnut[17] considered a model system consisting of N molecules, n of which are excited to a state of degeneracy ν. The internal energy of the system was assumed to be of the form,

$$\frac{E}{N} = \rho\varepsilon_o + \frac{1}{2}\varepsilon_1 \rho^2, \qquad \text{(III.3.1)}$$

where ε_o and ε_1 are parameters* of the model and $\rho = n/N$ is the particle density. The entropy of this system is given by,

$$\sigma/N = \rho \ln\nu - \rho \ln\rho - (1-\rho) \ln(1-\rho) \qquad \text{(III.3.2)}$$

* ε_o is the single particle energy required to create an excitation. The term in ε_1 can arise either due to particle-particle interaction in the excited state or due to a deformation of the lattice caused by the excitations.

Thus, the free energy of the system can be written as

$$\frac{F}{N} = \varepsilon_o \rho + \frac{1}{2} \varepsilon_1 \rho^2 - \frac{1}{\beta} \left[\rho \ln \nu - \rho \ln \rho - (1-\rho) \ln (1-\rho)\right]. \qquad \text{(III.3.3)}$$

Free energy is minimized with respect to ρ to obtain the equilibrium value of ρ as

$$\rho = \nu / \{\exp \left[\beta(\varepsilon_o + \varepsilon_1 \rho)\right] + \nu\}, \qquad \text{(III.3.4)}$$

together with the condition

$$\frac{1}{N} \frac{d^2 F}{d\rho^2} = \varepsilon_1 + \frac{1}{\beta \rho} \frac{1}{(1-\rho)} > 0 . \qquad \text{(III.3.5)}$$

When the equations (III.3.4) and (III.3.5) are solved, for various values of ε_o, ε_1 and $\nu > 1$, below a certain value of $(-\varepsilon_1/\varepsilon_o)$, ρ shows a gradual increase with temperature while above this value of $(-\varepsilon_1/\varepsilon_o)$, two equally stable minima are observed at a transition temperature. Above the transition temperature a higher value of ρ is preferred. The limiting value of ρ, as $T \to \infty$, is $\nu/(\nu+1)$. The jump in particle density, from ρ_1 to ρ_2, at the transition temperature is characterized by a symmetry around $\rho = 0.5$.

Bari and Sivardiere[16] extended Chestnut's model to explain low-spin-high-spin transition in solids and chose the Hamiltonian*,

---

* This Hamiltonian gives exactly the same form for internal energy, as assumed by Chestnut (eq. III.3.1). This can be seen by carrying out the displaced oscillator transformation $Q = \bar{Q} + (V/2\xi N) \sum_i n_i$ on this Hamiltonian.

$$H = N\xi Q^2 + \sum_i (\Delta - VQ)\, n_i, \qquad \text{(III.3.6)}$$

to describe the system. In eqn. (III.3.6) $n_i=0$ refers to the low-spin state and $n_i=1$ to the high-spin state, Q is a measure of the distance between the ion in question and its neighbours, ξ is an elastic constant and $(\Delta - VQ)$ is the energy gap between the two spin states. The model for low-spin-high-spin transition described by eqn. (III.3.6) shows exactly the same behaviour as the Chestnut model. Thus the model does not give any information about the change in symmetry. It also predicts a zero high-spin population at T=0 K. The saturation value of high-spin to low-spin population ratio predicted by this model for the case of cobalt (III) is 15 while from sec. III.2 we see that in cases of saturation the observed ratio is $\sim$1. This model gives a good qualitative description of the spin-state transition observed in transition metal complexes. Bari and Sivardiere introduced magnetic interaction between high-spin states, into the Hamiltonian (eqn. III.3.6) and observed interesting phase behaviour including 'heat magnetization'.[28,29] However, the model with magnetic interactions is also incapable of explaining some of the basic features of the transition in cobaltites (see section 1).

Bari,[18] Bari and Sivardiere[16] put forth a two-sublattice model to explain the change in symmetry observed in cobaltites. In the notation of eqn. (III.3.6), the model considered was,

$$= N \xi Q^2 + \sum_{i \in A} (\Delta - VQ)\, n_i + \sum_{i \in B} (\Delta + VQ) n_i \quad \text{(III.3.7)}$$

This model, in addition to the phase transition between low-spin and high-spin states, also shows a first or second order phase transition to a two-sublattice structure. This ordering transition is followed by a first or second order (if the preceding transition is second order, this transition is necessarily second order) low-spin-high-spin transition. This prediction is contrary to the experimental observation, where initially we observe a low-spin-high-spin transition and this is accompanied or followed by an ordering transition.

III.4 Models for Spin-State Transition Investigated in the Present Study

III.4.1 Dynamic Coupling Model : The models of Bari and Sivardiere are static models. To treat the lattice participation in a more complete manner, we have to incorporate the kinetic energy of the lattice into the Hamiltonian of the model. In order to examine the effect of the kinetic energy term on the phase transition, we shall consider the following one-sublattice model:

$$H = AI + B\,\sigma_z,$$
$$A = \frac{p_Q^2}{2M} + \frac{M \omega_b^2 Q^2}{2}, \quad B = \Delta + VQ, \qquad \text{(III.4.1)}$$

where I is the 2x2 unit matrix, σ_z is the familiar Pauli spin

matrix. The eigenstates of σ_z represent the low-spin and high-spin states of the transition metal ion. Q is the displacement caused by the appropriate normal mode (breathing mode). The low-spin and high-spin states are located at $-(\Delta + VQ)$ and $(\Delta + VQ)$ respectively. P_Q, M and ω_b have their usual meaning. For the present we shall assume that the low-spin and high-spin states are non-degenerate.

The partition function of this model is given by,

$$Z = \mathrm{Tr}\, e^{-\beta H} \qquad \text{(III.4.2)}$$

where, from eq. (III.4.1) we have

$$H = \begin{bmatrix} A+B & 0 \\ 0 & A-B \end{bmatrix} . \qquad \text{(III.4.3)}$$

Since the operator H is diagonal*, we can write the partition function as

$$Z = \mathrm{Tr} \begin{bmatrix} e^{-\beta(A+B)} & 0 \\ 0 & e^{-\beta(A-B)} \end{bmatrix} \qquad \text{(III.4.4)}$$

$$= \mathrm{Tr}\; e^{-\beta(A+B)} + \mathrm{Tr}\, e^{-\beta(A-B)} \qquad \text{(III.4.5)}$$

Thus, to calculate the partition function, we should first obtain the eigenvalues of (A+B) and (A-B). The operator (A+B), written more explicitly as

$$\frac{P_Q^2}{2M} + \frac{M \omega_b^2 Q^2}{2} + \Delta + VQ ,$$

*A function of a diagonal matrix is identically equal to the diagonal matrix formed by the functions of the diagonal elements.

can be trivially cast into the form of harmonic oscillator Hamiltonian by the transformation,

$$Q = Y - \frac{V}{2M\omega_b^2} \qquad \text{(III.4.6)}$$

The resulting operator is

$$(A+B)' = \frac{p_y^2}{2M} + \frac{M\omega_b^2 Y^2}{2} + \left(\Delta - \frac{V^2}{(2M\omega_b^2)^2}\right) . \qquad \text{(III.4.7)}$$

Hence we see that the eigen values of the operator $(A+B)$, are the same as that of a harmonic oscillator of fundamental frequency ω_b, with the zero of the energy shifted by $\Delta - V^2/(2M\omega_b^2)^2$. Similarly the eigen values of the operator $(A-B)$ are the same as that of a harmonic oscillator of fundamental frequency ω_b, with the zero of the energy shifted by, $-\Delta - V^2/(2M\omega_b^2)^2$. We can now write the partition function Z of eqn. (III.4.2) as

$$Z = 2\, Z_{vib}(\omega_b)\, e^{\frac{\beta V^2}{(2M\omega_b^2)^2}} \cosh(\beta\Delta) . \qquad \text{(III.4.8)}$$

This partition function being analytic, does not show any phase transitions. The mean displacement $\bar{Q} = \langle Q \rangle$ varies smoothly with temperature*. The difference in high-spin and low-spin population also varies gradually with temperature and is given by

$$\langle \sigma_z \rangle = -\tanh(\beta\Delta) . \qquad \text{(III.4.9)}$$

*This is easily calculated since the displacement can be written as a sum of phonon-creation and annihilation operators.

We see from this that the spin-state population ratio goes to unity at high temperature. The magnetic susceptibility calculated from this ratio varies smoothly as $\beta\,[1-\tanh(\beta\Delta)]$. If we consider the high-spin state to be ν-fold degenerate, the partition function of the system then would be given by

$$Z = \nu\ \mathrm{Tr}\ e^{-\beta(A+B)} + \mathrm{Tr}\ e^{-\beta(A-B)}. \qquad \text{(III.4.10)}$$

This partition function is also analytic. The mean displacement of the lattice, $\langle Q \rangle$, again shows smooth variation and the difference of low-spin and high-spin populations also shows a smooth variation. These results show that the kinetic energy term washes out the transition in the case of one-sublattice model.

The above result is quite general, in that any linear coupling of the crystal field strength to the lattice, is incapable of leading to a phase transition. This can be shown by considering a model with an arbitrary linear coupling of the crystal field strength to the lattice. Hamiltonian of such a system, in the second quantization notation, can be written as

$$H = \left(h \sum_k \omega_k\, b_k^*\, b_k\right) I + (\Delta + VX)\,\sigma_z\ , \qquad \text{(III.4.11)}$$

where b_k and b_k^* are the phonon annihilation and creation operators and X is a general displacement.* Any general

*For purpose of convenience, this displacement is taken to be the displacement of the phonon coordinate. Corresponding lattice displacement can be arrived at by the appropriate transformation.

displacement X can be written as a sum of the creation and annihilation operators in the form*

$$X = \sum_k C_k (b_k^* - b_{-k}), \quad C_k = \frac{1}{2i} \left(\frac{2h}{M\omega_k}\right)^{\frac{1}{2}} X \text{ constant.} \qquad \text{(III.4.12)}$$

The Hamiltonian (eqn. III.4.11) can now be diagonalized by the transformation,

$$b_k^* = a_k^* + \lambda_k \quad \text{and} \quad b_k = a_k - \lambda_k, \quad \lambda_k = VC_k/h\omega_k, \qquad \text{(III.4.13)}$$

to obtain a transformed Hamiltonian, which is identical to pure phonon Hamiltonian with the zero of energy shifted by a constant. If we now consider the displacement to correspond to the displacement in the two-sublattice model of Bari and Sivardiere (eqn. III.3.7), we arrive at the conclusion that the kinetic energy term washes away the phase transition in the case of the two-sublattice model also. Thus, dynamic coupling of the lattice to the crystal field strength, without causing a mixing of the spin states, is not the correct description of the systems showing spin-state transitions.

III.4.2 Dynamic Coupling Model with Mixing of Spin States : We now discuss another model in which the low-spin and high-spin states mix and are no longer the eigen states of the system. To bring about a mixing of the low-spin and high-spin states, we have to couple the crystal field strength to a lattice vibration in which the transition metal ion moves off-centre

*In this chapter for typographical convenience h is written for $\hbar$.

while the ions forming the octahedral cage remain static. Such a mode will couple the high- and low-spin states since the site symmetry around the transition metal ion is no longer octahedral. This mixing is expected to provide a non-trivial model in which the higher energy high-spin state is partially occupied even at absolute zero.

The mixing can be described as arising from the term,

$$H_1 = a\ Q^2\ \sigma_x, \qquad \text{(III.4.14)}$$

where σ_x is the Pauli spin matrix and Q is the displacement of the normal mode in which the transition metal ion moves against the cage. The coupling is taken to be quadratic since the mixing does not depend upon the sign of Q. The Hamiltonian of the model is now given by,

$$H = H_o\ I + A\ \sigma_z + B\ \sigma_x,$$
$$H_o = \frac{p_Q^2}{2M} + \frac{M\omega_o^2 Q^2}{2}, \quad A = \Delta \text{ and } B = a\frac{M\omega_o^2 Q^2}{2}, \qquad \text{(III.4.15)}$$

where ω_o is the frequency of the lattice mode and a is the coupling constant in dimensionless units. At this stage we make the following approximation*:

$$\frac{a^2M^2\omega_o^4 Q^4}{4}\sigma_x = \frac{a^2M^2\omega_o^4}{4}\langle Q^2\rangle^2\ \sigma_x \qquad \text{(III.4.16)}$$

*This approximation is necessary since a transformation that diagonalizes $A\ \sigma_z + B\ \sigma_x$ should commute with H_o so that H is diagonalized by the same transformation.

When we seek to find a transformation that diagonalizes H, we find that a rotation around Y-axis can transform H into diagonal form. In order to obtain the actual transformation, U, that diagonalizes H, we need to consider only $A\sigma_z + B\sigma_x$. Since U diagonalizes H, we can write

$$U(A\sigma_z + B\sigma_x)\, U^{-1} = C\sigma_z, \quad B = \frac{a\, M\, \omega_o^2 \langle Q^2 \rangle}{2} \qquad \text{(III.4.17)}$$

U being a rotation operator for rotation around Y-axis has the form[30]

$$U = \cos \phi/2 - i\, \sigma_y \sin \phi/2, \qquad \text{(III.4.18)}$$

where ϕ is the angle of rotation. Substituting the r.h.s. of eqn. (III.4.18) in the l.h.s. of eqn. (III.4.17) we have

$$U\,(A\sigma_z + B\sigma_x)\, U^{-1} = \sigma_z\,(A \cos \phi - B \sin \phi) + \sigma_x\,(B \cos \phi - A \sin \phi)\,. \qquad \text{(III.4.19)}$$

Therefore ϕ is determined by the condition that the coefficient of σ_x in eqn. (III.4.19) vanishes. This gives C as

$$C = (A^2 + B^2)^{\frac{1}{2}} \qquad \text{(III.4.20)}$$

Hence the transformed Hamiltonian is given by

$$H' = U\, H\, U^{-1} = \frac{p_Q^2}{2M} + \frac{M\, \omega_o^2 Q^2}{2}\, I + (\Delta^2 + \frac{a^2 M^2 \omega_o^4}{4} \langle Q^2 \rangle^2)^{\frac{1}{2}}\, \sigma_z \qquad \text{(III.4.21)}$$

The partition of this system can now be easily evaluated as

$$Z = \mathrm{Tr}\, e^{-\beta H} = \mathrm{Tr}\, U e^{-\beta H} U^{-1} = \mathrm{Tr} e^{-\beta H'}$$

$$= Z(\omega_o).2\cosh\{\beta(\Delta^2 + \frac{a^2M^2}{4}\langle Q^2\rangle^2\ \omega_o^{\,2})^{\frac{1}{2}}\} \qquad \text{(III.4.22)}$$

The difference in high-spin-low-spin population, $\langle\sigma_z\rangle$ is given by

$$\langle\sigma_z\rangle = \mathrm{Tr}\cdot e^{-\beta H}\sigma_z/\mathrm{Tr}\, e^{-\beta H}$$

$$= Z^{-1}\,\mathrm{Tr}\, U e^{-\beta H}\sigma_z U^{-1} = \mathrm{Tr}\, U e^{-\beta H} U^{-1} U\sigma_z U^{-1} \qquad \text{(III.4.23)}$$

From eq. (III.4.17), $U\sigma_z U^{-1}$ can be evaluated and is given by

$$U\sigma_z U^{-1} = \sigma_z \cos\phi + \sigma_x \sin\phi\ . \qquad \text{(III.4.24)}$$

Thus

$$\langle\sigma_z\rangle = Z^{-1}\,\mathrm{Tr}\, e^{-\beta H'}(\sigma_z\cos\phi + \sigma_x\sin\phi)$$

$$= Z^{-1}\{\cos\phi\,\mathrm{Tr}\, e^{-\beta H'}\sigma_z + \sin\phi\,\mathrm{Tr}\, e^{-\beta H'}\sigma_x\}\ . \qquad \text{(III.4.25)}$$

By expanding $e^{-\beta H'}$ in a series and using the properties of the Pauli matrices, the second term of eqn. (III.4.25) can be shown to be proportional to the sum of trace over σ_x and σ_y. Since the Pauli matrices are traceless, the second term vanishes. The first term can be similarly expanded and as before, by using the properties of Pauli matrices, we get,

$$\langle\sigma_z\rangle = Z^{-1} \cos\phi \; \mathrm{Tr}\, e^{-\beta H_o I} \{\sigma_z \cosh [\beta(A^2+B^2)^{\frac{1}{2}}] - I \sinh [\beta(A^2+B^2)^{\frac{1}{2}}]\}$$

$$= -Z^{-1} \cos\phi \cdot Z(\omega_o) \cdot 2 \sinh [\beta(A^2+B^2)^{\frac{1}{2}}] \qquad \text{(III.4.26)}$$

Using $\cos\phi = A/(A^2+B^2)^{\frac{1}{2}}$ and eqn.(III.4.22), we get,

$$\langle\sigma_z\rangle = - \frac{A}{(A^2+B^2)^{\frac{1}{2}}} \tanh [\beta(A^2+B^2)^{\frac{1}{2}}] . \qquad \text{(III.4.27)}$$

For a harmonic oscillator, $\langle Q^2\rangle$ is given by,

$$\langle Q^2\rangle = \frac{h}{2\omega_o} + \frac{h}{\omega_o} \times (e^{\beta h\omega_o} - 1)^{-1} \qquad \text{(III.4.28)}$$

Thus $(A^2+B^2)^{\frac{1}{2}}$ can be written as,

$$(A^2+B^2)^{\frac{1}{2}} = \Delta \left(1 + \frac{a^2 M^2 \omega_o^4}{4\Delta^2} g^2(\omega_o)\right)^{\frac{1}{2}}, \quad g(\omega_o) = \left[\frac{h}{2} + \frac{h}{e^{\beta h\omega_o} - 1}\right]$$

$$= \Delta\Phi \qquad \text{(III.4.29)}$$

Now, we have the expression for $\langle\sigma_z\rangle$ as,

$$\langle\sigma_z\rangle = - \frac{1}{\Delta\Phi} \tanh (\beta\Delta\Phi) \qquad \text{(III.4.30)}$$

From eqn.(III.4.30), we see that $\langle\sigma_z\rangle = -\frac{1}{\Delta\Phi}$, at T=0 implying non-zero high-spin population at absolute zero. In the limit $T \to \infty$, $\langle\sigma_z\rangle = -\beta\Delta$ and the variation of $\langle\sigma_z\rangle$ with temperature is completely smooth over the whole temperature range.

While this model does not predict a phase transition, it does show partial occupation of the high-spin states at T=0,

which indeed is observed in the systems belonging to the category of $HoCoO_3$. This model also explains the behaviour of inorganic complexes, where the spin-state transition is not accompanied by a phase transition. It appears that quadratic coupling of the crystal field strength to the lattice displacement, with mixing of the two spin states is not the correct description of the spin-state transition in inorganic solids although this mechanism may be operative in causing partial occupation of the high-spin state at absolute zero.

III.4.3 Order Parameter Model : In Section 2 of this chapter we saw that the spin-state transition in rare earth cobaltites is accompanied by a structural transition which should be explained by a successful model. In order that we get a structural transition, we should arrive at a free energy expansion in terms of a suitable lattice displacement, such that the displacement becomes non-zero above a certain temperature for the thermodynamically stable state. It is not possible to obtain an exact expansion of free energy in terms of the lattice displacement, if we consider the lattice dynamics of the system, as the displacement operator does not commute with the corresponding kinetic energy operator. However, from our previous results we see that the kinetic energy term plays an important role in determining the existence of a phase transition in the model. In order to include the effect of the kinetic

energy term and at the same time obtain an approximate free energy expansion in terms of the lattice displacement, we have employed the path integral method[31] for computing the partition function of our model system. In this method, the kinetic energy contribution to the partition function reduces to a constant and the partition function itself is given as a simple integral over lattice displacement.

To test the validity of this method, we shall first apply it to cases where the exact solution is known. One such case is the one-sublattice model studied in sub-section III.4.1. The partition function of this model is given by eqn. (III.4.5) as,

$$Z = \mathrm{Tr}\, e^{-\beta\left(\frac{p_Q^2}{2M} + \frac{M\omega_b^2}{2} Q^2 + \Delta + VQ\right)} + \mathrm{Tr}\, e^{-\beta\left(\frac{p_Q^2}{2M} + \frac{M\omega_b^2}{2} Q^2 - \Delta - VQ\right)}.$$

Employing the path integral method (see eqn. II.A.22 in the Appendix to this chapter), this can be written as,

$$Z \approx \left(\frac{MkT}{2\pi h^2}\right)^{\frac{1}{2}} \int e^{-\beta\left(\frac{M\omega_b^2}{2} \underline{Q}^2 + \frac{\beta h^2}{24}\omega_b^2\right)} \cdot 2\cosh\left[\beta(\Delta + V\underline{Q})\right] d\underline{Q} \qquad \text{(III.4.31)}$$

when the system consists of N such octahedra, in the limit of large N, the partition function can be approximated* by,

$$Z \approx e^{-\beta F(Q_m)},$$

where $F(Q_m)$ is the minimum value of the function $F(Q)$ given by,

$$F(Q) = \frac{M\omega_b^2}{2} Q^2 + \frac{\beta h^2}{24}\omega_b^2 - \frac{1}{\beta} \ln\{2\cosh\left[\beta(\Delta + VQ)\right]\} \qquad \text{(III.4.32)}$$

*The integral in eqn. (III.4.31) can be evaluated exactly. The results from such an integration are in agreement with the exact results; that is, in both cases we do not observe a phase transition and $\langle\sigma_z\rangle$, C_v and $\langle Q\rangle$ calculated from both the approaches are in agreement. However, we make the approximation in the text to arrive at a free energy expansion in terms of Q.

The free energy of our model can now be written as

$$F = F(Q_m) = \frac{M\omega_b^2}{2} Q_m^2 + \frac{\beta\hbar^2}{24} \omega_b^2 - \frac{1}{\beta} \ln\{2 \cosh [\beta(\Delta + VQ_m)]\}, \tag{III.4.33}$$

where Q_m is given by the condition,

$$\left[\frac{dF}{dQ}\right]_{Q=Q_m} = 0$$

Or

$$Q_m = \frac{V}{M\omega_b^2} \tanh [\beta(\Delta + VQ_m)]. \tag{III.4.34}$$

Equation (III.4.34) has only one solution and that is non-zero, as can be seen graphically. This fact rules out a phase transition in the system. $\langle Q \rangle^{exact}$ can be calculated easily and is given by

$$\langle Q \rangle^{exact} = \frac{V}{M\omega_b^2} \tanh (\beta\Delta) . \tag{III.4.35}$$

The difference of high-spin to low-spin population, $\langle \sigma_z \rangle$, from the path integral approach is given by,

$$\langle \sigma_z \rangle = - \tanh [\beta(\Delta + VQ_m)] \tag{III.4.36}$$

Comparison of Q_m with $\langle Q \rangle^{exact}$ and $\langle \sigma_z \rangle^{P.I}$ (eqn. (III.4.36)) with $\langle \sigma_z \rangle$ (eqn. (III.4.9)) shows that in the limit $\Delta >> VQ_m$, our approximation agrees with the exact results. Also in agreement with the exact results is the fact that this approximate approach does not predict a phase transition. Hence the

effect of the kinetic energy term on the phase transition is included in the approximation and at the same time we have been successful in arriving at a free energy expansion in terms of lattice displacement.

Let us now consider the two-sublattice case, where the displacements are such that octahedra on one sublattice expand while those on the other contract. The Hamiltonian for this model is

$$H = \sum_i \{ \frac{P_{Q_i}^2}{2M} + \frac{M\omega_b^2}{2} Q_i^2 \quad I + (\Delta + VQ_i)\sigma_z \}, \qquad \text{(III.4.37)}$$

$$Q_i = (-)^i Q.$$

It was shown in Section III.4.1 that such a model does not exhibit a phase transition. The exact values of $\langle \sigma_z \rangle$ and $\langle |Q_i| \rangle$ are the same as those in the one sublattice case and are given by eqns. (III.4.9) and (III.4.35) respectively.

We can now proceed to solve this model using the path integral method for computing the partition function. The partition function corresponding to a pair of contracting and expanding octahedra is given by,

$$Z = \mathrm{Tr}\, e^{-\beta(\frac{P_Q^2}{2M} + \frac{M\omega_b^2}{2} Q^2 + \Delta + VQ)} + \mathrm{Tr}\, e^{-\beta(\frac{P_Q^2}{2M} + \frac{M\omega_b^2 Q^2}{2} - \Delta - VQ)}$$
$$+ \mathrm{Tr}\, e^{-\beta(\frac{P_Q^2}{2M} + \frac{M\omega_b^2 Q^2}{2} + \Delta - VQ)} + \mathrm{Tr}\, e^{-\beta(\frac{P_Q^2}{2M} + \frac{M\omega_b^2 Q^2}{2} - \Delta + VQ)}$$

(III.4.38)

goes to unity starting from 0 at $Q_m=0$. The left hand side of eqn. (III.4.40) is a straight line with slope $M\omega_b^2$ and passing through the origin. A second solution of eqn. (III.4.40) is possible if the slope of the curve given by the right hand side of the equation near the origin is greater than the slope of the left hand side. Thus, a non-zero Q_m results, in addition to $Q_m=0$, if

$$k_B T \leq \frac{V^2}{M\omega_b^2} . \qquad \text{(III.4.42)}$$

The $Q_m \neq 0$ solution also corresponds to a minimum of $F(Q)$ (the second derivative of $F(Q)$ is greater than zero for all Q). We, thus, arrive at the result that the order parameter expansion of free energy in the two sub-lattice case indicates a phase transition in the system, while exact and path integral calculations rule out phase transition in the same model.

To resolve the discrepancy between the order parameter expansion results and the results from exact and path integral calculations, we need to examine the order parameter expansion in some detail. We assume that the displacement at each site, Q_i, can be written as,

$$Q_i = \bar{Q} + \Delta Q_i, \quad \langle Q_i \rangle = \bar{Q} \quad \text{and} \quad \langle \Delta Q_i \rangle = 0 \qquad \text{(III.4.43)}$$

and write the expression for the partition function of the whole system as,

$$Z = \int e^{-\beta \left[\sum_i \phi(Q_i) + \sum_{i \neq j} J_{ij} Q_i Q_j\right]} \prod_i dQ_i \,, \qquad \text{(III.4.44)}$$

Here, we have introduced a small coupling between the displacements on sites i and j. This coupling tends to make $\underline{Q}$ to be the same at each site. Using eqn. (III.4.43) in eqn. (III.4.44), we have,

$$Z = \int e^{-\beta \left[\sum_i \phi(\bar{Q}) + \sum_{i \neq j} J_{ij} \bar{Q}^2 + \sum_i f(\bar{Q}\Delta Q_i) + \sum_{i \neq j} J_{ij}(\bar{Q}\Delta Q_j + \bar{Q}\Delta Q_i + \Delta Q_i \Delta Q_j)\right]} d\bar{Q} \prod_i d\Delta Q_i \,, \qquad \text{(III.4.45)}$$

subject to the condition $\langle \Delta Q_i \rangle = 0$. Making a mean field approximation in eqn. (III.4.45), we obtain,

$$Z = \int e^{-\beta \left[N\phi(\bar{Q}) + \sum_{i \neq j} J_{ij} \bar{Q}^2\right]} d\bar{Q} \,. \qquad \text{(III.4.46)}$$

Eqn. (III.4.46) in the limit of large N (using asymptotic approximation) yields*,

$$Z \simeq e^{-\beta N \phi(\bar{Q}_m)} \,. \qquad \text{(III.4.47)}$$

We see that the free energy expansion in terms of order parameter implicitly includes coupling between various octahedra, in the mean field approximation, while exact and path integral calculations (where the integrals are calculated exactly) do not include such a coupling. This coupling, however, weak it may be, tends to cooperatively expand and contract the octahedra

* $\sum_{i \neq j} J_{ij} \bar{Q}^2$ term is neglected since J_{ij} is small and the coupling is assumed to be short-range. Neglecting this term does not affect the essential parameters of the phase transition.

thus giving rise to a phase transition. The exact solution discussed above corresponds to N pairs of octahedra expanding and contracting independently and hence one does not observe a phase transition. The order parameter expression for free energy in the one-sublattice case does not show the existence of a phase transition. This implies that the one-sublattice system with coupling between octahedra also does not undergo a phase transition.

We can determine the transition temperature by expanding the r.h.s. of eqn. (III.4.41) around $\beta\Delta$, for $Q=Q_m$, to obtain a series expansion of free energy in Q_m. This expansion yields,

$$F(Q_m) = \frac{\beta\hbar^2}{24}\omega_b^2 - k_B T \ln(2\cosh\beta\Delta) + \frac{1}{2}(M\omega_b^2 - \beta V^2) Q_m^2 + \frac{1}{12}(\beta^3 V^4) Q_m^4 + \ldots \quad \text{(III.4.48)}$$

The transition temperature is determined by equating the coefficient of Q_m^2 to zero. This gives the transition temperature as

$$T_c = \frac{V^2}{kM\omega_b^2} . \quad \text{(III.4.49)}$$

The value of Q_m below the transition temperature is given by

$$Q_m = \left[\frac{3}{2}\,\frac{(V^2 - M\omega_b^2)}{\beta^3 V^4}\right]^{\frac{1}{2}} . \quad \text{(III.4.50)}$$

The difference in high-spin and low-spin population is given by $\langle\sigma_z\rangle$. The expression for $\langle\sigma_z\rangle$ is

$$\langle \sigma_z \rangle = - \frac{\sinh \left[\beta(\Delta + VQ_m)\right] + \sinh \left[\beta(\Delta - VQ_m)\right]}{\cosh \left[\beta(\Delta + VQ_m)\right] + \cosh \left[\beta(\Delta - VQ_m)\right]}$$

$$= - \tanh (\beta\Delta) . \qquad \text{(III.4.51)}$$

Thus we see that although our system undergoes a structural phase transition, the spin-state population variation is smooth and similar to the variation in a system without coupling between octahedra. The susceptibility will also show a smooth variation with temperature. If we compute the variation in spin-state population difference on each sublattice, we find,

$$\langle \sigma_z \rangle_{\text{sublattice}} = - \frac{1}{2} \tanh (\beta\Delta) \pm \frac{1}{2} \tanh (\beta V Q_m), \qquad \text{(III.4.52)}$$

shows a smooth dependence on the order parameter, below T_c.

The two-sublattice order parameter model we have considered shows a second order structural phase transition with a smooth variation of low-spin-high-spin population ratio. Although the available experimental data in the literature on systems showing gradual spin-state transitions is not exhaustive to enable a good comparison between theory and experiment, systems showing gradual spin-state transitions have indeed been found to exhibit anomalous Debye-Waller factor changes indicating occurrence of structural transition. Typical of these systems are $NdCoO_3$, $GdCoO_3$, and the iron (II) complex $[Fe(papt)_2]$.

Systems exhibiting spin-state transitions are also known to undergo thermodynamically first order phase transitions at the spin-state transition temperature. We have examined a two-sublattice model with the spin-states coupled to the cube of the breathing mode displacement. The Hamiltonian considered by us is,

$$H = \sum_i \left[\left(\frac{p_{Q_i}^2}{2M} + \frac{M\omega_b^2}{2} Q_i^2 \right) I + (\Delta + VQ_i^3)\sigma_z \right], \text{where } Q_i = (-)^i Q. \tag{III.4.53}$$

As before, employing the path integral approximation and order parameter expansion for free energy, we get the following expression for free energy:

$$F(Q_m) = \frac{\beta h^2}{24} \omega_b^2 - \frac{1}{\beta} \ln \left[2 \cosh (\beta\Delta) \right] + \frac{M\omega_b^2}{2} Q_m^2 - \frac{1}{\beta} \ln \left\{ \cosh \left[\beta \left(\frac{\beta h^2}{4M} VQ_m + VQ_m^3 \right) \right] \right\}, \tag{III.4.54}$$

where, Q_m satisfy

$$M\omega_b^2 Q_m = V \left(\frac{\beta h^2}{4M} + 3Q_m^2 \right) \tanh \left[\beta \left(\frac{\beta h^2}{4M} VQ_m + VQ_m^3 \right) \right] \tag{III.4.55}$$

Equation (III.4.54) has two solutions viz., a non-zero solution and a $Q_m=0$ solution. Thus, the two-sublattice system with cubic coupling also shows a phase transition. To arrive at the transition temperature and the order of the phase transition, we have expanded the r.h.s. of eqn. (III.4.54) in a power series in Q_m as follows:

$$F(Q_m) = \frac{\beta h^2}{24}\omega_b^2 - \frac{1}{\beta}\ln\left[2\cosh(\beta\Delta)\right] + Q_m^2\left[\frac{M\omega_b^2}{2} - \frac{\beta^3 h^4}{32M^2}V^2\right] + Q_m^4\left[\frac{\beta^3}{12}\left(\frac{\beta h^2}{4M}\right)^4 V^4 - \frac{\beta}{2}\left(\frac{\beta h^2}{2M}\right)V^2\right] + Q_m^6\left[\left(\frac{\beta h^2}{4M}\right)^6\left(\frac{\beta^5}{2880}\right)V^6 + \left(\frac{\beta h^2}{4M}\right)^3\left(\frac{\beta^3}{48}\right)V^4 - \left(\frac{\beta}{2}\right)V^2\right] \quad \text{(III.4.56)}$$

The condition for a first order phase transition is that the coefficient of Q_m^2 should vanish, coefficient of Q_m^4 should be negative and the coefficient of Q_m^6 should be positive at $T=T_c$. These are satisfied when,

$$\left(\frac{\beta h^2}{4M}\right)^6\left(\frac{\beta^5}{2880}\right)V^6 \gg \frac{\beta}{4}V^2 .$$

The transition temperature is given by

$$\beta_c^3 = \frac{16\,M^3\,\omega_b^2}{V^2\,h^4} \quad \text{(III.4.57)}$$

Like in the previous case, we can estimate $\langle\sigma_z\rangle$, the difference in high-spin and low-spin population. $\langle\sigma_z\rangle$ is given by the expression,

$$\langle\sigma_z\rangle = -\tanh(\beta\Delta), \quad \text{(III.4.58)}$$

that is zero population of high-spin state at T=0 and equal population of the two spin states as $T\to\infty$. We once again notice that the low-spin and high-spin population difference over the whole system is independent of Q_m. We see from our calculations that unless there is coupling of the spin states to the lattice displacement in even power, we will always have the above

expression for $\langle\sigma_z\rangle$. However, this difference in population on any one of the sublattices depends upon Q_m by the relation,

$$\langle\sigma_z\rangle_{\text{sublattice}} = -\frac{1}{2}\tanh(\beta\Delta) \pm \frac{1}{2}\tanh\left[\beta\left(\frac{\beta h^2}{4M}VQ_m + VQ_m^3\right)\right] \qquad \text{(III.4.59)}$$

Thus, an abrupt change in Q_m will lead to ordering of the low-spin and high-spin ions on different sublattices.

In the two-sublattice model with cubic coupling, we can have either a first order or a second order transition. Systems where the spin-state transition is first order are known. However, thermodynamics of such systems have not been studied in detail to see whether the first order spin-state transition is also accompanied by a thermodynamically first order phase transition. The drawback of a model with pure cubic coupling is that it predicts the net low-spin-high-spin population ratio to be independent of the order parameter. In real systems the net low-spin-high-spin population rationshows a jump at T_c. This feature can be incorporated into the model by adding an additional coupling term which couples the spin-states to the square of the lattice displacement.

III.4.4 Two Phonon Model : We saw under sub-section III.4.2 that coupling of the spin states to an optical (ion versus cage) mode leads to a non-zero population of the high-spin state at T=0 K. In this sub-section we shall make a preliminary study of a model in which the spin states are coupled to two phonon modes,

viz., a breathing mode and an optical mode. The breathing mode to which the spin states are coupled is the one in which the octahedra on one sublattice expand while those on the other contract (two-sublattice model). The coupling to the optical mode mixes the spin states and is brought about by a quadratic term in the off-center displacement of the transition metal ion. The system we shall study is described by the following Hamiltonian:

$$H = \sum_i \left[\left(\frac{P_{Q_i}^2}{2M} + \frac{P_{X_i}^2}{2M} + \frac{M\omega_b^2}{2} Q_i^2 + \frac{M\omega_o^2}{2} X_i^2 \right) I + (\Delta + VQ_i)\,\sigma_z + a\, X_i^2\, \sigma_x \right], \qquad \text{(III.4.60)}$$

$$Q_i = (-)^i Q \quad \text{and} \quad X_i = x.$$

ω_b and ω_o are the frequencies of the breathing and the optical mode, Q is the breathing mode displacement and X, the optical mode displacement.

The transformation defined by eqn. (III.4.18) does not diagonalize this Hamiltonian because of the presence of the linear term in Q.* To obtain preliminary results from the model of eqn. (III.4.60), we shall make the following approximations: (i) we shall approximate the off-diagonal term in the model by writing,

*Even after making the approximation $x^2 = \langle x^2 \rangle$, diagonalization by the transformation operator U of eqn. (III.4.18) is not possible since U now becomes dependent on Q and thus does not commute with, H_o, the harmonic oscillator part of the Hamiltonian.

$$a\,x^2\,\sigma_x = a\,\langle x^2\rangle\,\sigma_x\ ; \qquad \text{(III.4.61)}$$

and (ii) we shall treat the model as classical while considering the coupling to the breathing mode. That is to say, in the estimation of the partition function, we can independently integrate over Q and P_Q. The integration over P_Q gives a constant. This approximation can be justified since in the path integral approximation, a linear term in displacement, in the potential function does not contribute to quantum mechanical correction (quantum mechanical correction is proportional to the second derivative of the potential taken with respect to displacement) and a quadratic term gives rise to a constant correction. Hence we saw in the linear two-sublattice and one-sublattice case, the partition function was classical except for a proportionality constant. Further the agreement between results from the path integral calculation and exact calculation shows that classical model is a good approximation. It was also shown that any discrepancy between the order parameter expansion results and the exact results was due to the inherent assumption of coupling between octahedra in the order parameter approximation and (the discrepancy) does not have its origin in the path integral approximation. Hence we are justified in approximating the Hamiltonian of eqn. (III.4.60) by

$$H = \sum_i \left[\left(\frac{P_{x_i}^2}{2M} + \frac{M\omega_o^2 x_i^2}{2} + \frac{M\omega_b^2 Q_i^2}{2} \right) I + (\Delta + VQ_i)\,\sigma_z + a\,\langle x_i^2\rangle\,\sigma_x \right] \qquad \text{(III.4.62)}$$

This Hamiltonian is now diagonalized by the transformation of eqn. (III.4.18) as in sub-section (III.4.2).

The partition function of the above Hamiltonian in the case of a pair of octahedra - one contracting and the other expanding - can now be written as

$$Z \sim Z(\omega_o)\ e^{-\beta\left(\frac{M\omega_b^2 Q^2}{2}\right)} \cdot 2\{\cosh\beta\left[(\Delta + VQ)^2 + a^2\langle x^2\rangle^2\right]^{\frac{1}{2}} + \cosh\beta\left[(\Delta - VQ)^2 + a^2\langle x^2\rangle^2\right]^{\frac{1}{2}}\}\, dQ, \qquad \text{(III.4.63)}$$

$Z(\omega_o)$ is the partition function of the optical mode. We see that the lim $a \to 0$, the partition function reduces to the linear two-sublattice partition function in the path integral approximation (eqn.(III.4.39)). In the lim $V \to 0$, the results are identical to the results of the model studied in subsection (III.4.2). Making an order parameter expansion we find that the free energy is given by

$$F(Q_m) = F(0) + \frac{M\omega_b^2 Q_m^2}{2} - \frac{1}{\beta}\ln\{\cosh\beta\left[(\Delta + VQ_m)^2 + a^2\langle x^2\rangle^2\right]^{\frac{1}{2}} + \cosh\beta\left[(\Delta - VQ_m)^2 + a^2\langle x^2\rangle^2\right]^{\frac{1}{2}}\}, \qquad \text{(III.4.64)}$$

where Q_m satisfies the equation

$$M\omega_b^2 Q_m = -\frac{1}{\beta}\left[\frac{V(\Delta + VQ_m)\sinh\beta\left[(\Delta + VQ_m)^2 + a^2\langle x^2\rangle^2\right]^{\frac{1}{2}}}{\left[(\Delta + VQ_m)^2 + a^2\langle x^2\rangle^2\right]^{\frac{1}{2}}} - \frac{V(\Delta - VQ_m)\sinh\left[\beta(\Delta - VQ_m)^2 + a^2\langle x^2\rangle^2\right]^{\frac{1}{2}}}{\left[(\Delta - VQ_m)^2 + a^2\langle x^2\rangle^2\right]^{\frac{1}{2}}}\right] \times \left[\cosh\beta\left[(\Delta + VQ_m)^2 + a^2\langle x^2\rangle^2\right]^{\frac{1}{2}} + \cosh\beta\left[(\Delta - VQ_m)^2 + a^2\langle x^2\rangle^2\right]^{\frac{1}{2}}\right]^{-1} \qquad \text{(III.4.65)}$$

We see that $Q_m=0$ is a solution of the above equation. For large values of Q_m, the r.h.s. of the equation behaves as $\tanh(\beta V Q_m)$ and hence if the slope of the r.h.s. is greater than $M\omega_b^2$ a second solution for Q_m exists and this solution will be a non-zero solution of the equation. This indicates that the system undergoes a phase transition. The transition temperature is obtained by the condition that the r.h.s. and l.h.s. of the expressions in eqn. (III.4.65) have the same slope near the origin. This condition gives the transition temperature as

$$T_c = \frac{V^2}{k_B M\omega_b^2}, \qquad \text{(III.4.66)}$$

which is the same as that given by eqn. (III.4.49). This phase transition could be second order, in which case it agrees with the phase behaviour of the linear two-sublattice model of the previous subsection. To see whether the system can show a first order phase transition, the free energy of eqn. (III.4.64) should be expanded in a power series in Q_m and as before, we should see whether the coefficient of Q_m^4 is negative while the coefficient of Q_m^6 is positive, at T_c. The evaluation of the coefficients is rather tedious and has not been carried out for the present. However, spin-state population difference can be computed easily, in the same manner as in subsection (III.4.2). The expression for $\langle\sigma_z\rangle$ is given by

$$\langle\sigma_z\rangle = -\left[\frac{(\Delta+VQ_m)\sinh\beta\left[(\Delta+VQ_m)^2 + a^2\langle x^2\rangle^2\right]^{\frac{1}{2}}}{\left[(\Delta+VQ_m)^2 + a^2\langle x^2\rangle^2\right]^{\frac{1}{2}}} + \frac{(\Delta-VQ_m)\sinh\beta\left[(\Delta-VQ_m)^2 + a^2\langle x^2\rangle^2\right]^{\frac{1}{2}}}{\left[(\Delta-VQ_m)^2 + a^2\langle x^2\rangle^2\right]^{\frac{1}{2}}}\right] \times \left[\cosh\beta\left[(\Delta+VQ_m)^2 + a^2\langle x^2\rangle^2\right]^{\frac{1}{2}} + \cosh\beta\left[(\Delta-VQ_m)^2 + a^2\langle x^2\rangle^2\right]^{\frac{1}{2}}\right]^{-1} \quad \text{(III.4.67)}$$

We see that $\langle\sigma_z\rangle$ tends to zero as $\beta\to 0$ or $T\to\infty$. Also as $T\to 0$ or $\beta\to\infty$, $\langle\sigma_z\rangle$ is given by

$$\langle\sigma_z\rangle \sim -\frac{(\Delta + VQ_m)}{\left[(\Delta + VQ_m)^2 + a^2\langle x^2\rangle^2\right]^{\frac{1}{2}}} \quad \text{(III.4.68)}$$

This implies a non-zero population of the high-spin state at absolute zero. Another noteworthy feature in eqn. (III.4.67) is that the net difference between the two spin-state populations depends on the order parameter, a feature which was lacking in the earlier models. This may give rise to more interesting variations of the magnetic susceptibility with temperature.

The results presented here are not complete and the model itself may be studied in the quantum mechanical framework. Studies in this direction are being pursued at present.

III.5. Summary

From the Tanabe-Sugano diagrams, it is known that the ground state of a transition metal ion in d^4, d^5, d^6 or d^7 configuration changes from one spin state to another as the crystal field strength is varied. In solid state systems where the crystal field strength is close to such a crossover point, a variety of interesting magnetic and structural behaviours is observed. Such observations include abrupt or gradual change in the ratio of high-spin state population to the low-spin state population, a plateau in the inverse susceptibility versus temperature curve and change in symmetry at the spin-state transition temperature. These transitions are thermodynamically first or second order. Examples of systems undergoing spin-state transitions are the Fe^{2+} complexes like $[Fe(Phen)_2(NCS)_2]$ and $[Fe(Phen)_2(NCSe)_2]$, MnAs, MnP, Co_2O_3 and the family of rare earth cobaltites, $LnCoO_3$ (Ln = rare earth ion).

Bari and Sivardiere put forward a theory to explain spin-state transitions, particularly in the $LaCoO_3$ system. Their theory does not include the dynamics of the lattice and besides does not explain the observed changes such as the ratio of spin-state populations being unity in the high temperature phase and the non-zero population of the high-spin states even at absolute zero. In view of this, we have examined some models for spin-state transitions in solids. We observe that Bari and

Sivardisra's one- and two-sublattice models do not show a phase transition even when a kinetic energy term is added to the Hamiltonians, provided we do not introduce coupling between the octahedra. The spin-state populations vary smoothly with temperature. The inverse susceptibility shows smooth variation with temperature; while the behaviour at very low and very high temperatures match the observed behaviour, the plateau at intermediate temperature is not reproduced by the model.

We have examined a model in which the spin states are coupled to a mode in which the central transition metal ion in the octahedron moves off-center. This coupling is assumed to provide a mixing of the spin states since the symmetry of the octahedron is lost when the central ion moves off-center. This model does not exhibit any phase transition although there is some population of the high-spin state even at absolute zero.

To study the spin-state transition and the accompanying structural transition, we have arrived at a free energy expansion in lattice displacement. This cannot be done exactly because of the presence of the kinetic energy term in the Hamiltonian. But, by using a standard path integral approximation for evaluating the partition function, in which the kinetic energy term is treated approximately, we could write the partition function as an integral over displacement only. Later by making an order parameter expansion of the free energy, in the limit of large N, we have succeeded in obtaining an expansion

of free energy in terms of lattice displacement. In this approximation, the two-sublattice model exhibits a second order phase transition. This fact is in apparent contradiction with the exact results. The discrepancy between the order parameter theory and the exact results is explained by a closer examination of the order parameter method. In the order parameter method, coupling between octahedra is tacitly assumed, in the mean field approximation, since we use a single displacement parameter for all octahedra. In the exact solution, on the other hand, displacements of each pair of octahedra are treated independently. Thus, we see that a linear two-sublattice model with coupling between octahedra exhibits a second order phase transition. The inverse susceptibility variation with temperature is the same as in the exact model. The net spin-state population ratio is independent of the order parameter while the same on each sublattice depends smoothly upon the order parameter.

The two-sublattice model with cubic coupling between the spin states and the displacement is capable of exhibiting a first order phase transition. However, the net spin-state population ratio is again independent of the order parameter. By inspection it is seen that this ratio can depend on the order parameter only when the coupling is to an even power in the displacement.

We have investigated a two phonon model in which the coupling to off-center displacement mixes the spin states while the coupling to breathing mode is linear and without mixing. The breathing mode displacement is considered to alternate in sign from site to site. This model is solved by assuming it to be classical with respect to the breathing mode. This is justified from the results on the models of subsections (III.4.2) and (III.4.3). This model shows a spin-state transition accompanying a structural transition. Besides it predicts a non-zero population of the high-spin state at absolute zero. The net spin-state population ratio is also dependent on the order parameter - a feature which can explain the observed first or second order spin-state transition associated with the structural transition and anomalous magnetic susceptibility variation with temperature.

The models that we have considered are simple two and four state models and do not include spin-orbit coupling or charge transfer between different spin states. However, our models do show the existence of thermodynamically first or second order phase transitions accompanying spin-state transitions. Some of them also predict a non-zero population of the high-spin state at absolute zero and a ratio of the spin-state populations tending to unity at high temperatures. The last model deserves to be examined more closely and particularly, for variation of inverse

magnetic susceptibility with temperature. None of our models, however, can predict the unusual higher temperature lower symmetry phase observed in the rare earth cobaltite systems. Before commenting any further on the applicability and limitations of these models, it would be necessary to obtain well defined data on the thermodynamic and crystal structure changes accompanying spin-state transitions. Experimental studies in this direction are now in progress in this laboratory.

References

1. Y. Tanabe and S. Sugano, J. Phys. Soc. (Japan), 11, 864 (1956).

2. C. J. Ballhausen, 'Introduction to Ligand Field Theory', McGraw Hill, New York (1962).

3. B. N. Figgis, 'Introduction to Ligand Fields', John Wiley and Sons, New York (1966).

4. E. Konig and G. Ritter, Mössbauer Effect Methodology, 9, 1 (1974).

5. E. Konig, G. Ritter and H. A. Goodwin, Chem. Phys. Letts., 44, 100 (1976).

6. E. Konig and G. Ritter, Solid State Commun., 18, 279 (1976).

7. M. Sorai and S. Seki, J.Phys. Chem. Solids, 35, 555 (1974).

8. J. B. Goodenough, 'Magnetism and the Chemical Bond', John Wiley and Sons, New York (1963).

9. J. B. Goodenough, D. H. Ridgley and W. A. Newman, Proceedings of the International Conference on Magnetism, Nottingham, 1964, page 542, Institute of Physics and the Physical Society, London, (1965).

10. J. Chenavas and J. C. Joubert, Solid State Commun., 9, 1057 (1971).

11. P. M. Raccah and J. B. Goodenough, Phys. Rev., 155, 932 (1967).

12. V. G. Bhide, D. S. Rajoria, G. Rama Rao and C. N. R. Rao, Phys. Rev., B6, 1021 (1972).

13. V. G. Bhide, D. S. Rajoria, Y. S. Reddy, G. Rama Rao and C. N. R. Rao, Phys. Rev., B8, 5028 (1973).

14. L. P. Landau and E. M. Lifshitz, 'Statistical Physics', Pergamon Press, Oxford (1970).

15. G. A. Gehring and K. A. Gehring, Rep. Progr. Phys., 38, 1 (1975).

16. R. A. Bari and J. Sivardiere, Phys. Rev., B5, 4466 (1972).

17. D. B. Chestnut, J. Chem. Phys., 40, 405 (1964).

18. R. A. Bari, in Proceedings of the Seventeenth Annual Conference on Magnetism and Magnetic Materials, Chicago, 1971 (Eds.) C. D. Graham and J. J. Rhyne, page 290, American Institute of Physics, New York (1972).

19. D. S. Rajoria, V. G. Bhide, G. Rama Rao and C.N.R. Rao, J. Chem. Soc., Farad. Trans. II, 70, 512 (1974).

20. V. G. Jadhao, R. M. Singru, G. N. Rao, D. Bahadur and C. N. R. Rao, J.Phys. Chem. Solids, 37, 113 (1976).

21. V. G. Jadhao, R. M. Singru, G. Rama Rao, D. Bahadur and C. N. R. Rao, J. Chem. Soc., Farad. Trans. II, 71, 1885 (1975).

22. D. Bahadur, Ph.D. Thesis, Kanpur University (1977).

23. D. Bahadur, Ind. J. Chem., 14A, 204 (1976).

24. G. Rama Rao, Ph.D. Thesis, Indian Institute of Technology, Kanpur (1974).

25. V. G. Jadhao, Ph.D. Thesis, Indian Institute of Technology, Kanpur (1975).

26. C. N. R. Rao and V. G. Bhide, in Proceedings of Nineteenth Annual Conference on Magnetism and Magnetic Materials, Boston, 1973, page 504, American Institute of Physics, New York (1974).

27. R. Marx and H. Happ, Phys. Stat. Solidi, (b) 67, 181 (1975).

28. M. Blume, Phys. Rev., 141, 517 (1966).

29. Y. Kitano and G. T. Trammell, Phys. Rev. Letts., 16, 572 (1966).

30. A. Messiah, 'Quantum Mechanics', North-Holland Publishing Company, Amsterdam, (1961).

31. R. P. Feynman and A. R. Hibbs, 'Quantum Mechanics and Path Integrals', McGraw-Hill, New York (1965).

APPENDIX

PATH INTEGRAL METHOD IN STATISTICAL MECHANICS[31]

The partition function of a system can be written as the trace over the density matrix, ρ, of the system:

$$Z = Tr\,[\rho] = \int \rho(x,x)\, dx, \qquad \text{(III.A.1)}$$

where $\rho(x,x)$ is the diagonal element of the density matrix. The density matrix element $\rho(x_2,x_1)$ is given by

$$\rho(x_2,x_1) = \sum_i \phi_i(x_2)\ \phi_i^*(x_i)\ e^{-\beta E_i}, \qquad \text{(III.A.2)}$$

where ϕ_i s are the eigen functions of the system and E_i the corresponding eigen value. The form of the above expression is similar to that of a kernel for the probability of taking a system from (x_1,t_1) to (x_2,t_2), viz.,

$$K(x_2,t_2;\ x_1,t_1) = \sum_j \phi_j(x_2)\ \phi_j^*(x_1)\ e^{-i/h\ E_j(t_2-t_1)} \qquad \text{(III.A.3)}$$

The close similarity between eqn. (III.A.2) and eqn. (III.A.3) can be seen by making the substitutions $u_2=\beta h$ and $u_1=0$ in the earlier equation.

The kernel of eqn. (III.A.3) can be represented by a path integral of the form

$$K(x_2,t_2;\ x_1,t_1) = \sum_{\text{all paths}} e^{i/h\ S[x(t)]} = \int_1^2 e^{i/h \left[\int_1^2 L(x,\dot{x},t)dt\right]} Dx(t), \qquad \text{(III.A.4)}$$

where $S[x(t)]$ is the action for a path connecting (x_2,t_2) and (x_1,t_1), $L(x,\dot{x},t)$ is the Lagrangian of the system and $Dx(t)$ implies integration over all paths connecting (x_2,t_2) and (x_1,t_1). Since $K(x_2,t_2;\ x_1,t_1)$ and $\rho(x_2,x_1)$ are similar in form and also can be shown to satisfy similar equations of motion*, $\rho(x_2,x_1)$ can be represented as a path integral by performing the change of variable from t to -iu, in eqn. (III.A.4). Thus the density matrix element can be written as

$$\rho(x_2,x_1) = \int e^{\frac{1}{h}\left[\int_o^h L_u(x,\dot{x}_u,u)\,du\right]} Dx(u), \qquad \text{(III.A.5)}$$

where $\dot{x}_u$ is the differential of x w.r.t U. The path integration is performed over all paths connecting the points $(x_1,0)$ and $(x_2,\beta h)$. For systems where Lagrangian can be written in the form

$$L = \frac{m}{2}\dot{x}^2 - V(x)\ , \qquad \text{(III.A.6)}$$

the change of variable from t to -iu gives the 'Lagrangian' of eqn. (III.A.5) as

$$L_u = -\frac{m}{2}\dot{x}_u^2 - V(x)\ . \qquad \text{(III.A.7)}$$

Thus the density matrix element of such a system can be written as

$$\rho(x_2,x_1) = \int e^{-\frac{1}{h}\left[\int_o^{\beta h}\{\frac{m}{2}\dot{x}_u^2 + V(x)\}du\right]} Dx(u)\ . \qquad \text{(III.A.8)}$$

The partition function now becomes

---

* In the case of the density matrix, $-i\beta h$ assumes the role of time.

$$Z = \int \rho(x_1,x_1)\, dx_1 = \int dx_1 \int_{x_1}^{x_1} \left[e^{-\frac{1}{h}\left[\int_0^h (\frac{m}{2}\dot{x}_u^2 + V(x))du\right]} Dx(u) \right] \qquad \text{(III.A.9)}$$

The paths over which integration is performed begin and end at x_1. At high temperatures, the 'time' (βh) in which a path has to be completed is small. Hence longer paths will have higher 'kinetic energy'. Consequently they do not contribute significantly to the integral. Since paths which contribute significantly are shorter, the potential $V(x)$ can be considered to be a constant for the entire path. The path integral that need be evaluated now is just a free particle path integral and can be evaluated easily. The resulting partition function has the form

$$Z \simeq \left(\frac{mkT}{2\pi h^2}\right)^{\frac{1}{2}} \int e^{-\beta V(x_1)} dx_1 \,. \qquad \text{(III.A.10)}$$

For our purpose, we need to estimate the partition function over all temperatures. At low temperatures longer paths do make significant contributions to the path integral. So, we no longer can treat the potential as a constant and should take into account the change in the potential along a path. We can approximately treat the variation of the potential along a path, by expanding the potential around a point x in Taylor series. For convenience and accuracy, we can take this point to be the mean position of a path, $\underline{x}$, defined by

$$\underline{x} = \frac{1}{\beta h} \int_0^{\beta h} x(u)\, du. \qquad \text{(III.A.11)}$$

The path integration is carried out over all paths which have the same $\underline{x}$. A second integration over $\underline{x}$ will give the partition

function. Expanding the potential in Taylor series upto the 3rd term, we can write

$$\int_0^{\beta h} V\left[\underline{x}(u)\right]du = \beta h\, V(\underline{x}) + \int_0^{\beta h} \left[\underline{x}(u)-\underline{x}\right] V'(\underline{x})\, du + \frac{1}{2}\int_0^{\beta h} \left[\underline{x}(u)-\underline{x}\right]^2 V''(\underline{x})\, du. \qquad \text{(III.A.12)}$$

The second term in the expansion vanishes from the definition of $\underline{x}$ (eqn. III.A.11). Hence, we have for the partition function

$$Z = \int e^{-V(\underline{x})}\, d\underline{x} \int_{x_1}^{x_1} \left[e^{-\frac{1}{h}\left[\int_0^{\beta h} \{\frac{m}{2}\dot{x}^2 + \frac{(x(u)-\underline{x})^2}{2} V''(\underline{x})\}du\right]} \right] Dx(u) \qquad \text{(III.A.13)}$$

$V(\underline{x})$ is a constant since $\underline{x}$ is a constant for the set of paths considered in the path integration.

The constraint, eqn. (III.A.11), can be incorporated into the path integral by rewriting it as

$$\int_0^{\beta h} (x-\underline{x})\, du = 0 . \qquad \text{(III.A.14)}$$

Substituting $y = x - \underline{x}$ gives the constraint in the form

$$\int_0^{\beta h} y\, du = 0 . \qquad \text{(III.A.15)}$$

The path integral then assumes the form

$$\text{P.I.} = \int_{x_1-\underline{x}}^{x_1-\underline{x}} \left[e^{-\frac{1}{h}\left[\int_0^{h} \{\frac{m}{2}\dot{y}^2 + \frac{1}{2} y^2 V''(0)\}\, du\right]} \right] Dy(u). \qquad \text{(III.A.16)}$$

The constraint, now written in the form of eqn. (III.A.15) can be incorporated into the path integral in the following way.

Since all the paths in the path integral have the same average position, y=0, we multiply the path integral by $\delta(\int_0^{\beta h} y\, du)$. Now, we use the integral representation of the δ function viz.,

$$\delta\left(\int_0^{\beta h} y\, du\right) = \int_{-\infty}^{\infty} e^{ik \int_0^{\beta h} y\, du} \frac{dk}{2\pi} . \qquad \text{(III.A.17)}$$

Thus the path integral with the constraint now becomes

$$\text{P.I. with constraint} = \int_{-\infty}^{\infty} \frac{dk}{2\pi} \int_{x_1-\underline{x}}^{x_1-\underline{x}} e^{-\frac{1}{\hbar}\left[\int_0^{\beta h} \{\frac{m}{2}\dot{y}^2 + \frac{1}{2} y^2 V''(0) - ihky\} du\right]} \mathcal{D}y(u) \qquad \text{(III.A.18)}$$

The path integration in eqn. (III.A.18) is performed over all paths beginning and ending at $x_1-\underline{x}$. To complete the path integration, integration over x_1 (to include all initial points) also has to be carried out.

The path integration in eqn.(III.A.18) is carried out by first writing the paths y(u) as

$$y(u) = y_{Cl}(u) + g(u), \qquad \text{(III.A.19)}$$

where y_{Cl} is the classical path corresponding to the Lagrangian in the exponent and g(u) gives the difference between the classical path and the path in question. The end points of g(u) are (0,0) as y_{Cl} satisfies the required boundary conditions. Substituting eqn. (III.A.19) in eqn. (III.A.18), the latter equation can be re-written as

$$\text{P.I.} = \int_{-\infty}^{\infty}\int_{-\infty}^{\infty} \frac{dk}{2\pi}\, dx_1\, e^{-\frac{1}{h}S_{Cl}} \int_{o}^{o} e^{-\frac{1}{h}\left[\int_0^{\beta h}\left\{\frac{m}{2}\dot{g}^2+\frac{1}{2}g^2V''(0)\,du\right\}\right]} Dg(u), \tag{III.A.20}$$

where S_{Cl} is the classical action. First order terms in g and $\dot{g}$ do not appear in the exponent of the above equation as the classical path is determined by setting the first order correction to zero. The path integral over g can be easily evaluated since g can be extended odd periodically in u (this is possible since $g(u)=0$ at $u=0$ and $u=\beta h$) with a period $2\beta h$. The function g can then be expressed as a Fourier sine series. Integration over all the paths, g(u), is now reduced to a set of simple integrals over the Fourier coefficients and the integrations yield a constant times $(\beta h)^{\frac{1}{2}}$. Integrations over k and x_1 can be performed after expanding S_{Cl} correct to first order in $V''(0)$. The path integral is finally given by

$$\text{P.I.} = \sqrt{\frac{m\omega}{2\pi h \sin(\omega\beta h)}}\cdot e^{-\frac{\beta^2h^2}{24M}V''(\underline{x})}, \quad \omega^2 = -V''(\underline{x})/m$$

$$\simeq \left(\frac{mkT}{2\pi h^2}\right)^{\frac{1}{2}} e^{-\frac{\beta^2h^2}{24M}V''(\underline{x})}, \tag{III.A.21}$$

for small $V''(\underline{x})$. Substituting this in eqn. (III.A.13) gives the partition function as

$$Z \simeq \left(\frac{mkT}{2\pi h^2}\right)^{\frac{1}{2}} \int e^{-\beta\left[V(\underline{x}) + \frac{h^2}{24m}V''(\underline{x})\right]} d\underline{x} \tag{III.A.22}$$

Thus, we see that in the expression for the partition function, only the distance $\underline{x}$ appears and the kinetic energy contribution to the partition function appears as a correction to the potential.